

HIGH REPETITION RATE GATED PHOTOMULTIPLIER



By



ALAIN POIRIER, B.Sc.

A Thesis

Submitted to the School of Graduate Studies

in Partial Fulfilment of the Requirements

for the Degree

Master of Science

McMaster University

May 1980

HIGH REPETITION RATE GATED PHOTOMULTIPLIER

MASTER OF SCIENCE (1980)
(Physics)

McMASTER UNIVERSITY
Hamilton, Ontario

TITLE: High Repetition Rate Gated Photomultiplier

AUTHOR: Alain Poirier, B.Sc. (University of Montreal)

SUPERVISOR: Professor E. A. Ballik

NUMBER OF PAGES: xii , 126

ABSTRACT

A high repetition rate, high voltage pulse generator was built and was used to gate a photomultiplier for the detection of relatively high levels of radiation.

A unique design has been developed which is capable of a much higher repetition rate than any system described in the literature. The pulse risetime is 1.7 ns, and the width is continuously adjustable from 4 ns. The highest achievable repetition rate is 100 MHz for a train of six consecutive pulses repeated every 2.5 μ s. A continuous train of pulses can be generated for repetition rates below 2.5 MHz. The pulse amplitudes range between 0V and 220V.

The gated photomultiplier is a versatile low-noise pulsed detector. One, two or three dynodes can be pulsed with positive or negative pulses, and the cut-off ratio can, within limits, be set to any desirable level. We have achieved ratios ranging between 0 and 2400. The gated photomultiplier can be adjusted to be gated on or off during intense radiation. The latter allows detection of weak radiation occurring before or after the intense radiation.

The effect that changes in the potential drop between the dynodes has on the total current gain of the photomultiplier is investigated. Also, investigated are the saturation

properties of photomultipliers at high anode currents. These studies explain the behaviour of the gated photomultipliers and indicate how to choose amongst the various photomultiplier parameters.

The capability of the gated photomultiplier system in a given application is tested with a dye laser. This is done by carrying out measurements on the amplified spontaneous emission (ASE).

ACKNOWLEDGEMENTS

I wish to express my appreciation to my thesis supervisor, Dr. E. A. Ballik, for his guidance and support in this work. The financial support from the National Research Council and McMaster University is also acknowledged. I wish to thank Mr. M. Roberts for his excellent construction of equipment and Mr. G. Lienweber for his help and advice.

I am grateful for the excellent work done by Mrs. Kennelly in typing this manuscript.

GLOSSARY

CONSTANTS

Boltzmann's constant
Planck's constant
Stephen's constant
Vacuum permittivity
Vacuum permeability
Velocity of light in vacuum

SYMBOLS

$k = 1.380 \times 10^{-23} \text{ J} \cdot \text{K}^{-1}$
 $h = 6.626 \times 10^{-34} \text{ J} \cdot \text{s}$
 $\sigma = 5.67 \times 10^{-8} \text{ J} \cdot \text{s}^{-1} \cdot \text{m}^{-2} \cdot \text{K}^{-4}$
 $\epsilon_0 = 8.8542 \times 10^{-12} \text{ (A} \cdot \text{s)}^2 \cdot \text{kg}^{-1} \cdot \text{m}^{-3}$
 $\mu_0 = 4\pi \times 10^{-7} \text{ (A} \cdot \text{s)}^{-2} \cdot \text{kg} \cdot \text{m}$
 $c = 2.997925 \times 10^8 \text{ m} \cdot \text{s}^{-1}$

UNITS

Ampere
Angstroms
Electron-volt
Farad
Henry
Hertz
Joule
Kelvin
Liter
Meter
Mole
Moles per liter
Ohm
Second
Volt
Watt

SYMBOLS

A
 $\text{\AA} = 10^{-10} \text{ m}$
 $\text{eV} = 1.6 \times 10^{-19} \text{ J}$
f
h
Hz
J
 $^{\circ}\text{K}$
 ℓ
m
M
M/ ℓ
 Ω
s
V
W

<u>MULTIPLICATION FACTOR</u>	<u>SYMBOL</u>
Giga - 10^9	G
Mega - 10^6	M
Kilo - 10^3	K
Milli - 10^{-3}	m
Micro - 10^{-6}	μ
Nano - 10^{-9}	n
Pico - 10^{-12}	p

<u>TERM</u>	<u>ABBREVIATION</u>
Amplified Spontaneous Emission	ASE
Capacitor	C
Direct current	dc
Gain, amplification factor	G
Half Width at Half Maximum	HWHM
Internal Diameter	ID
Inductor	L
Light Emitting Diode	LED
Outer Diameter	OD
Printed Circuit	PC
Resistor	R
Rhodamine 6G	R6G
Silicon Controlled Rectifier	SCR
Ultraviolet radiation	UV
Potential difference	ΔV
Wavelength	λ

TABLE OF CONTENTS

	<u>PAGE</u>
ABSTRACT	iii
ACKNOWLEDGEMENTS	v
GLOSSARY	vi
LIST OF FIGURES	x
CHAPTER 1	
INTRODUCTION	1
1.1 Outlines of the contents of the thesis	2
CHAPTER 2	
PULSE GENERATOR FOR PHOTOMULTIPLIER GATING	
2.1 The gating switch	4
2.1.1 The transistors	7
2.1.2 The speed-up circuit	8
2.1.3 The reverse biased junction	10
2.1.4 More about transistors	12
2.2 The transmission lines	14
2.3 The multiple gates	18
2.4 Conclusion	24
CHAPTER 3	
THE GATED PHOTOMULTIPLIER	
3.1 Introduction	27
3.2 The basic principles	27
3.2.1 The photocathode	28
3.2.2 The dynode chain	29
3.2.3 The anode	30
3.3 The photomultiplier gating circuit	32
3.3.1 Literature review	33
3.4 Description of the gating circuit	38
3.5 The multiplication process	42
3.6 Experimental results	49
3.7 Saturation effect	57
3.7.1 The DC mode	57
3.7.2 The pulsed mode	65
3.8 Conclusion	75

		<u>PAGE</u>
CHAPTER 4	TIME DEPENDENCE OF INTENSE LIGHT PULSE	77
	4.1 Introduction	77
	4.1.1 Literature review	78
	4.2 Theory of gain in Rhodamine 6G	80
	4.2.1 The computer program: DYGAIN	88
	4.3 Experimental	91
	4.3.1 Gain measurements in a dye amplifier	91
	4.3.2 Problems and discussion	92
	4.4 Time dependent spectrum of ASE	95
	4.5 Discussion and conclusion	110
CHAPTER 5	CONCLUSION	112
APPENDIX A	A NANOSECOND LIGHT PULSER	115
APPENDIX B	PULSE TRANSFORMER FOR USE AS A NANO-SECOND PULSE INVERTER	119
REFERENCES		124

LIST OF FIGURES

<u>FIGURE</u>		<u>PAGE</u>
2-1	The gating switch	6
2-2a	The speed-up circuit	9
2-2b	Current and voltage waveforms for the speed-up circuit	9
2-3	Pulse in a reverse biased junction	11
2-4	Heating of the transistors junctions	17
2-5	First multiple gate design	19
2-6	Second multiple gate design	22
2-7	Generation of high frequency pulses	25
3-1a	Gated photomultiplier with dynode D1 pulsed	36
3-1b	Gated photomultiplier with whole resistive chain pulsed	36
3-1c	Gated photomultiplier with dynodes D10 and D11 pulsed	36
3-2	First gated photomultiplier circuit	39
3-3	Gain Variations for photomultiplier type RCA 6199 and type HTV R212UH when dynode D6 is pulsed	45
3-4	Gain variation for photomultiplier type RCA 6199 when two dynodes, D4 and D6, are pulsed	47
3-5	Gain variation for photomultiplier type RCA 6199 when three dynodes D2, D4 and D6 are pulsed	48
3-6	Gain variation for photomultiplier type RCA 6199 when dynode D3 is pulsed	50
3-7	Second gated photomultiplier circuit	53

<u>FIGURE</u>		<u>PAGE</u>
3-8	Third gated photomultiplier circuit	56
3-9	Divergence (D) from linearity for photomultiplier type RCA 6199 operating at 600V in the dc mode	60
3-10	Divergence (D) from linearity for photomultiplier type HTV R212UH operating at 800V in the dc mode	61
3-11	Divergence (D) from linearity for photomultiplier type RCA 6199 operating at 900V in the dc mode	62
3-12	Divergence (D) from linearity for photomultiplier type HTV R212UH operating at 1000V, pulsed for 600 ns	66
3-13	Divergence (D) from linearity for photomultiplier type HTV R212UH operating at 1000V, pulsed for 8 ns during a 600 ns light pulse	67
3-14	Divergence (D) from linearity for photomultiplier type RCA 6199 operating at 900V, pulsed for 8 ns	69
3-15	Divergence (D) from linearity for photomultiplier type HTV R212UH operating at 900V, pulsed for 8 ns. Last stage resistance is 100 K Ω	70
3-16	Divergence (D) from linearity for photomultiplier type HTV R212UH operating at 900V, pulsed for 8 ns. Last stage resistance is 150 K Ω and last stage capacitance is 0.005 μ F	72
3-17	Divergence (D) from linearity for photomultiplier type HTV R212UH operating at 900V, pulsed for 8 ns. Last stage resistance is 150 K Ω and last stage capacitance is 0.002 μ F	73

<u>FIGURE</u>		<u>PAGE</u>
3-18	Divergence (D) from linearity for photomultiplier type HTV R212UH operating at 900V, pulsed for 8 ns. Last stage resistance is 180 K Ω and last stage capacitance is 0.005 μ F	74
4-1	Energy levels for Rhodamine 6G	81
4-2	Flow chart of computer program DYGAIN	89
4-3	Schematic of the experimental arrangement	96
4-4a	Superposition of pumping pulse and ASE pulse	98
4-4b	Superposition of ASE pulse and sampled output from the gated photomultiplier	98
4-5	ASE spectrum at time 0 ns	99
4-6	ASE spectrum at time 100 ns	100
4-7	ASE spectrum at time 200 ns	101
4-8	ASE spectrum at time 300 ns	102
4-9	ASE spectrum at time 400 ns	103
4-10	ASE spectrum at time 500 ns	104
4-11	ASE spectrum at time 600 ns	105
4-12	ASE spectrum at time 700 ns	105
4-13	Time characteristics of ASE spectra	108
A-1	Circuit for a nanosecond light pulser	116
B-1	A nanosecond pulse transformer	120

CHAPTER 1

INTRODUCTION

Many areas in physics e.g., nuclear physics, molecular physics, and laser physics, use photomultipliers because of their very high sensitivity. Sometimes, desirable weak radiation immediately precedes and/or follows intense radiation pulses. The latter can permanently damage the sensitive components of the photomultiplier or at the very least saturate the detector, which can greatly reduce the sensitivity of the detector for hours or even days. This is a similar phenomenon as occurs when looking directly at the sun. In order to avoid damage, and to maintain high sensitivity, the photomultiplier was gated using a transistorized switch. Thus, the detector is turned on during the measurement period and off during the presence of strong radiation. This must be done reliably and the system must have the capability of gating short time durations. Relatively strong radiation can also be measured by gating the photomultiplier for a very short period (~ 10 ns). This prevents dynode damage while giving improved signal-to-noise ratio (SNR).

Therefore, a gated photomultiplier can either be used to extract very weak radiation separated in time from high

intensity radiation. These measurements can not be performed in normal dc operation of a photomultiplier.

1.1 Outline of the Contents of the Thesis

Approximately half of the research effort involved the design of the high voltage, high repetition rate pulse generator described in Chapter 2. There, the different parts of the circuit are described, the principle of operation is given, and comments are made concerning further improvements to the present circuit.

Chapter 3 is devoted to the gated photomultiplier, which utilizes the pulse generator described in Chapter 2. The basic principles of a photomultiplier are discussed to provide an understanding about the interrelation of its three different parts, namely, the photocathode, the dynodes, and the anode. The gated photomultiplier is described in detail and the physical principles involved are discussed. Finally, an extensive investigation of the gain variations in the dynode chain and of the non-linear behaviour of the anode current complete the work done on the gated photomultiplier.

The fourth chapter of this thesis deals with an experiment involving a dye laser, and is intended to test the capabilities of the gated photomultiplier system described in the previous chapter. A computer program has been written to predict the spectrum of the amplified spontaneous emission (ASE) from the dye laser, as measured by the gated photomultiplier. Chapter 4 also describes problems in implementing

a system to measure the single pass gain using a high-pressure Xe lamp as a probe source.

The last chapter (5) summarizes the overall research.

CHAPTER 2

PULSE GENERATOR FOR PHOTOMULTIPLIER GATING

Several techniques can be employed for pulse generation and for gating a photomultiplier [4-7,11,12]. Some are complex, involving monostable (or bistable) multivibrators. Others are simpler, as efficient, and therefore more attractive.

The best technique for our application employs a generator utilizing pulse forming cables and high speed avalanche switching transistors [4,5,7].

2.1 The Gating Switch

The basic circuit, shown in Fig. 2-2a, utilizes three avalanche transistors (Motorola 2N3725) connected in series, which act as a very fast switch. This configuration greatly improves the risetime and the amplitude of the generated pulse (Fig. 2-2b).

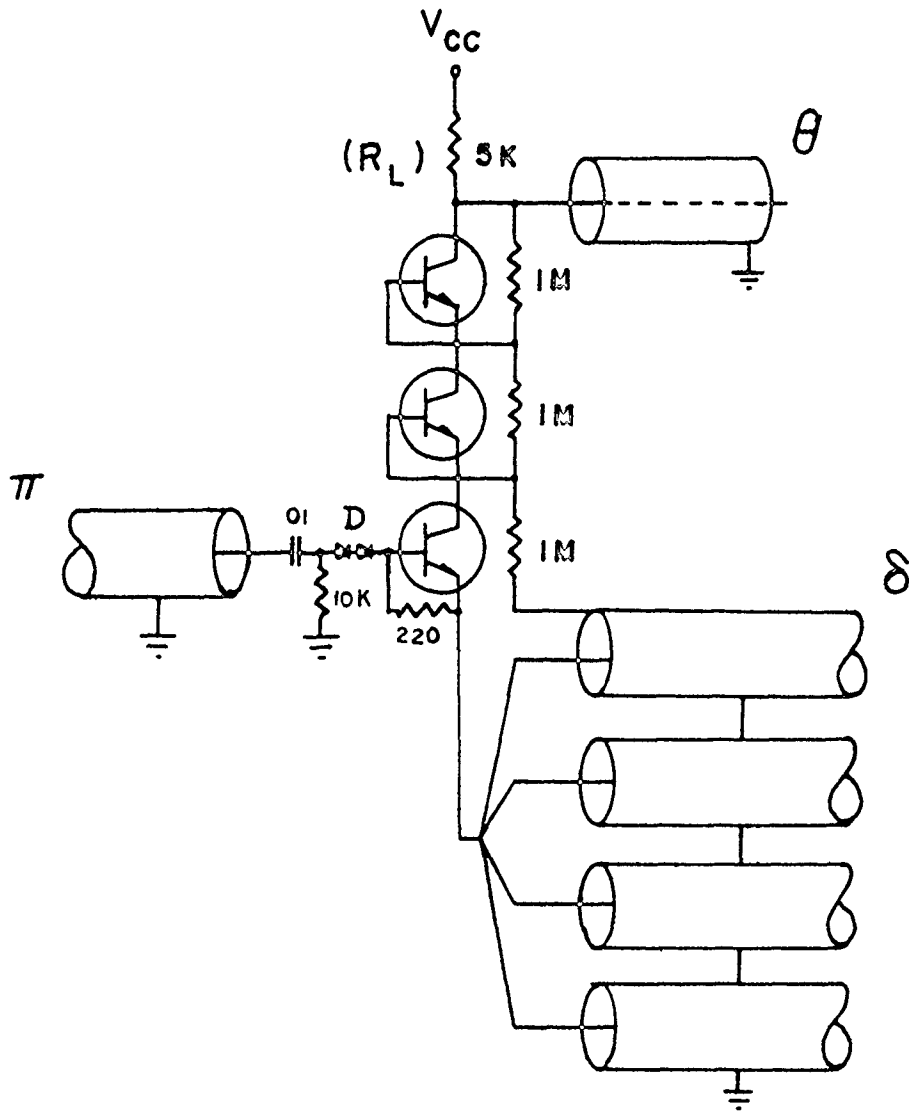
Several transistors, in series, are needed to increase the working voltage applied between the top and the bottom of the switch. There exist single transistors that can tolerate the voltage but, as a rule, a higher breakdown voltage means a longer turn-on and turn-off time. This is undesirable because it affects the performance of the switch. For example, the risetimes of transistors 2N3725 and 2N3109

are the same. However, the highest attainable repetition rate with the 2N3725 is 1.25 MHz when $BV_{CES} \sim 80V$ (breakdown voltage with emitter and base shorted together), and only 100 KHz with 2N3109 at $BV_{CES} \sim 120V$.

A high positive voltage ($\sim 350V$) is applied through R_L to the collector of the top transistor and to the coaxial cable (charging cable). The resistors across each transistor form a potential divider which provides the same voltage across each transistor. It is necessary that these resistors have a high impedance compared with the charging resistor (R_L) to ensure that most of the potential drop appears across the transistors. The emitter of the bottom transistor is connected to the delay cables. These delay cables feed the pulses into the photomultiplier (see next chapter).

The trigger circuit, in Fig. 2-1, brings the pulse from a standard pulse generator (20V into 50Ω) into the base of the bottom transistor. The resistor across the base-emitter junction forward biases this junction when a pulse is applied to the base, and turns on the transistors. The diodes protect the pulse generator from high voltage transients coming from the emitter when the transistors switch. The coupling between the pulse generator and the gate employs a capacitor, and a resistor, connected to ground. This differentiating circuit provides the pulse spike needed to trigger the switch, and to recover the switching network quickly.

Fig. 2-1 The gating switch. The components are the charging cable (RG58A/U) θ , the delay cables δ (RG62/U), the transistors (2N3725), the diodes D (1N4148). The voltage applied to the switch (V_{cc}) is +320V or less. The trigger pulse comes from a standard pulse generator π (20V, 50 Ω).



2.1.1 The Transistors

The choice of avalanche (fast switching) transistors is governed by:

- 1) very fast risetime and fall time (to generate rectangular pulses).
- 2) high breakdown voltage (to generate high voltage pulses).
- 3) short storage time and delay time (to achieve a high repetition rate)
- 4) good power dissipation factor (for high duty cycle).

We tested transistors types 2N3725, 2N3109, 2N3019 and 2N704. The only transistor capable of meeting all of the above criteria is the 2N3725. Its characteristics include a risetime and a fall time of 1 ns, a total switching time (turn-on and turn-off) of 90 ns, and a second breakdown voltage of $\sim 160V$. The second breakdown voltage is the maximum potential drop that can be sustained by the transistor without damage - the first breakdown is the avalanche process.

It is not the purpose of this thesis to fully discuss the theory of transistor switching. The interested reader is referred to references [12-14]. Two important factors, the risetime and the achievable repetition rate, are discussed in the following sections.

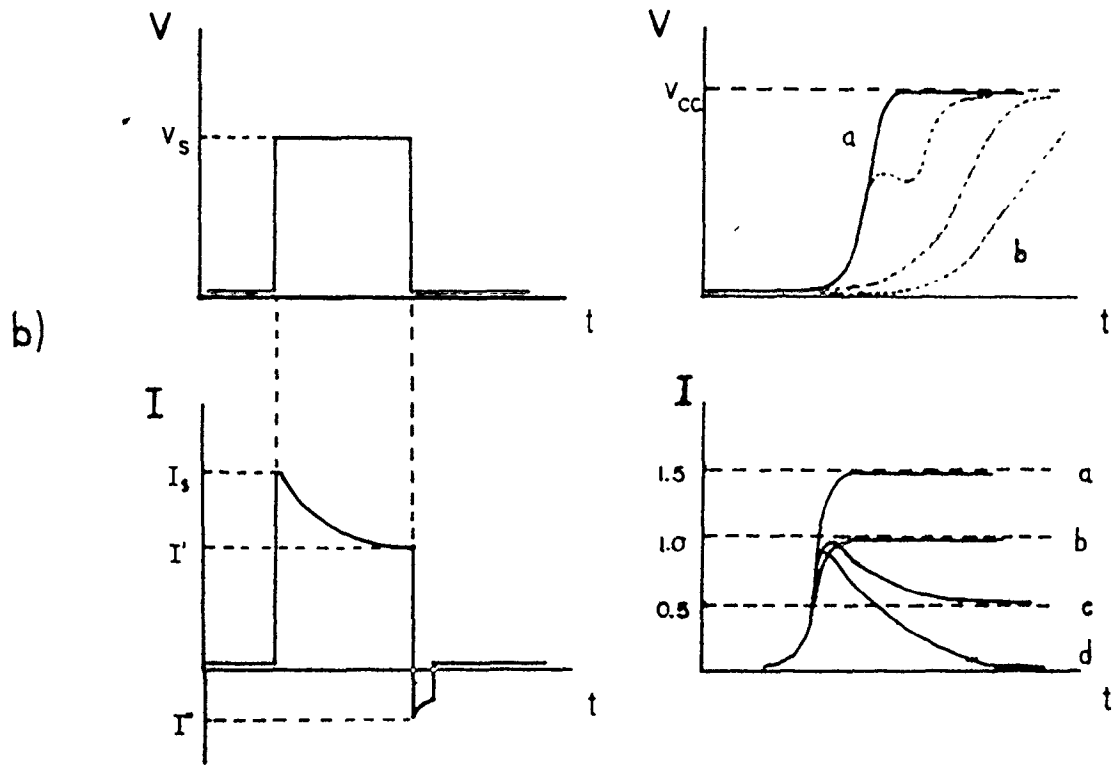
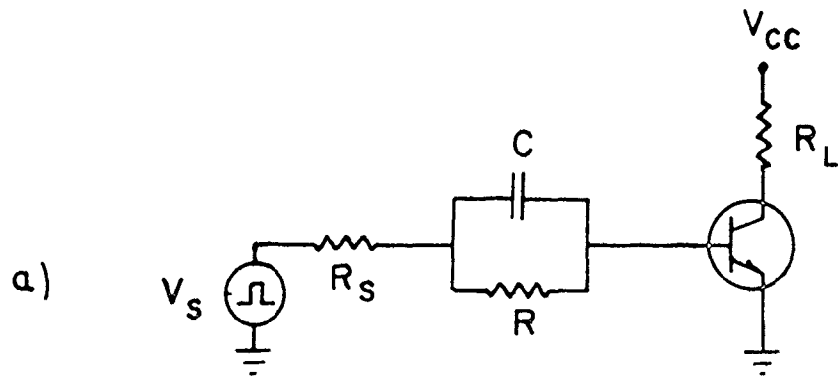
2.1.2 Speed-Up Circuit

One way of reducing the risetime is to use a speed-up capacitor [13,15] as shown in Fig. 2-2a. During the transient stage, i.e. when a fast pulse arrives from a standard pulse generator, the capacitor C acts like a short-circuit and the parallel resistor R acts like an open-circuit. As soon as C is charged, the impedance becomes large compared to R. The latter then limits the current injected into the base of the transistor. The effect on the transistor is a much reduced storage of holes at the base-emitter junction. Consequently, the transistor is less strongly driven into saturation. Thus, a speed-up circuit gives a high turn-on current (faster risetime), together with less storage of holes, resulting in shorter storage time and faster fall time. Fig. 2-2b illustrates the effect of C on the risetime and the effect of R on the shape of the pulses [15]. The determination of proper values for R and C requires experimentation because there are no straightforward analytic methods readily applicable. The optimum values depend on the input capacitance, the input resistance, and the bandwidth product (f_T), which is typically 250 MHz for transistor type 2N 3725. For the usual transistor, it is believed [13] that the optimum resistance is approximately given by

$$R \approx h_{fe} / 2\pi C f_T ,$$

where h_{fe} is the current amplification factor. The optimum C

Fig. 2-2 The speed-up circuit. V_s and R_s are the voltage and impedance, respectively 20V and 50Ω , of the standard pulse generator; I_s is the corresponding current. V_{CC} is the voltage applied to the switch, C and R are the capacitive and resistive components of the speed-up circuit. The time scale is arbitrary, but ~ 15 ns is typical for the standard generator pulse width. The voltage scale is arbitrary, V_{CC} depends on the transistor type used.



is approximately

$$C = Q_T/V,$$

where V is the voltage applied to the junction (base-emitter) and Q_T the total charge stored in the base. A range of values for R and C were tested but were not able to improve the risetime significantly. This may result from the fact that the capacitance and impedance of the base-emitter junction of an avalanche transistor vary greatly with time under pulse conditions. It is clear that further work is required to achieve significant reduction of the risetime.

2.1.3 The Reverse Biased Junction

The risetime of the switch may be improved by reverse biasing the base-emitter junction, as illustrated by the waveforms in Fig. 2-3. When reverse biased, no large accumulation of charges remain at the base-emitter junction. If a large positive current is injected into the base, the collector current (I_C) starts to increase exponentially. The maximum value attainable for I_C is either determined by

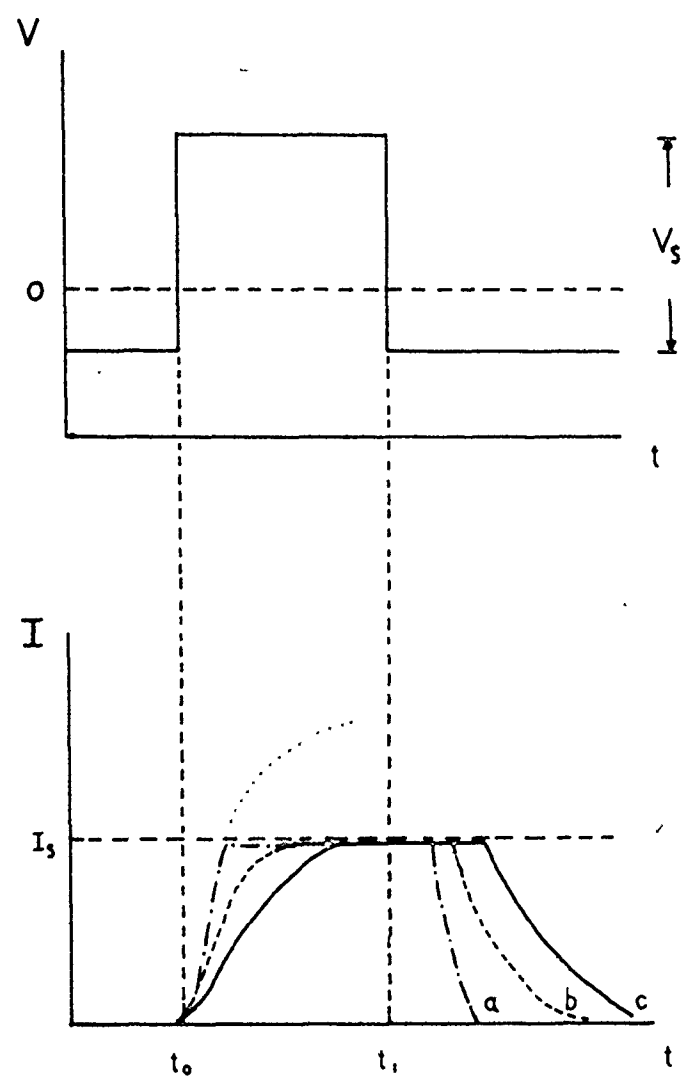
$$I_C = \beta I_B,$$

where I_B is the base current and β , the current amplification factor, is ~ 60 (for transistor type 2N3725), or I_C is limited by the charging resistor,

$$I_C = V_{CC}/R_L,$$

where V_{CC} is the voltage across the switch. Three different

Fig. 2-3 Pulse in a reverse biased junction. V_s is the amplitude of the voltage pulse coming from the standard pulse generator. t_0 is the time related to the leading edge and t_1 is related to the trailing edge. Typically, $t_1 - t_0 \sim 15$ ns, and I_s , the maximum collector current, is ~ 100 mA.



situations are depicted in Fig. 2-3,

- 1) $\beta I_B \gg I_S$: the base is over-driven and strongly reverse biased.
- 2) $\beta I_B > I_S$: the base is fully-driven and moderately reverse biased.
- 3) $\beta I_B \lesssim I_S$: the base is under-driven and not reverse biased.

Here I_S is the maximum value of I_C .

From Fig. 2-3, the best performance is achieved in the over-driven case when the base is strongly reverse biased (case (1)). Regretfully, this situation could not be reached, in our experiment owing to the limits imposed by the maximum output available from the pulse generator used. A reverse biased voltage, approximately 5V corresponding to case (2), has been applied to a single transistor used as a switch. In this case, the risetime was improved by 10%. Therefore, it is demonstrated that this technique can be used successfully to improve the risetime of the switch.

2.1.4 More About the Transistors

With ordinary transistors, the risetime is proportional to

$$D = 1 + \alpha \omega_T R_L C_C ,$$

where $\alpha \sim 1$, ω_T is $2\pi f_T$ and C_C is the collector input capacitance (~ 50 pf). The only parameter that can be easily varied

is the value of the charging resistor (R_L). It was found that the lowest resistance possible is $4.7 \text{ K}\Omega$ (for R_L). A smaller value allows too large collector current to pass and the transistors behave improperly, i.e., either they switch randomly or the switch simply remains closed.

The fastest risetime and the highest repetition rate (for the switch) are expected for $D \sim 1$. That is why D usually provides a good estimate of the deterioration of the high speed performance of a transistor. Thus, one can see that a value of $D \sim 400$, obtained with $R_L \sim 4.7 \text{ K}\Omega$ and $f_T \sim 250 \text{ MHz}$, implies that the high speed performance could be improved. Different values for R_L , between $1 \text{ M}\Omega$ and $4.7 \text{ K}\Omega$, were tested with no significant ($\sim 20\%$) effect on the risetime of the switch. This shows that the factor D does not describe the behaviour of avalanche transistors as well as ordinary transistors, but is still an appropriate reference for high speed performance. This also shows that the only adjustable parameter (R_L) cannot be used to significantly improve high speed performance.

It should be noted that the fastest response time, together with the lowest leakage current, occur when the base and the emitter are shorted together, i.e. in the common-emitter configuration [13]. For the circuit in Fig. 2-1, the risetime was 2 ns , as measured with an oscilloscope. Using the approximate relation,

$$2ns \approx \sqrt{t_s^2 + 3t_t^2},$$

where t_s is the oscilloscope risetime (Tektronix 7834) and t_t the transistor risetime (type 2N3725). For $t_s = 1$ ns,

$$t_t \approx \sqrt{(4 - t_s^2)/3} = 1 \text{ ns.}$$

This indicates that the risetime of an individual transistor is, at best, 1 ns, and that the best risetime of the gating pulse (for the photomultiplier) is

$$\sqrt{3} t_t \approx 1.7 \text{ ns.}$$

2.2 The Transmission Lines

The time needed to charge the charging cable to the power supply voltage, through the charging resistor (R_L in Fig. 2.1), is approximately given by the $R_L C$ time constant. The charging cables and delay cables consist of standard coaxial cables. The capacitance of these cables is typically 80 pf/m. The charging time has to be reduced below 100 ns to achieve a very high repetition rate (≥ 10 MHz). Araki et al. [7] state a repetition rate of 100 KHz (period of 10 μ s) which is limited by the $R_L C$ of their charging cables.

R_L can be varied, but not C because it depends on the length of coaxial cable used, which is determined by the fixed width of the gating pulse. As mentioned before, the

minimum safe resistance for R_L is $4.7 \text{ K}\Omega$, resulting in a charging time of $\sim 400 \text{ ns}$. This is one step toward the 10 MHz region.

7
Whilst the transistors are switching, the collector of the top transistor is short-circuited to the emitter of the bottom transistor. This implies that the charging cable, in Fig. 2-1, is directly connected to the delay cables. If the impedances of the parallel delay cables and the charging cable are matched, two voltage waves of equal amplitudes and opposite polarities, travelling in opposite directions, are created in the charging cable as soon as the switch is closed. Only one is fed into the delay lines. The voltage falls to zero (end of the pulse) when the second wave returns, after reflection from the open end, to the connected end of the charging cable. Thus the delay lines carry a voltage pulse of amplitude equal to half the voltage applied to the charging cable, and of width determined by the round-trip time in the charging cable. In general, the delay time in a coaxial cable is approximately 4.6 ns/m . In our circuit, a charging cable 0.75 m long produced a pulse width of 8 ns .

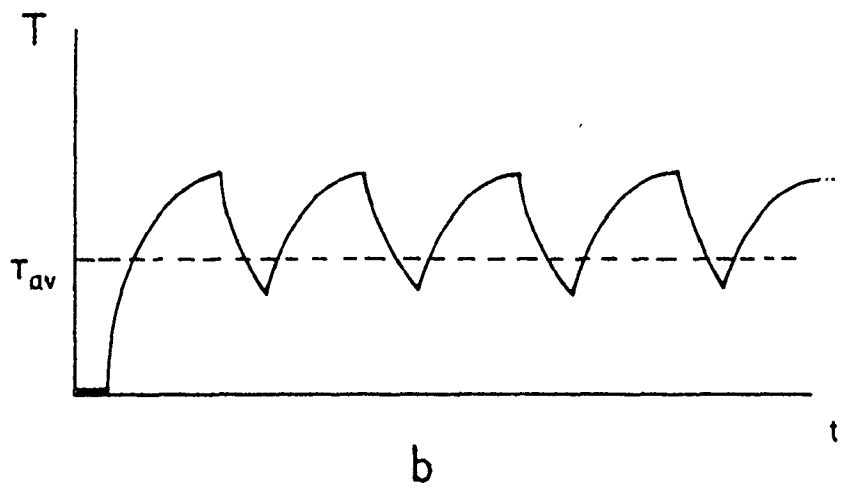
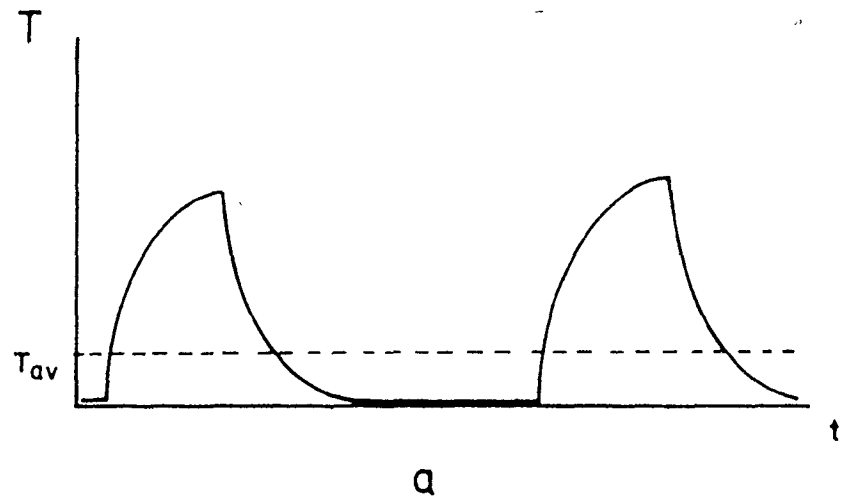
What happens if the impedance of the two sets of cables are not matched? In such a case, which is closer to reality, the amplitude of the signal, sent down the delay lines, is decreased and reflections appear. For example, consider the case where the charging cable has an impedance of

50 Ω (RG58A/U) and the delay lines have an impedance of 93 Ω (RG62/U). The pulse has to travel from a medium with a 50 Ω impedance into a medium with a 23.25 Ω impedance (4 cables in parallel). Only 63% of the "matched" pulse amplitude is transmitted into the delay cables. The reflections have one third of the main pulse amplitude (21%), and are negative. It is shown in the next chapter why these reflections are necessary. The impedance can easily be matched by using two charging cables connected in parallel. However, the capacitance is increased, the charging time is longer and the repetition rate lower, and this consequently, is undesirable.

The duty cycle is very important. At a 100 KHz pulse rate, the transistors get very hot, and this causes a degradation of performance, i.e. the amplitude of the pulses decreases, and random switching is observed. Even if a high repetition rate (1 MHz) is allowed for only a short period of time ($\sim 30 \mu\text{s}$) when the pulse width is $\sim 10 \text{ ns}$, the same effect is observed. If the time between two pulses is shorter than the time constant of the thermal dissipation, then a net heating is observed (Fig. 2-4). Therefore, the highest repetition rate attainable is either limited by the charging time constant ($R_L C$) or by the temperature increase due to the duty cycle. For transistors type 2N3725, these two effects occur at about the same frequency ($\sim 1.25 \text{ MHz}$) for

Fig. 2-4 Heating of the transistors junctions.

T is the temperature (arbitrary units), and T_{AV} represents the range temperature related to a particular duty cycle. In (a) the duty cycle is longer than the thermal dissipation time ($\sim 1 \mu s$). In (b) the duty cycle is shorter than the thermal dissipation time resulting in a higher T_{AV} .



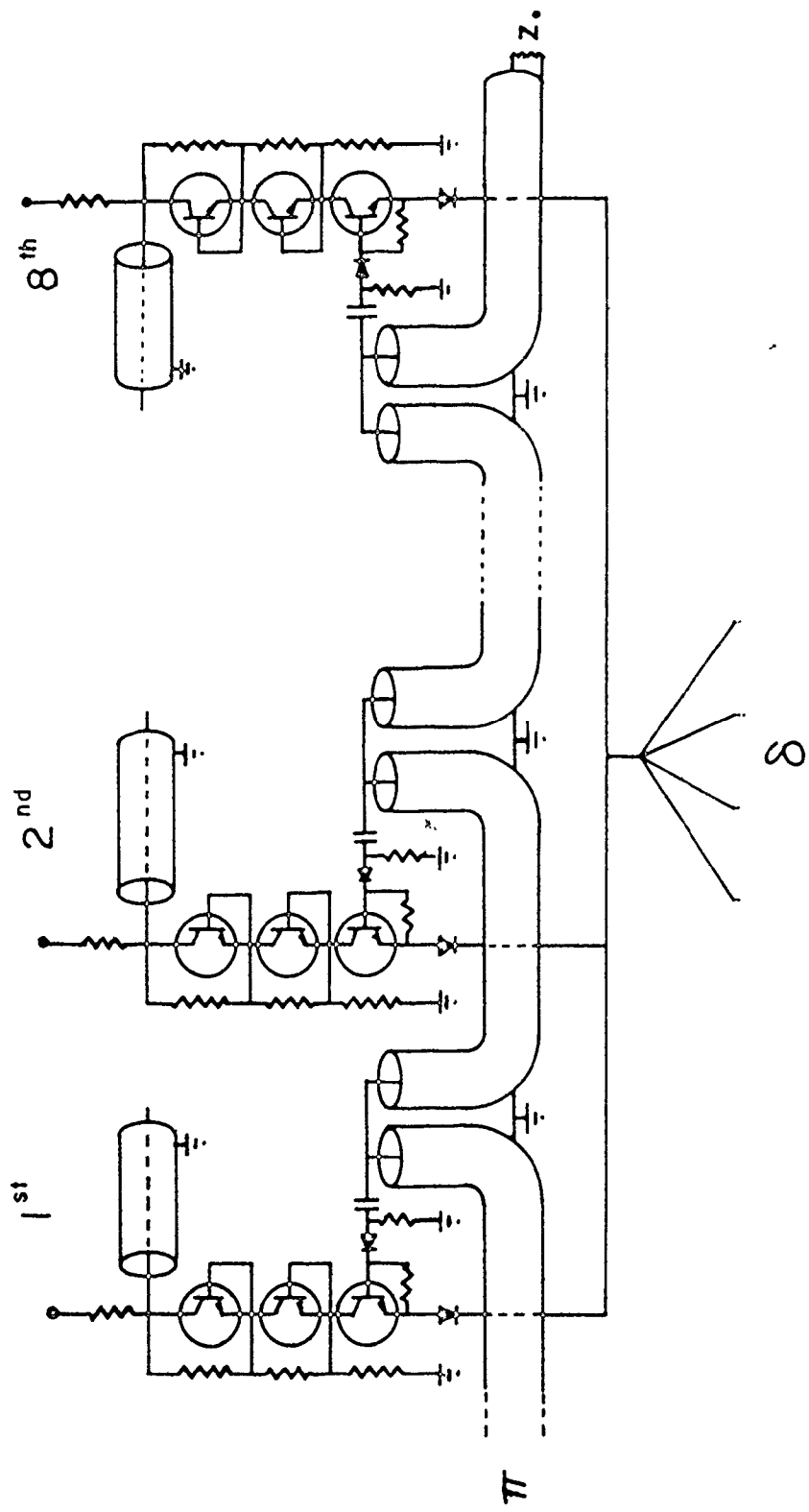
pulse width of ~ 10 ns. However, the temperature effect is the first to appear. This emphasizes the importance of a high power dissipation capability for any transistors used.

2.3 Multiple Gates

Approximately 100 ns is required between pulses in order to achieve a desirable sampling rate of 10 MHz (see next chapter). However, the circuit in Fig. 2-1 is limited to a repetition rate of about 0.4 MHz. The solution is to build eight gates and to switch them in sequence into the delay lines, with a delay of 100 ns between consecutive pulses. When the eighth gate has switched, the cycle is started again. Since each gate operates at 0.4 MHz with a 100 ns delay between subsequent gates, the effective repetition rate is 10 MHz.

In principle, this solution looks simple, but there are some serious subjacent difficulties. One would prefer to isolate each gate from the others, due to the high voltage transients (~ 100 V) present when a gate is switched. However, in order to drive all the gates with the same pulse generator, and to feed all the pulses into the same photomultiplier the gates must inevitably be connected together. Much effort was spent to provide at least some isolation of the gates shown in Fig. 2-5. When the circuit was constructed, only six of the eight gates would switch properly. The main problem comes from the driving circuit, i.e. the pulse from

Fig. 2-5 First multiple gate design. Same basic circuit as in Fig. 2-1. The driving circuits of each gate are connected by a coaxial cable 20 m long (RG58A/U) inducing a delay of 100 ns. Two diodes (type 1N4148) are introduced in series with the emitters of the bottom transistors. A total of eight gates are connected in parallel.



the pulse generator loses too much amplitude whilst traveling down the 139 m. long coaxial cable that distributes sequentially the triggering pulse to each gate. At least two synchronized pulse generators would be required to accomplish this task properly. Moreover, each of the eighteen transistors involved did not have exactly the same breakdown voltage. This situation resulted in a variation as large as 5% in the amplitude of the pulses generated from different gates.

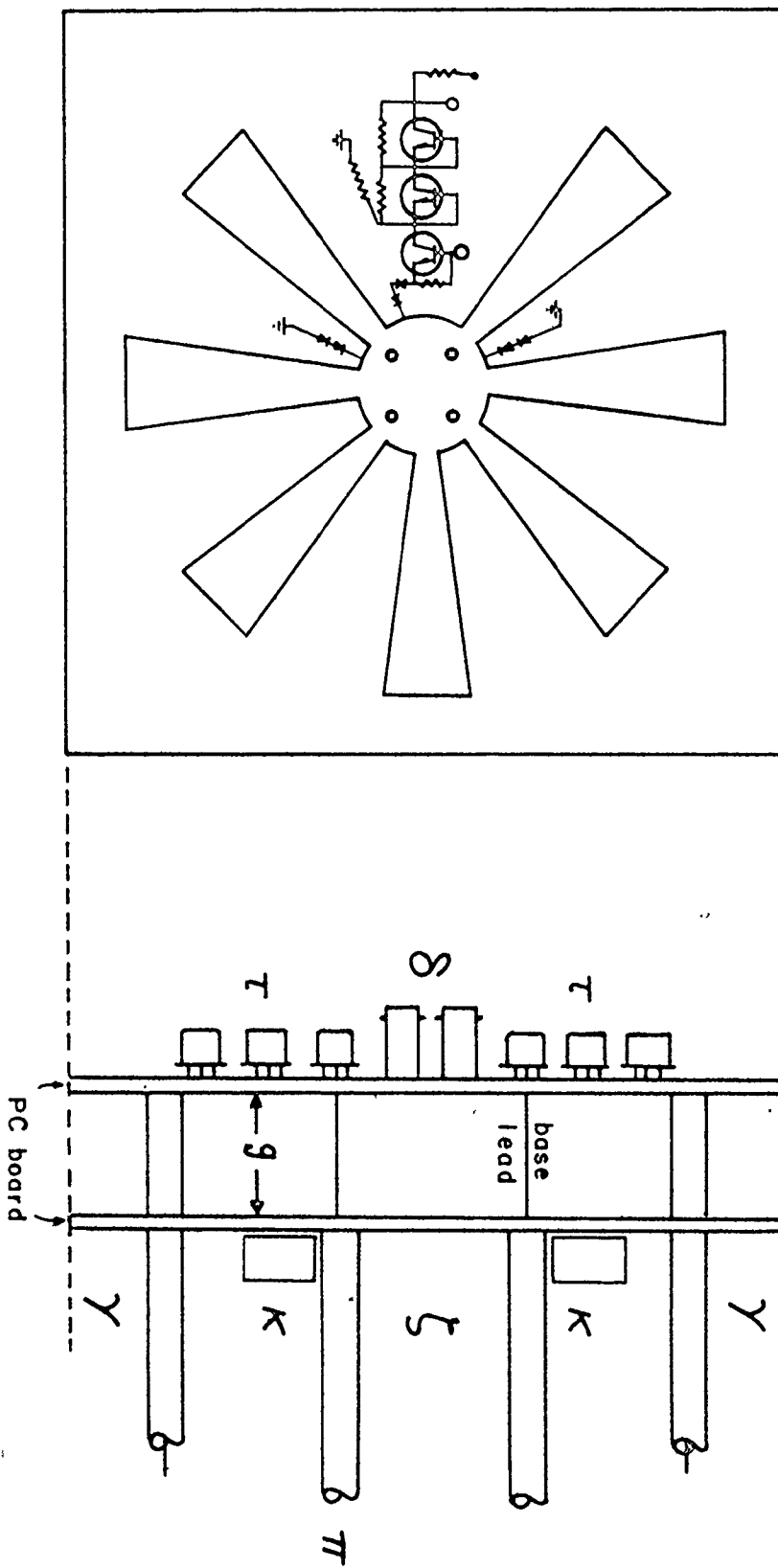
The first design that was attempted consisted of four lengths (20 m each) of RG58A/U coaxial cable (delay of 100 ns) to distribute the driving pulse to each of eight gates. Only four cables are needed when used together with pulse inverters. All the gates were in-line on a PC (printed circuit) board, similar to the circuit in Fig. 2-5. The distance between the first and eighth gate was 18 cm. This meant a lead length of about 8 cm from the gates at the extremities to the input of the delay cables. The inductance introduced by the leads caused a reshaping of the pulse, i.e. a longer risetime. In addition, all the gates employed a common ground, which caused serious problems due to the high transients generated in the ground (mainly from the charging cables). These transients were present almost everywhere in the gating circuit, and caused all the gates to switch either at the same time or randomly. It was found that this multi-

gating circuit would work properly if the base-emitter junctions of all the bottom transistors are free of any transients higher than $\sim 10V$. This specifies how well each gate must be isolated from its neighbours.

The second design, shown in Fig. 2-6, performed better than the first design. The gates were located radially in a circular configuration. The distance between the emitter of the bottom transistor and the input to the delay lines was about 1 cm, providing a low inductance. The inductance of the circuit was further reduced by soldering the transistors (short leads) directly to the PC board. The driving circuit was built on a second PC board (double-sided) so as to introduce a grounded copper sheet between the PC board with the transistors, and the PC board comprising the driving circuit. Therefore most of the electromagnetic field, originating from the transistors and acting on the driving circuit, would be shielded. Each gate had its own ground so that transients generated in the ground could not travel across the circuit. In the driving circuit, the gates were temporally isolated using a coaxial cable (20 m, delay of 100 ns).

Fast-recovery diodes type 1N4148, 1N4151, 1N904 and MBD101 were tested for use in blocking transients. Only the type 1N4148 had a reverse recovery time less than 2 ns, and it therefore was used in the circuit. Two diodes are needed

Fig. 2-6 Second multiple gate design. Same basic circuit as in Fig. 2-1. The gates are located radially in a circular configuration. Grounded copper sheets are provided for shielding and two diodes (type 1N4148) connected between the input to the delay cables and the ground eliminate the negative transient pulses. The delay lines (δ), the transistors (τ) and the charging cables (γ) are on one PC board. The triggering circuit (K), the delay cable (ζ) and the input cable (π) are on a second PC board. The grounded planes are indicated by g.



to the base of each bottom transistor, Fig. 2-1, to isolate the driving circuit from the transistors. Two other diodes are required between the emitters of the bottom transistors and the input to the delay cables in order to block the positive transients. Finally two more diodes must be connected between ground and the input to the delay cables in order to eliminate the negative transients, Fig. 2-6.

With the above arrangement, the multiple gates system worked properly. The only problem came from the resistors across the base-emitter junctions of the bottom transistors. These resistors acted like a potential divider with the terminating resistors of the delay cables, and, moreover, they are seen in parallel with the driving coaxial cables resulting in an unmatched impedance. Consequently, the fifth gate saw only 58% of the main driving pulse, of which only 29% appears across the base-emitter junction, because of the potential divider arrangement of the resistors. Below 45% of the amplitude of the driving pulse, a gate could not be turned on.

It was mentioned earlier in this chapter that the highest repetition rate attainable with a single gate was 0.4 MHz. Each gate generates pulses at this rate. When six gates were operated sequentially, with a delay of 400 ns between each one, a rate of 2.5 MHz could be achieved. When the delay is reduced to 100 ns between each gate, a burst

of six pulses was produced at an effective rate of 10 MHz, repeatable every 2.5 μ s. The highest repetition rate attainable for six consecutive pulses was 100 MHz. If several pulse generators are used to drive several multiple gates systems, very high repetition rate would be possible for more than six consecutive pulses.

Two standard pulse generators are used to operate the multiple gate, as shown schematically in Fig. 2-7. The main-pulse generator, used also for timing the flashlamp of the dye laser (see chapter 4), producing pulses 50 μ s long at a repetition rate of 1 KHz, is used to gate the second pulse generator. The second pulse generator generates pulses (20V, 15 ns) at a repetition rate of 0.4 MHz within the gating period. This arrangement reduces the duty cycle of the transistors. The pulse burst triggers the multiple gate, and this results in the generation of pulses of \sim 75V (8 ns) at a rate of 10 MHz.

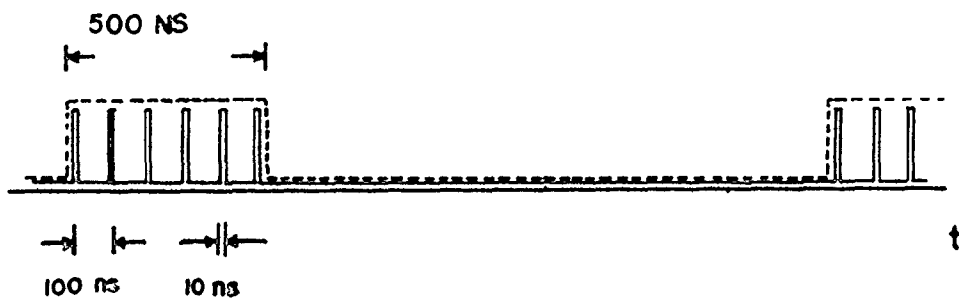
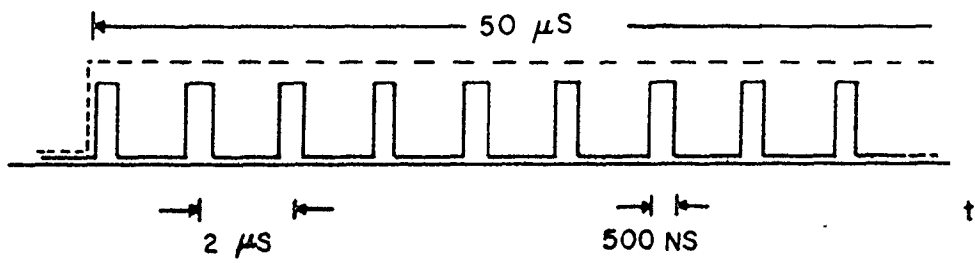
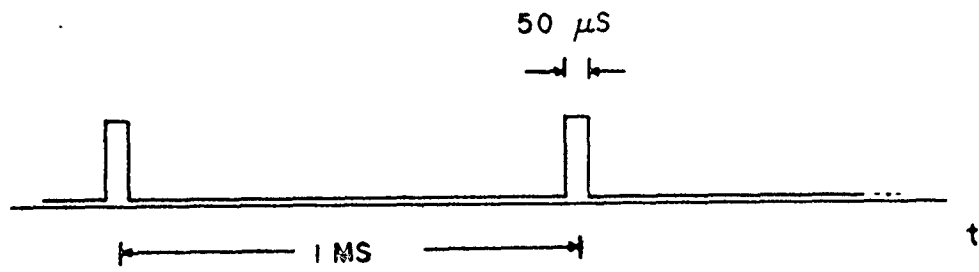
2.4 Conclusion

Pulses with amplitudes ranging between 0V and 220V were generated with a risetime and falltime of 2 ns. The maximum of 220V was obtained with four transistors and two parallel charging cables. The width of the pulses was adjustable with an accuracy of 0.2 ns from 4 ns (minimum due to circuit risetime). The repetition rate was up to 100 MHz for



Fig. 2-7 Generation of high frequency pulses.

In (a), the pulses are from the main pulse generator. In (b), the dashed line represents the pulses in (a) and the solid line represents the pulses from the second pulse generator. In (c), the dashed line represents the pulses drawn in the solid line in (b). The timing pulses, in solid line, are produced by the multiple gate.



six consecutive pulses every 2.5 μ s. The complete system was used to successfully gate a photomultiplier (see next chapter).

The work indicates that many improvements can still be made to the system, especially in the driving circuit. Here, multiplexing looks like more promising technique to introduce a delay between the gates than the coaxial cable technique.

CHAPTER 3

THE GATED PHOTOMULTIPLIER

3.1 Introduction

A photomultiplier is chiefly a radiation (light) detector. Photomultipliers are capable of detecting extremely low light level because of their built-in wideband high gain amplifier. They also have a good response time, typically 3 ns, which provides a good resolution in time for many experiments in physics and chemistry. Photomultipliers work mainly in the ultraviolet and the visible part of the spectrum, and consequently cover a wide range of laser wavelengths. The gated photomultiplier is intended to work under strong radiation intensity. Such situations very often occur when a laser is involved.

The above features justify the use of a photomultiplier as the signal detector in the system described in this thesis. This is followed by a literature review, a description of the circuitry, and experimental results.

3.2 The Basic Principles

Mainly, a photomultiplier can be divided into three parts characterized by their particular functions,

- 1) the photocathode: light detection,

- 2) the dynode chain: wideband high gain amplifier,
- 3) the anode: signal output.

3.2.1 The Photocathode

The photocathodes are generally divided into two groups: opaque and metallic or the semi-transparent semi-conductor type. The most sensitive photocathodes belong to the second group, which is the main concern of this thesis. These photocathodes are formed by a thin layer of semi-conducting material deposited on the inside surface of a window. A photon impinging on such a window has a probability, given by the quantum efficiency of the particular semi-conducting material ($\sim 10\%$), to release an electron. The energy of the emitted electron is determined by Einstein's equation,

$$E = h\nu - \phi,$$

where ϕ is the work function of the semi-conducting material. The purpose of the photocathode is then to convert the photon flux into an electron flux (electrical current). Unfortunately, electrons can be emitted from the photocathode even if no photons fall on it (complete darkness). That phenomenon is called thermionic emission. It produces a "dark current" proportional to the area of the photocathode and is a function of the temperature. The total photocathode dark current is the minimum detectable current (signal to noise ratio equal to ~ 1):

$$i_d = jA + i' ,$$

where i_d is the total dark current, j is the thermionic current, A is the photocathode area and i' is the total of all other sources of current such as leakage current caused by a poor insulation, and ionization and bombardment from stray electrons. Usually i' is minimized by geometrical considerations. Typically, i_d is not larger than a few femtoamperes (10^{-15} A) at the photocathode, corresponding to an equivalent power (light signal) of $\sim 10^{-13}$ W. A typical photocathode radiant sensitivity (S-11 phosphor) is ~ 36 mA/W.

An electrode is provided to guide and to focus the emitted electrons into the second part of the photomultiplier in order to ensure the efficient collection of most of the electrons. For the same reasons, i.e., to minimize the losses, this region, as well as the other parts of the photomultiplier, is under a very high vacuum.

3.2.2 The Dynode Chain


The very small current coming from the photocathode must be amplified. The second part of the photomultiplier consists of several amplification stages in series. The number of stages (dynodes) varies between six and sixteen. These stages provide an amplification factor, ranging between 10^4 to 10^8 , for the original current coming from the photocathode. The multiplication process occurring at each dynode will be

described later in this chapter. Essentially, one electron impinges on a dynode, which is a secondary emission electrode, and several electrons are then emitted. A potential drop must be applied between successive dynodes (e.g., by means of a resistor chain (potential divider)) to provide an electric field that accelerates and focusses the electrons from dynode to dynode. Because of their good emission properties, the dynodes can be easily damaged if the DC current reaches too high a level (~ 1 mA, corresponding to a power of 10^{-7} W falling on the photocathode). This is one of the reasons why the photomultiplier has to be gated in some situations. In the gated mode, high current is allowed only for a few (~ 8 ns) nanoseconds. Because of the short period of time involved, the damage level can be raised by a factor of ~ 100 , i.e., the current can reach values of ~ 100 mA for a few nanoseconds.

After the last amplification stage, all the electrons are focussed on a collector electrode (anode), the third part of the photomultiplier.

3.2.3 The Anode

This electrode (anode) has a special bowl shape to make sure all the electrons are collected. A grid, located between the last dynode and the anode, screens the inductive effect caused by the electrons travelling toward the anode. This is very important for increasing the time resolution, i.e., for reducing the risetime of the signal at the anode. The anode



should be protected against any other sources of electrons, against ground loops and capacitive effects with the dynodes. Because the anode is usually so isolated, it is easy to match it into high impedance devices.

The highest current in the photomultiplier occurs between the last dynode and the anode. When this current reaches a high level (close to 1 mA) the space charge density becomes very large and screens the potential drop in this region. Therefore, the electrons emitted from the last dynode see a smaller potential drop. The effect is that the output current at the anode no longer follows a linear relationship with the power incident on the photocathode. The output current is, in fact, lower than expected. The photomultiplier is said to saturate when it starts to behave non-linearly. This is the second reason why a photomultiplier must be gated when dealing with strong light signals. The shorter the gating time, the less strongly the photomultiplier is driven into saturation.

In summary, photons impinging on the photocathode produce electrons. The small current generated (\sim pA) is amplified by going through successive amplification stages (dynodes). The resulting amplified current (\sim μ A) is measured at the anode. The noise in the system consists of dark current (Richardson noise), and noise from the measuring device or the output load impedance (Johnson noise).

3.3 The Photomultiplier Gating Circuit

To gate or to pulse a photomultiplier means that for a certain period of time, the ability of the detector to "detect" a light signal is impaired to a certain level determined by the cut-off ratio. It also means that the gain of the multiplication stages and/or the collection efficiency at the photocathode is lower than it is during normal operation. Therefore, the photomultiplier can be gated only through an action in its first or second part as outlined above.

The pulsing of photomultipliers has been used in nuclear physics for observation of nuclear phenomena immediately following intense α - or β -radiation. Another class of experiments in physics in which this pulsed photomultiplier proves to be useful is in the application of lasers to molecular and solid-state physics. Here, there is often a need for observing a spontaneous incoherent light scattering process following an intense, coherent molecular or atomic excitation arising from a stimulated process. In these cases, the photomultiplier is gated off during the intense radiation pulse, and gated on just before, or just after the pulse. In the experiment described in this thesis, the photomultiplier is gated on during the intense radiation consisting of spontaneous emission from a laser amplifier.

A very large cut-off efficiency is required in order to protect the photomultiplier against dynode damage, or tem-

porary loss of linearity in the output current. It is then necessary, not only to shut off the detector during the high intensity photon flux, but also to switch it back to normal working conditions in a very short time. The cut-off ratio is defined as the ratio of the maximum gain value (in normal operation) to the minimum gain value in the gated (off) state.

3.3.1 Literature Review

Several methods have been employed or proposed to gate photomultipliers. By pulsing the photocathode [1] with a positive pulse of the order of the first dynode potential (photocathode being grounded), it is possible, in some cases, to block completely the electron flux. In such a case, the potential drop between the photocathode and the first dynode is zero or positive. To restore the normal voltage distribution and thus the maximum gain available, a voltage pulse is externally applied to the photocathode. The claimed cut-off ratio is appreciably large ($\sim 10^4$), but the time needed to reach the full gain is of the order of 30 μ s, however fast the risetime of the gating pulse. The explanation comes from the fact that the very thin layer of semiconductor forming the photocathode behaves like a high impedance transmission line and delays the trailing edge of the gating pulse traveling in it. The only good point with this technique is the large cut-off ratio.

The next step is to gate the first dynode [1,2]. A satisfactory cut-off ratio cannot be obtained owing to the high amplification of the following dynodes. The voltage pulse needed to sufficiently impair (down to 1%) the electron flow is large enough (> 150 V) to introduce sparking between the first and second dynodes. Naturally, this adversely affects the life of the photomultiplier. The gain risetime, i.e., the time needed to go back to the normal gain, is only limited by the risetime of the voltage pulse used to gate on the photomultiplier. The cut-off ratio is low (~ 30), since a minimum value of 1000 is desirable to avoid the previously mentioned effects of intense radiation pulse.

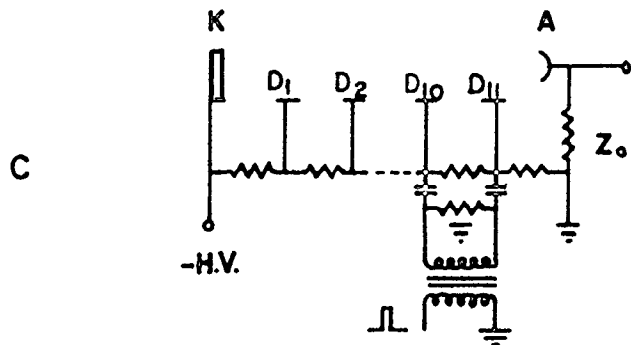
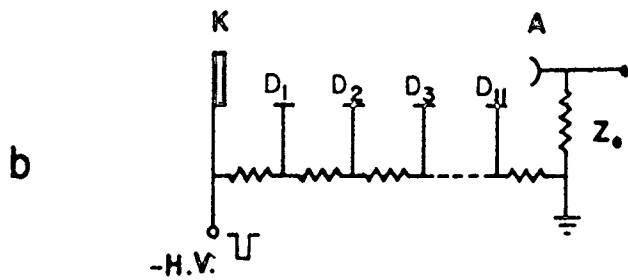
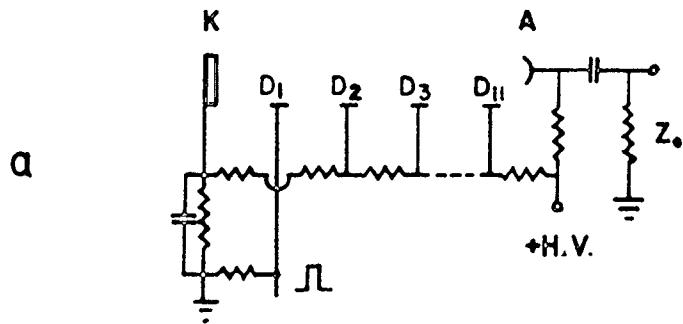
For photomultipliers designed so that the shield or focussing electrode can be gated, the problem is conveniently solved. At sufficiently negative voltages (~ 50 V), usually of the same order as the potential drop relative to the photocathode, this method gives very good results, i.e., low noise, a high cut-off ratio ($\sim 10^4$) and a good risetime which is limited by the risetime of the voltage pulse. Unfortunately, few photomultipliers have that property of allowing us to gate the focussed electrode. Most of them are not suitable for our requirements, i.e., they do not have a high gain ($> 10^6$), a UV window and a low dark current.

In order to achieve a higher cut-off ratio, one would like to gate more than one multiplication stage. Therefore,

a group of dynodes can be pulsed [3]. When the first dynodes are pulsed with respect to the photocathode, as shown in Fig. 3-1a, De Marco et al. [3] found a cut-off ratio of $\sim 10^4$, but with a long gain risetime ($\sim 1.5 \mu\text{s}$). By pulsing the whole resistive chain (Fig. 3-1b), De Marco et al. obtained a very high cut-off ratio with a gain risetime limited only by the gating pulse risetime. Unfortunately, very large spurious signals are present due to the very high voltage of the gating pulse (kilovolt range). This method is undoubtedly unapplicable for our purpose. Finally, the last dynodes can be gated, Fig. 3-1c. At these stages, the current is very large and it is difficult to impair the electron flux. The result is a cut-off ratio of ~ 300 . The gain risetime, for this configuration, is the lowest De Marco et al. could achieve ($\sim 10 \text{ ns}$).

As described in Ref. [4], a transmission line built from inductive ($1.6 \mu\text{H}$) and capacitive (3pF) elements can be constructed to distribute the proper voltage to each dynode when a voltage wave is initiated at its input. The speed of the travelling wave matches the transit time of the electrons between the dynodes. In this way, the photomultiplier is progressively turned on from a state of zero gain to a state of very high gain achieving intrinsically a very good cut-off ratio ($\sim 10^6$) and the best possible time resolution ($\sim 2 \text{ ns}$). However, such a circuit is difficult to calibrate

Fig. 3-1 On all cases, K is the photocathode, HV is the high voltage, A is the anode and Z_0 is the load impedance. (a) Gated photomultiplier with dynode D1 pulsed. (b) Gated photomultiplier with whole resistive chain pulsed. (c) Gated photomultiplier with dynodes D10 and D11 pulsed.



because the transit time is not the same between each dynode. In addition, there is noise due to the travelling voltage wave (few hundred volts).

More recently, the trend is towards the pulsing of isolated dynodes [5,7]. This method does not need the high voltage required with some other techniques, therefore reducing the amplitude of the spurious signals. This method allows a compromise between the advantages and disadvantages of gating dynodes in the early and last multiplication stages. The sequence is usually among dynodes D2, D4, D6 or D8. This method, together with the method employing a transmission line described above, has been applied by Araki et al. [7]. They measured a cut-off ratio of $\sim 10^3$ and a time resolution of 2 ns.

The gated photomultiplier, in this thesis, was part of a system designed to provide data needed to compute the gain of a dye amplifier. The gain exists in the dye solution, when pulsed by a coaxial flashlamp, for a period of ~ 800 ns. Due to the intense spontaneous emission, the photomultiplier must be gated at a very high repetition rate (10 MHz) for very short period of time (~ 10 ns) to sample adequately the 800 ns pulse.

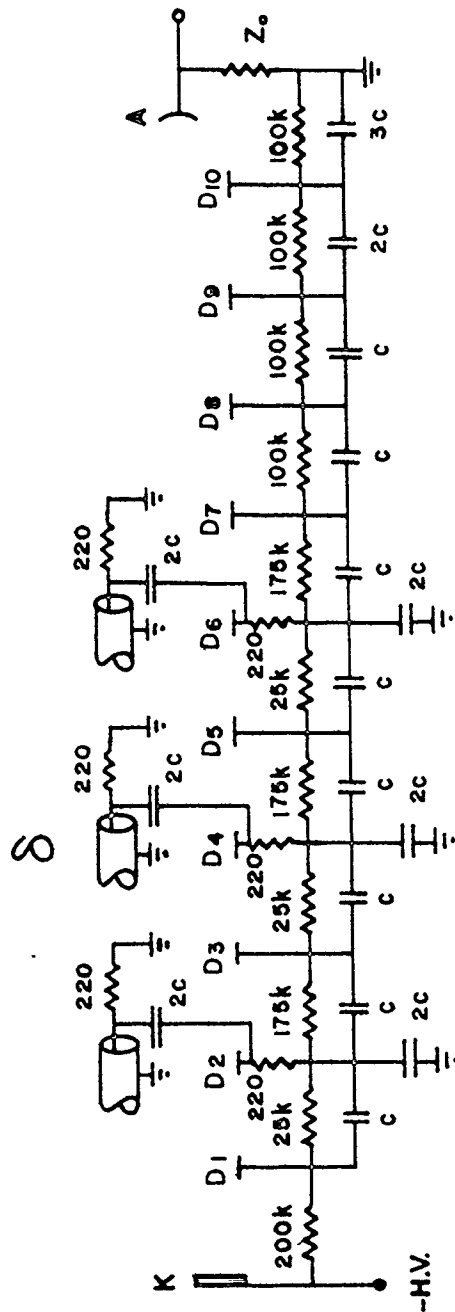
Therefore, a choice must be done among the previously proposed techniques. The most promising one has been published by Araki et al. [7]. The gain risetime (or time resolution) and the cut-off ratio is appropriate for this experiment, but the repetition rate they claimed is only 100 KHz.

3.4 Description of the Gating Circuit

The principle of the first circuit employed (Fig. 3-2) is similar to the transmission line type [4]. A voltage pulse of the proper amplitude, width and risetime is fed to the common input of the delay cables. The way this gating pulse is formed and sent to the dynodes at the desired repetition rate is the subject of the previous chapter. The voltage pulse reaches the output of the delay cables at a particular dynode. The length (delay) of the cables is chosen so that the times of arrival of the pulses at the dynodes match the transit time of the electron between the dynodes. Thus, the principle is the same as the transmission line type except that only some dynodes are gated.

For example, when 1 kV is applied to the photocathode, the normal operation, the total transit times for the two photomultipliers investigated, RCA6199 and HTRV212UH, are 33ns and 24 ns, respectively. This provides a good estimate for the transit time per stage. With the ten stages of photomultiplier RCA6199, (Fig. 3-2), three dynodes are gated D2, D4 and D6. The average transit time between two consecutive gated dynodes, e.g., D2 and D4, was experimentally measured as 7.2 ± 0.5 ns. Consequently, the lengths of delay cables (RG59/U, ~ 4.5 ns/m) were 1 m for D2, 2.6 m for D4 and 4.2 m for D6. When a time resolution of the order of the risetime of the gating pulse is required, the lengths of the cables

Fig. 3-2 First gated photomultiplier circuit. Dynodes D2, D4 and D6 are pulsed. The delay cables δ are RG59/U (75Ω); the capacitance C is $0.001 \mu\text{F}$. K is the photocathode, A is the anode, Z_0 is the load impedance and HV is the high voltage.



must be adjusted precisely to maximize the output signal. Accordingly, the width of the gating pulse can be considerably reduced, typically down to ~ 2 ns. No special care is needed for pulse width significantly larger than the transit time between two consecutive dynodes, e.g., 3.6 ns for the RCA6199. The pulse width used was 8 ns, narrow enough to ensure a good time resolution, but long enough to avoid any timing problems.

Fig. 3-2 shows that the delay cables are coupled to the dynodes by a capacitor (0.002 μ f) and terminated with a resistor (220 Ω) to ground. The resistor is intended to match the impedance of the delay cable to a particular dynode. When a pulse is injected into the photomultiplier, this resistor is essentially in parallel with a second resistor of equal value. Therefore, the input impedance is 110 Ω compared to 75 Ω and 93 Ω for coaxial cables type RG59/U and RG62/U, respectively. The impedances are sufficiently unmatched so that the negative reflections (less than 5%) helps to reach the cut-off state more quickly. The coupling capacitors are needed to maintain the DC voltages applied to the dynodes. Their capacitances must be sufficiently high to avoid pulse distortion, and the time constant (RC) should be suitable for high repetition rate (10 MHz).

Usually the voltage applied to the dynodes is fixed by the resistor chain. When a voltage pulse is sent down the

delay cables, a potential drop of the same amplitude appears across the appropriate resistor on the pulsed dynode and changes the voltage applied to that particular dynode. Thus, the voltage applied to a gated dynode can be adjusted at will by varying the amplitude of the gating pulses. However, the voltage pulses from the delay cables must not disturb the other dynodes. That is the purpose of the capacitors to ground at each gated dynode. These capacitors, together with the other capacitors across each dynode, help to stabilize the voltage applied to the dynodes. This is particularly important at the last stages where the space charge effect becomes important.

Fig. 3.2 also shows that the fixed voltage applied to each dynode is unequally distributed. Usually, a balanced (uniform) resistor chain or voltage distribution is required to achieve the best gain for the photomultiplier. This non-uniform voltage distribution is crucial because it determines the cut-off state of the photomultiplier. The value of the gain is lowered when the potentials are unbalanced. Fig. 3.3 shows how the gain varies when the potential drop is altered between dynodes D5-D6 and D6-D7. More precisely, the voltage applied to dynodes D5 and D7 is fixed. However, the voltage applied to dynode D6 is changed by a value equal to the gating pulse amplitude. One can see that the maximum gain is, in fact, achieved when

$$\Delta V_{5,6} = \Delta V_{6,7} ,$$

i.e., when the potential drop across D5-D6 equals the potential drop across D6-D7. When the equilibrium is not established, the gain can go down by one order of magnitude for the focussed type photomultiplier (RCA6199) and by two orders of magnitude for the elaborately focussed type (HTV R212UH). These two categories are defined by Sharpe [8].

Now the question is why does the photomultiplier is in a cut-off state when one or several dynodes are held at a different voltage than the manufacturer's specifications. Two phenomena can be involved. The first is the secondary electron emission process or the phenomenon of amplification at a dynode, and the second phenomenon is strictly the statistical process.

3.5 The Multiplication Process

Consider an electron in the space between two dynodes. Owing to the electric field filling this space, the electron is accelerated toward one of the dynodes. The proper design (geometry) of the dynodes [30] arranges the voltage equipotential between the dynodes so that the electron beam is focused on each dynode. A less elaborate design would simply allow the equipotentials to guide the electron flow toward the anode. The potential drop between the dynodes typically ranges between 50V and 200V. Therefore, the electrons reach the next dynode with an energy of about 50 eV to 200 eV.

The electron collides with a dynode and dissipates its kinetic energy. This energy is shared among several electrons

at a certain depth below the surface. If the energy of the electrons is sufficient to overcome the work function of the material (~ 1 eV), they are ejected. Typically, between 0 and 10 secondary electrons are emitted from one primary electron, depending on the material, and potential. These secondary electrons exit from the dynode with almost no velocity (~ 0.5 eV [30]). Again, the electric field accelerates and focusses them on the next dynode. This produces the multiplication process. The most common materials for the dynodes are CsSb, AgMgO-Cs, MgO and BeO.

The cumulative effect of multiplication at each dynode gives rise to photomultiplier gain which can be expressed as

$$G = K(\eta\delta)^n ,$$

where n is the number of stages, δ is the number of secondary electrons emitted for one incident electron (multiplication factor per stage), and K and η are the collection efficiencies of the first dynode and subsequent dynodes, respectively, i.e., the ability of the dynode to collect the secondary electrons emitted from the previous dynode (or photocathode). For example, with CsSb dynodes an empirical equation [8] gives

$$\delta = 0.2 V^{0.7} ,$$

where V is the potential drop between dynodes. Thus δ decreases when the voltage decreases. Moreover, the beam is less well focussed with a lower voltage, which results in a decrease

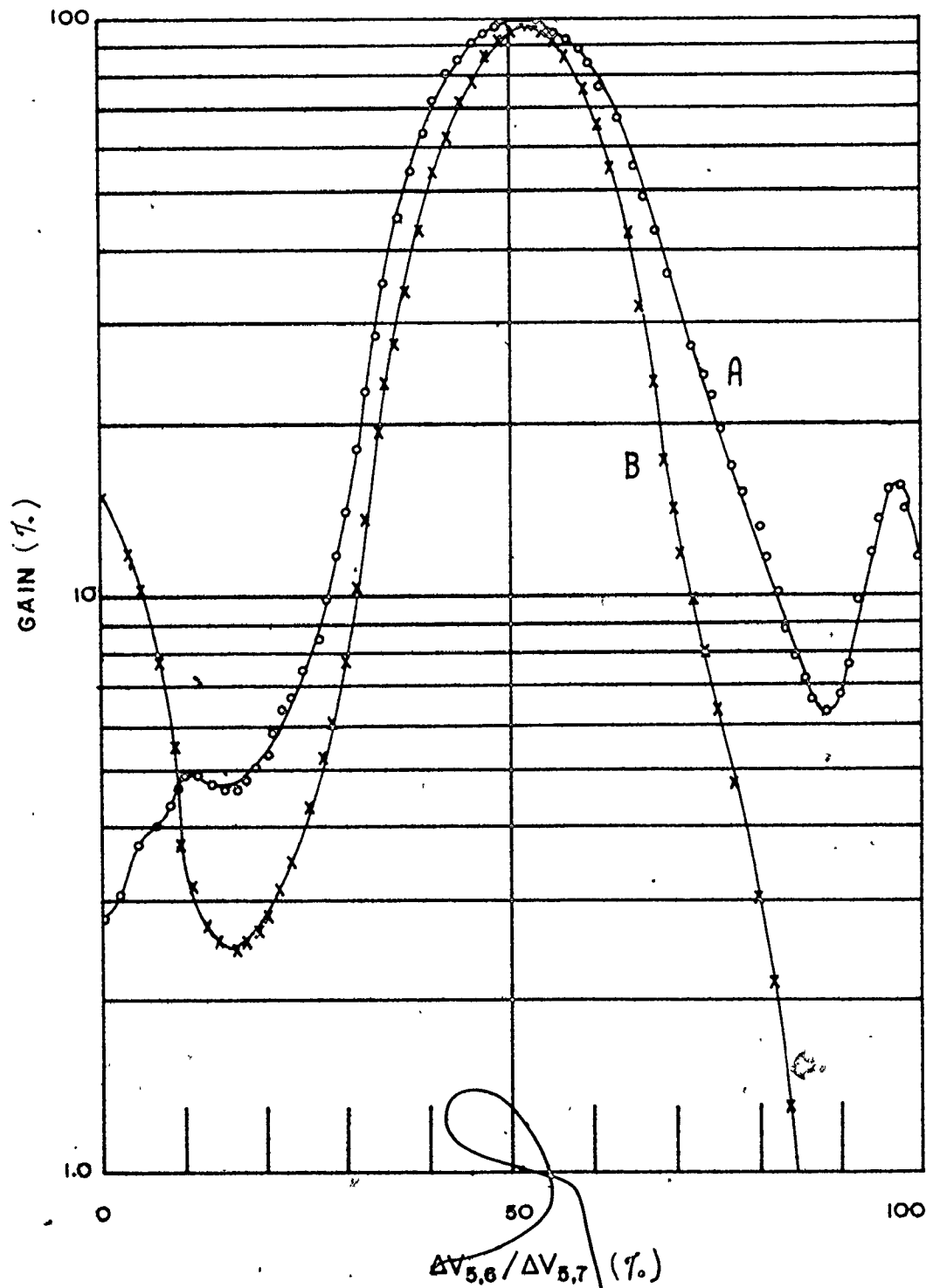
of η and/or K . The figures for η are typically [9] as follows for the box and grid type and venetian blind type [8], which are not focussed:

δ	1.5	2.0	2.5	3.0	5.0
η	58	80	89	94	99

It is different with the focussed and elaborately focussed type, i.e., the value of η drops very fast when the voltage is varied. Therefore, the gain goes down when the voltage is changed from the optimum value, mainly because the electron beam is defocussed and to a lesser extent because the effective δ , for two combined stages, also decreases with voltage changes from the optimum ($\sim 20\%$). Consequently, it is expected that gating would be more effective on an elaborately-focussed photomultiplier. Fig. 3-3 clearly shows that this is the case.

A second possible mechanism that could affect the gain of the photomultiplier is inherently related to the statistical nature of δ . In theory, it is assumed that the distribution of the number of secondary electrons emitted from a dynode follows a Poisson's distribution. Moreover, the probability of emission along the surface of a dynode also varies following a Poisson's distribution, for the focussed type photomultiplier. The cumulative effect of all the stages is a weighted convolution of all these distributions [28]. In practice, better results are obtained if Polya's distributions are used. When

Fig. 3-3 Gain variations for photomultipliers type RCA 6199 and type HTV R212UH when dynode D6 is pulsed. The circles (A) correspond to the focussed type (RCA 6199 operated at 100V per stage). The crosses (B) correspond to the elaborately focussed (HTV R212UH operated at 100V per stage). $\Delta V_{i,j}$ is the potential drop between dynodes i and j.



δ is the same for all stages, the total convolution remains a Poisson's (Polya's) distribution. If some of the δ 's are different, then the distribution is no longer Poisson's (Polya's) but broader and more Gaussian. This is the only difference that appears in the computer simulation of the multiplication process. The average still follows δ^n (or more precisely $\delta_1 \delta_2 \dots \delta_n$ for n stages). Therefore, it appears that the statistical distributions are not a significant factor in the change of the gain with the applied voltage. This result confirms the importance of η and K in causing large variations of the gain with the interdynode voltages.

It is very difficult to predict the cut-off ratio of a given photomultiplier because usually no data are available for η . Figs. 3-3, 3-4, 3-5 show the type of changes occurring in the gain (G) when one, two and three dynodes are gated, respectively. These data are more realistic than those published by Sharpe [8] and demonstrate that the gain can increase when one expects it to decrease and vice-versa. We obtained similar curves with the photomultiplier type RCA 6199 and HTV 212UH. Both our results and those of Sharpe [8] show that it is better to use the right side of the graph (gain versus voltage) to gate the photomultiplier. In other words, this means that the cut-off ratio is larger for a given voltage pulse amplitude, from the gate, when the potential drop between the gated dynode and the previous dynode (e.g., $\Delta V_{5,6}$)

Fig. 3-4 Gain variation for photomultiplier type RCA 6199 when two dynodes, D4 and D6 are pulsed. The dc potential $\Delta V_{5,6}$ was kept constant at 52.5V and the dc potential $\Delta V_{3,4}$ was varied.

N.B.: In normal operation $\Delta V_{5,6} = 100V$; $\Delta V_{i,j}$ is the potential drop between dynodes i and j.

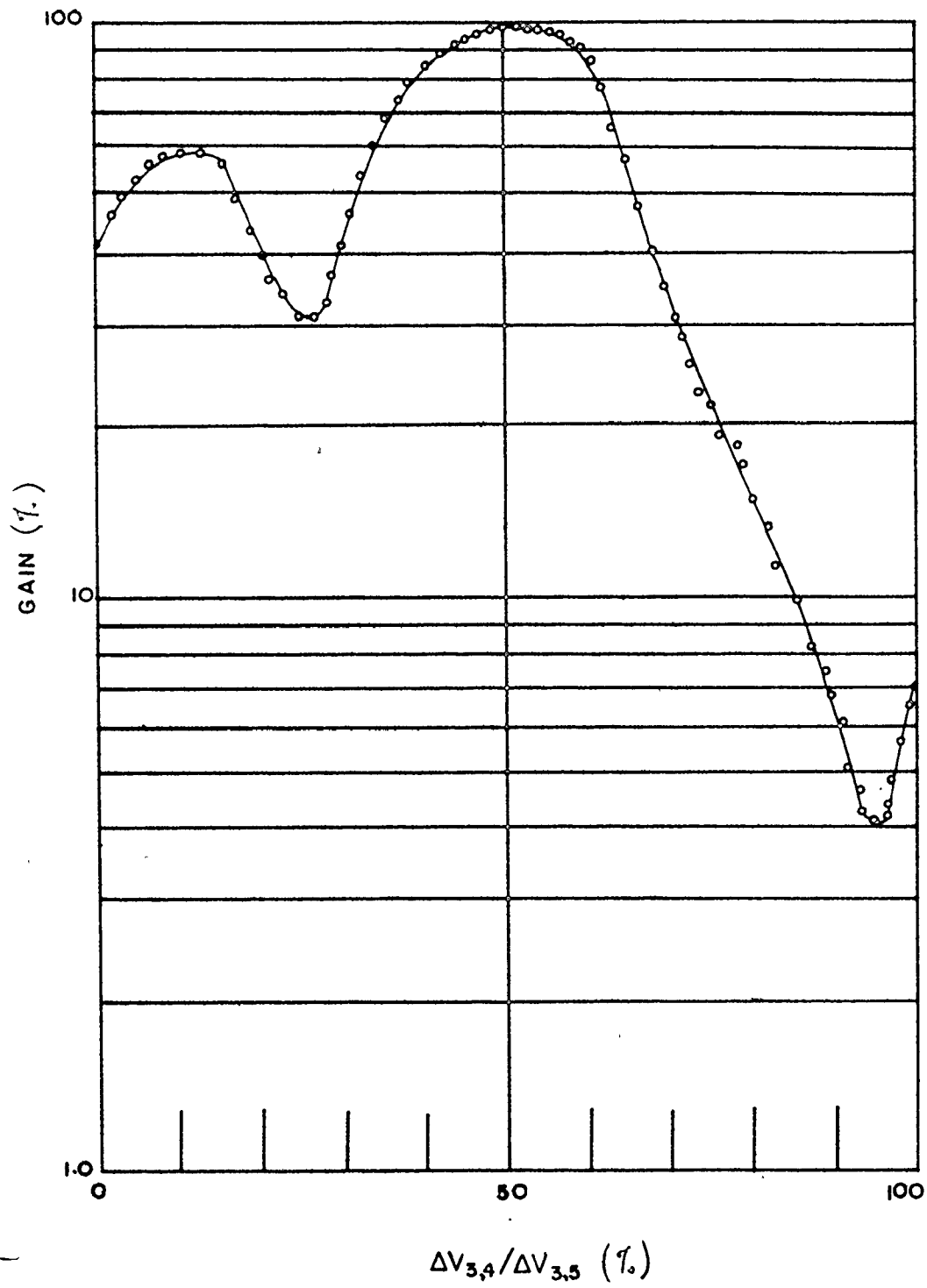
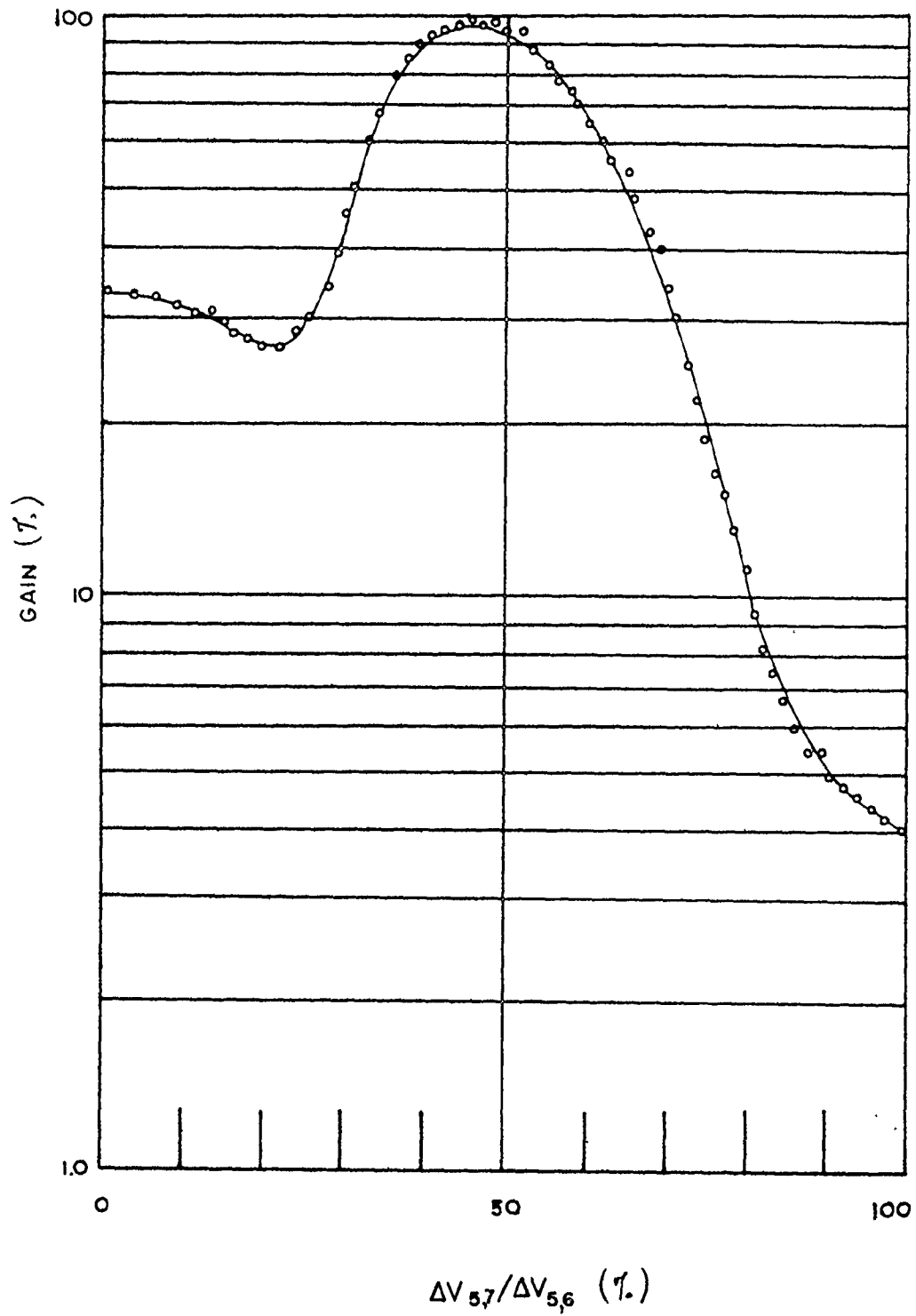


Fig. 3-5 Gain variation for photomultiplier type RCA 6199 when three dynodes, D2, D4 and D6, are capable of being pulsed. $\Delta V_{1,2}$ and $\Delta V_{3,4}$ were kept constant at 150V dc and $\Delta V_{5,6}$ was varied. For these measurements, only D6 was pulsed. Pulsing D2 and D4 increases the optimum gain by a factor of 100.

N.B.: In normal operation, $\Delta V_{1,2} = \Delta V_{3,4} = 100$; ΔV_{ij} is the potential drop between dynodes i and j.



is larger than the potential drop across the gated dynode and the following dynode (e.g., $\Delta V_{6,7}$), i.e., when

$$\Delta V_{i,j} > \Delta V_{j,k}$$

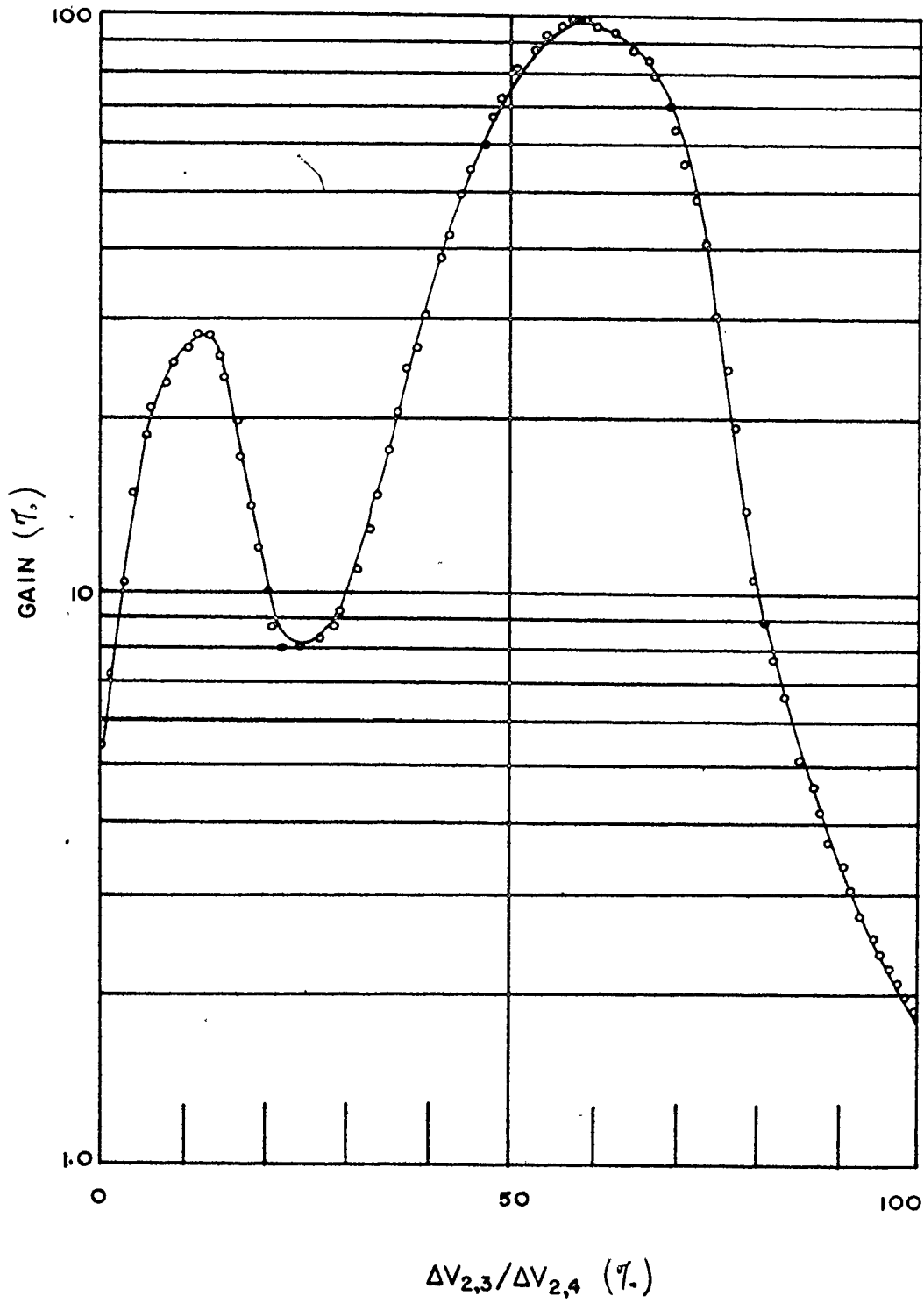
where $i < j < k$. More information on the geometry of the dynodes and η is needed to infer quantitative information.

3.6 Experimental Results

The major problem in this thesis was to build a versatile and noiseless gated photomultiplier. The first circuit to be built is represented in Fig. 3-2. Because the pulse generator (the gate) provides only positive voltage pulses, this circuit works only in the region on the left side of the graphs in Figs. 3-3, 3-4, 3-5. It turned out that the cut-off ratio was much too low (~ 300) and the amplitude of spurious signals (due to gating) was very large. The very low cut-off ratio can be understood using Fig. 3-5. It was observed that the shape of the gain curve (Fig. 3-3), for a particular setting of the resistive chain, changes significantly when a second (Fig. 3-4) and a third dynode (Fig. 3-5) is gated. With some dynodes, it was observed that the maximum gain did not occur at the expected equilibrium point (see, e.g., Fig. 3-6) showing that the gain curves are generally shifted, more or less, around the normal working point.

Since only one voltage pulse is created at the input of the delay cables, this means that all the dynodes are gated

Fig. 3-6 Gain variation for photomultiplier type
RCA 6199 when dynode D3 is pulsed. $\Delta V_{i,j}$ is the
potential drop between dynodes i and j.



with the same pulse amplitude. Because all the dynodes do not behave similarly, each one should be adjusted independently to give the maximum cut-off ratio for the gating pulse given. For example, a comparison between Fig. 3-3 (D6) and Fig. 3-6 (D3) shows that when dynodes D3 and D6 are gated at a voltage ratio of 40% to 50%, the gain goes down by 70% from D3, but by only 30% from D6. Now if the resistive chain is changed so that the voltage ratio varies between 30% and 40% instead of between 40% and 50% for D6, the gain changes by 78%. This is a factor of 2.5 better for the cut-off ratio, with an overall loss of maximum gain of only about 30%. These observations together with the fact that the gain curve changes significantly when several dynodes are gated, demonstrated the importance of fine adjustments for the resistors distributing the voltages to the gated dynodes. Consequently, PC board potentiometers, one for each gated dynode, were used in the circuit shown in Fig. 3-8. This resulted in a much more versatile gated photomultiplier as discussed in detail later in this chapter.

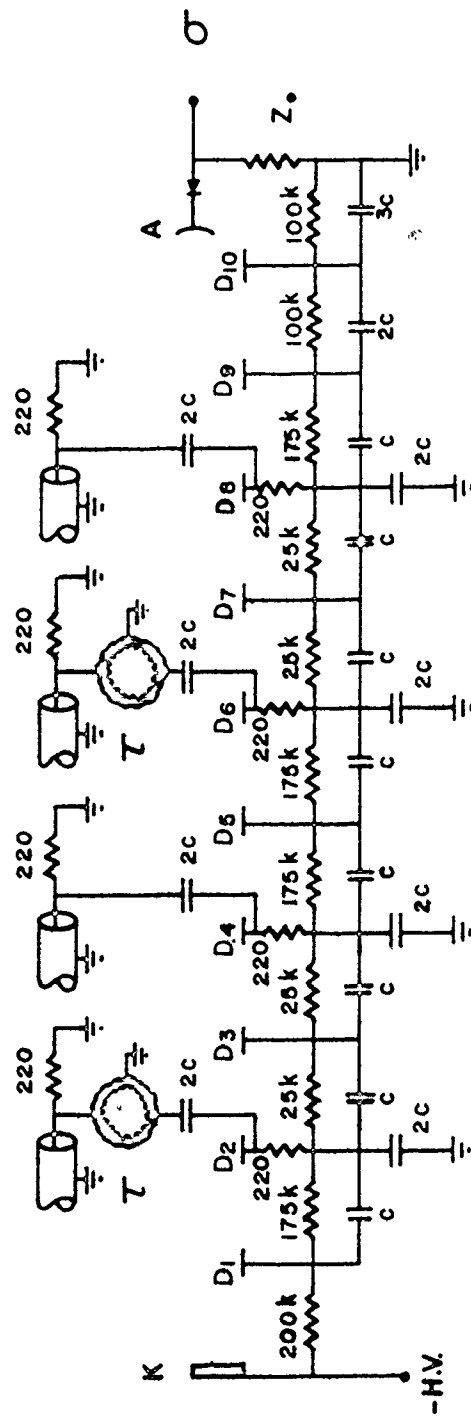
In the first circuit, high spurious signals, similar to the observations of other workers [3,6,11,29] . . . Because of the capacitance between the dynodes and the anode (~ 6 pF) and the output load resistance (25Ω), the gating pulse (50V, 4 ns) is differentiated at the anode. The amplitude at the anode is approximately given by

$$V = RC \frac{dV'}{dt} \sim RC \frac{\Delta V}{\Delta t} ,$$

where $R = 25 \Omega$, $C = 6 \text{ pF}$, $\Delta V' \sim 50\text{V}$ and $\Delta t \sim 4 \text{ ns}$. The result is a perturbing signal synchronized with the gating pulse, i.e., suffering no delay due to the transit time. The measured amplitude was 1V, compared to $\sim 3.8\text{V}$ obtained with the above rough calculation. Because each gating pulse produces its own spurious signal, the three delayed gating pulses give a very noisy output, in which a small signal of a few millivolts is buried. A solution to this problem, proposed by De Marco et al. [3], is to put a diode (or two) in series with the anode as shown in Fig. 3-7. A suitable diode type is the 1N4148. This diode has a reverse recovery time of 2 ns and a junction capacitance of 2 pF. Therefore, all positive spurious pulses with a risetime larger than 2 ns are eliminated, and the capacitance of the system is reduced from $\sim 6 \text{ pF}$ to $\sim 1.5 \text{ pF}$. Consequently, the amplitude of the negative spurious signals is decreased by a factor of 4, and the noise is decreased by a factor of 8. Moreover, the use of an oscilloscope with a bandwidth close to the bandwidth of the observed signal, provided further reduction of noise amplitude without affecting the signal amplitude. It should be mentioned that the diode affects the shape of the signal to be observed, i.e., the signal is higher (2 times) and narrower (2 times), as tested using a LED as a pulsed light source (see appendix A). A second diode in series with the first one did not affect the signal signifi-

Fig. 3-7 Second gated photomultiplier circuit. Dynodes D2, D4, D6 and D8 are pulsed. A pulse transformer is used with dynodes D2 and D6 (appendix B). The delay cables are RG62/U (93Ω), the capacitance C is $0.001 \mu\text{f}$. K is the photocathode, A is the anode, Z_0 is the load impedance, D is for diode (1N4148) and H.V. is the high voltage.

8



cantly but reduced the noise by another factor of 2. A third diode introduces deterioration of the signal and was therefore not used. Using a Tektronix 466 storage oscilloscope (4 ns risetime), the noise was down to ~ 5 mV.

Before a final circuit was built using both the diodes and the potentiometers, a simple modification of the previous circuit (Fig. 3-2) led to the circuit of Fig. 3-7. In this circuit, four dynodes are gated. Dynodes D4 and D8 are gated with a positive pulse and, D2 and D6 with a negative pulse. A pulse transformer (see appendix B) is needed to invert the positive pulse coming from the pulse generator (gate). Therefore, if the cable lengths going to dynodes D2 and D4 are the same (similarly for dynodes D6 and D8), and if the two dynodes of each set (e.g., D2 and D4) receive a positive pulse and a negative pulse simultaneously, the spurious signal should cancel out [10]. For identical pulses, a reduction of 99% is expected [10]. However, there are three problems with this method. First, the transit time between the dynodes requires much longer gating pulses (longer by the transit time) so that there is an overlap of the gating pulses as seen by the electrons in the photomultiplier. This implies longer charging cables (refer to previous chapter). Consequently, the achievable repetition rate is decreased. The second problem comes from the modifications of the gating pulse going through the pulse transformer. On our case, the amplitude of the pulse is decreased by 10%, the risetime is increased by 15% and there

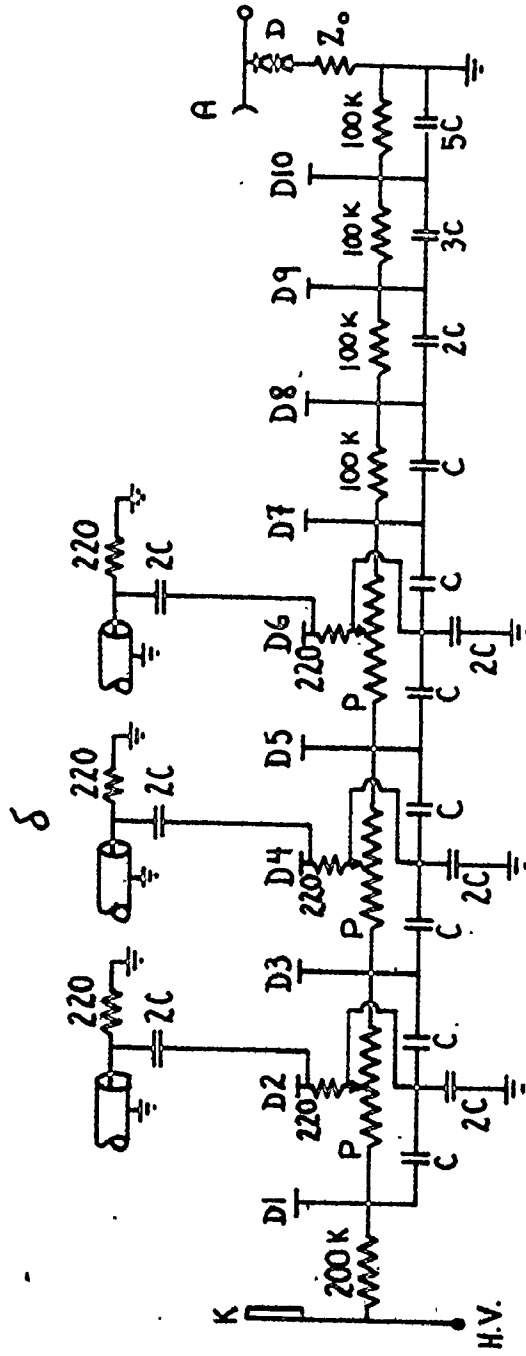
is a drop of $\sim 5\%$. Finally, the capacitance between all dynodes and anode is not necessarily the same. The net result was that the two pulses did not completely cancel and only a 70% reduction of noise was observed. This shows that the technique of pulse transformers is not justified for noise reduction if one considers all the problems involved. Nevertheless, some dynodes must be gated by a negative pulse in order to achieve a high cut-off ratio. Hence, pulse transformers must still be used to invert pulses.

Finally, a third circuit was built using potentiometers instead of fixed resistors (Fig. 3-8). Therefore, "fine tuning" was possible and improvements in the cut-off ratio were observed (factor ~ 3). The maximum cut-off ratio obtained using positive and negative gating pulses ($\sim 50V$) was 700 and 900, respectively, with the photomultiplier type RCA 6199 and, 1400 and 2400, respectively, for photomultiplier type HTV R212UH. The "fine tunings", for fixed gating pulse amplitude, maximize the cut-off ratio and minimize the noise.

The potentiometers make it possible to use the photomultiplier as a gated or non-gated device, at will. Moreover, the cut off ratio may be set to any possible level. This is useful for two reasons. Firstly, when the photomultiplier must be used as a non-gated device (normal operation), the potentiometers can be used to reduce the gain instead of varying the high voltage applied to the photocathode. By keeping the high voltage at its maximum value, the risetime and the transit time are kept to their shortest values. Therefore, better

Fig. 3-8 Third gated photomultiplier circuit.

Dynodes D2, D4 and D6 are pulsed. The delay cables (δ) are RG59/U (75Ω); the capacitance C is 0.001 μF . K is the photocathode, A is the anode, Z_0 is the load impedance, D is the diodes (1N4148) and HV is the high voltage.



time characteristics are achieved with the photomultiplier. Secondly, when the photomultiplier is used as a gated device, the potentiometers offer two possibilities. The photomultiplier can be gated on (normal operation) most of the time and gated off only during strong radiation or else, the photomultiplier is gated off most of the time and gated on during weak radiation. All these adjustments can be performed within minutes.

The circuit of Fig. 3-6 has been built for photomultiplier type HTV R212UH. Three dynodes are gated (D2, D4 and D6) and the corresponding delay cable lengths are 41 cm, 146 cm and 215 cm, respectively. The capacitance between the anode and the dynodes is the same as type RCA 6199 (~ 6 pF) and the spurious signal amplitude is also the same.

This circuit is more versatile than the previous one, is easier to build, and allows use of the photomultiplier in the normal working conditions, when desired. It should be stressed that the system described in this thesis emphasizes the use of the gated photomultiplier during an intense radiation pulse (see next chapter).

3.7 Saturation Effect

3.7.1 The DC Mode

High intensity, together with a reasonable gain in the photomultiplier ($\sim 10^6$), can produce a high dc anode current, e.g., one milliampere. This high current can drive the photomultiplier into a non-linear region or into sufficiently strong

saturation for permanent damage to occur. The initial non-linearity originates from the fact that the dynode current and the resistor chain current are closely related. Kirchhoff's law states that the sum of currents is zero at a node. This means that the sum of the resistor chain current and dynode current between two stages must be relatively constant. Also, the total voltage applied across the whole resistor chain remains constant since the supply is generally stable.

When a dynode current increases, the chain current for that particular dynode must decrease. Therefore, the potential drop also decreases. Since the total voltage drop across all stages must be a constant, the current drawn from the power supply must increase slightly to compensate for this reduction in voltage. The dynode current is usually high only in the last stages. Thus a substantial voltage drop can occur in the last stages and a small voltage increase would be observed in the first stages. The magnitude of the change depends on the value of the chain resistors. It can be shown [31] that most of the voltage drop occurs only in the last two stages. This voltage redistribution has been determined experimentally by Stump and Talley [35]. At relatively low intensity levels the net effect is a gain increase. Basically, the photomultiplier is inherently a non-linear device. However, space charge effect and other factors discussed below, can produce larger non-linearities, even at low intensities, as can be seen from Figs. 3-9 to 3-18.

A simple theory has been worked out by Baker et al. [31] which shows a linear deviation from photomultiplier linearity at small anode current. They show that the deviation from linearity is linear (first approximation) until the anode current is $\sim 10\%$ of the chain current. A more detailed theory [33,34], which includes second order effects, is more appropriate for deviations up to $\sim 40\%$ of the chain current. Figs. 3-10 and 3-11 show the type of agreement between this theory and the behaviour of photomultiplier types RCA 6199 and HTV 212UH. As mentioned by Moatti [33], the agreement can not be perfect owing to the approximations made and to the space charge effects present in the last stages [32]. The space charge originates from the fact that the secondary electrons leave the surface of a dynode with almost zero velocity, which results in an accumulation of charges near the surface of the dynode. This cloud of electrons screens the electric field between the dynodes so as to decrease the potential drop seen by the electrons leaving the surface of the dynode. Although the overall potential drop between the dynodes is not changed, there is a reduction of the dynode current and consequently the anode current drops. Data on the geometry of the dynodes, on the properties of the material for the dynodes, and on the shape of the equipotential between the dynodes, was not available. Therefore, it was impossible to even estimate the magnitude of the space charge.

Fig. 3-9 Divergence (D) from linearity for photo-multiplier type RCA 6199 operating at 600V and in the dc mode. Region α has the voltage redistribution effect plus the space charge effect. Region β is the saturation part due to a dynode current significant compared to the chain current. Perfect linearity is achieved when $D=1$.

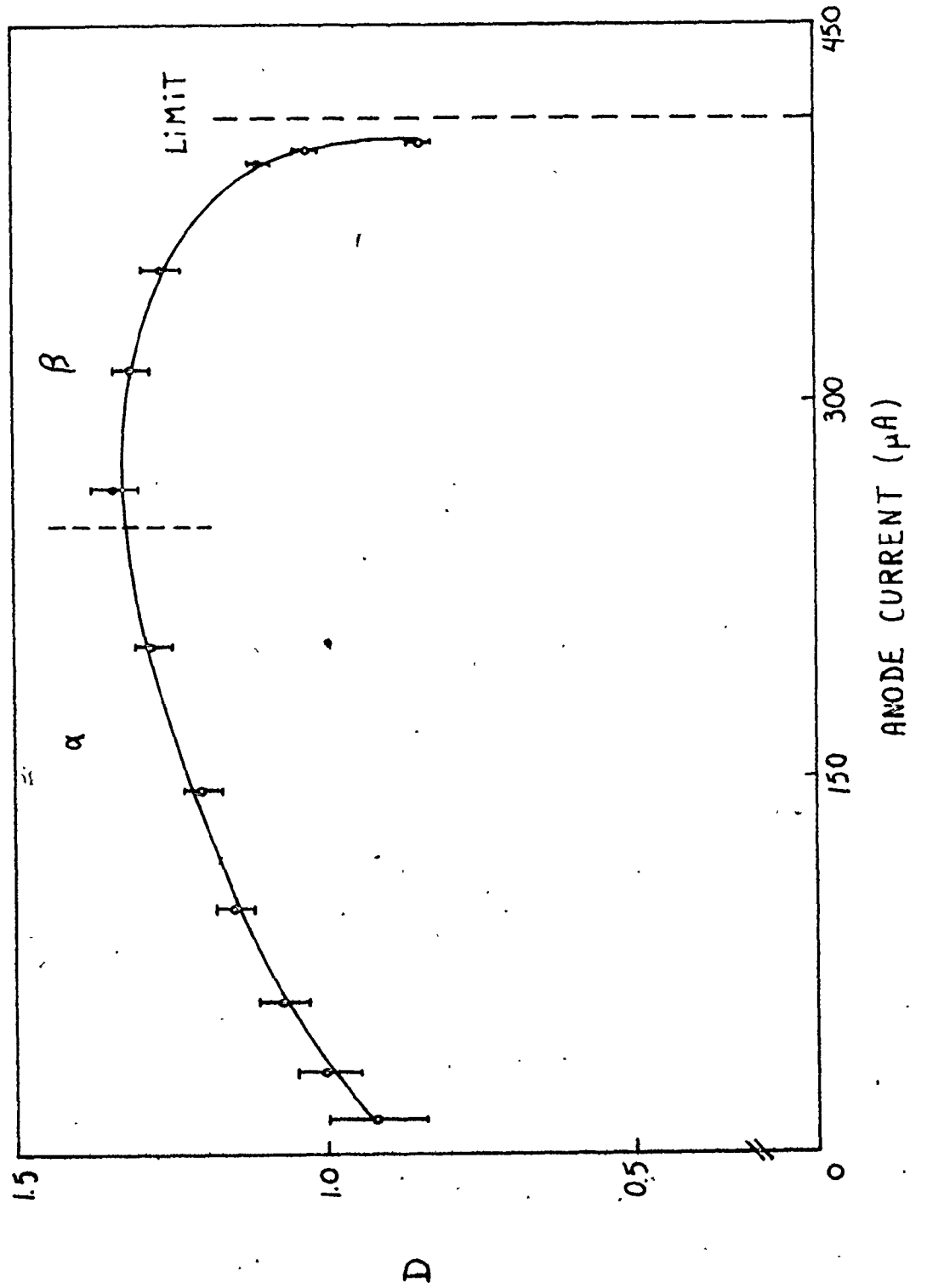




Fig. 3-10 Divergence (D) from linearity for photo-multiplier type HTV R212UH operating at 800V and in the dc mode. The theoretical curve (dashed) is from Lush et al. [34], with $k = 1.5$ corresponding to a last stage resistance of $150 \text{ K}\Omega$. Perfect linearity is achieved when $D=1$.

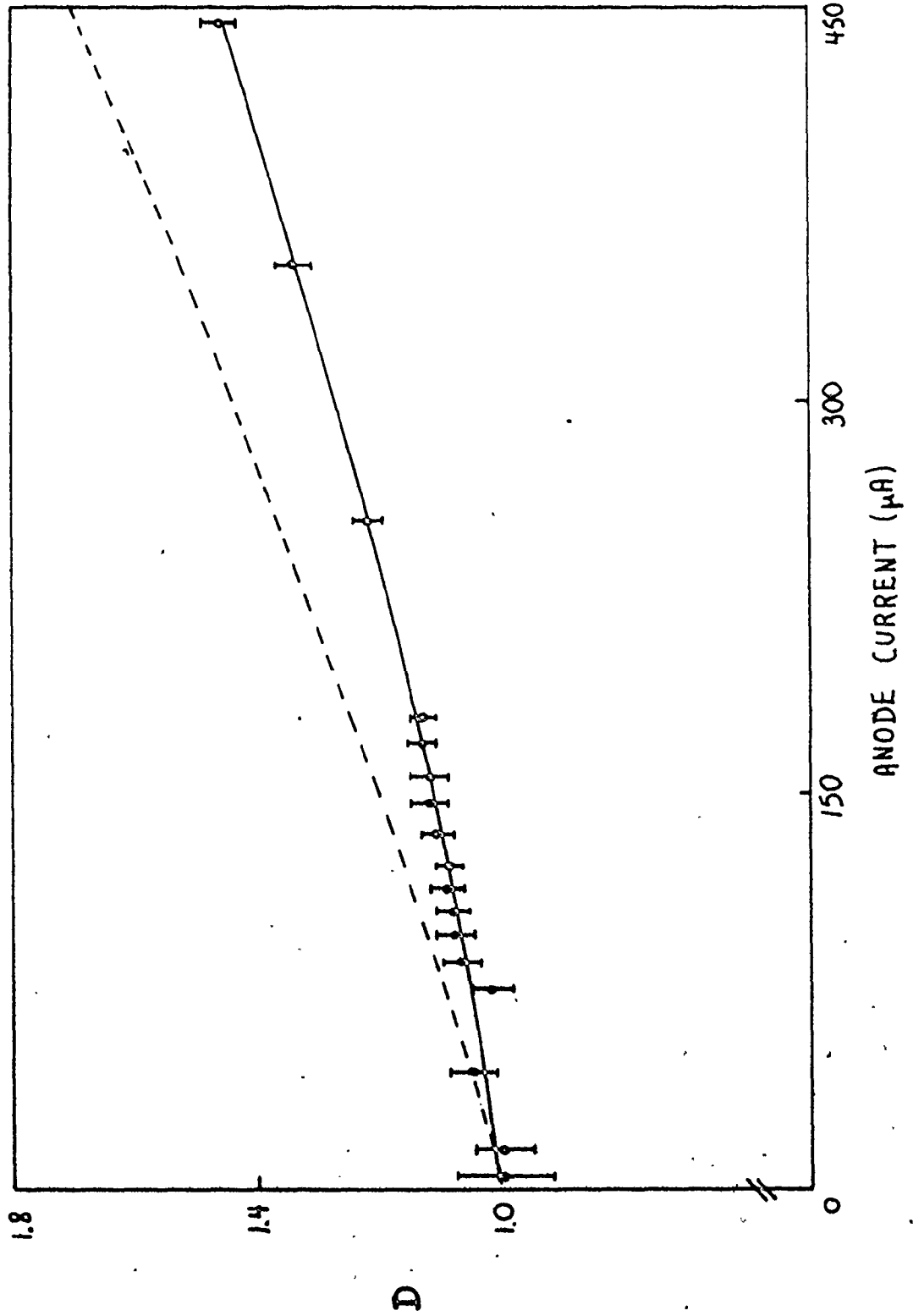
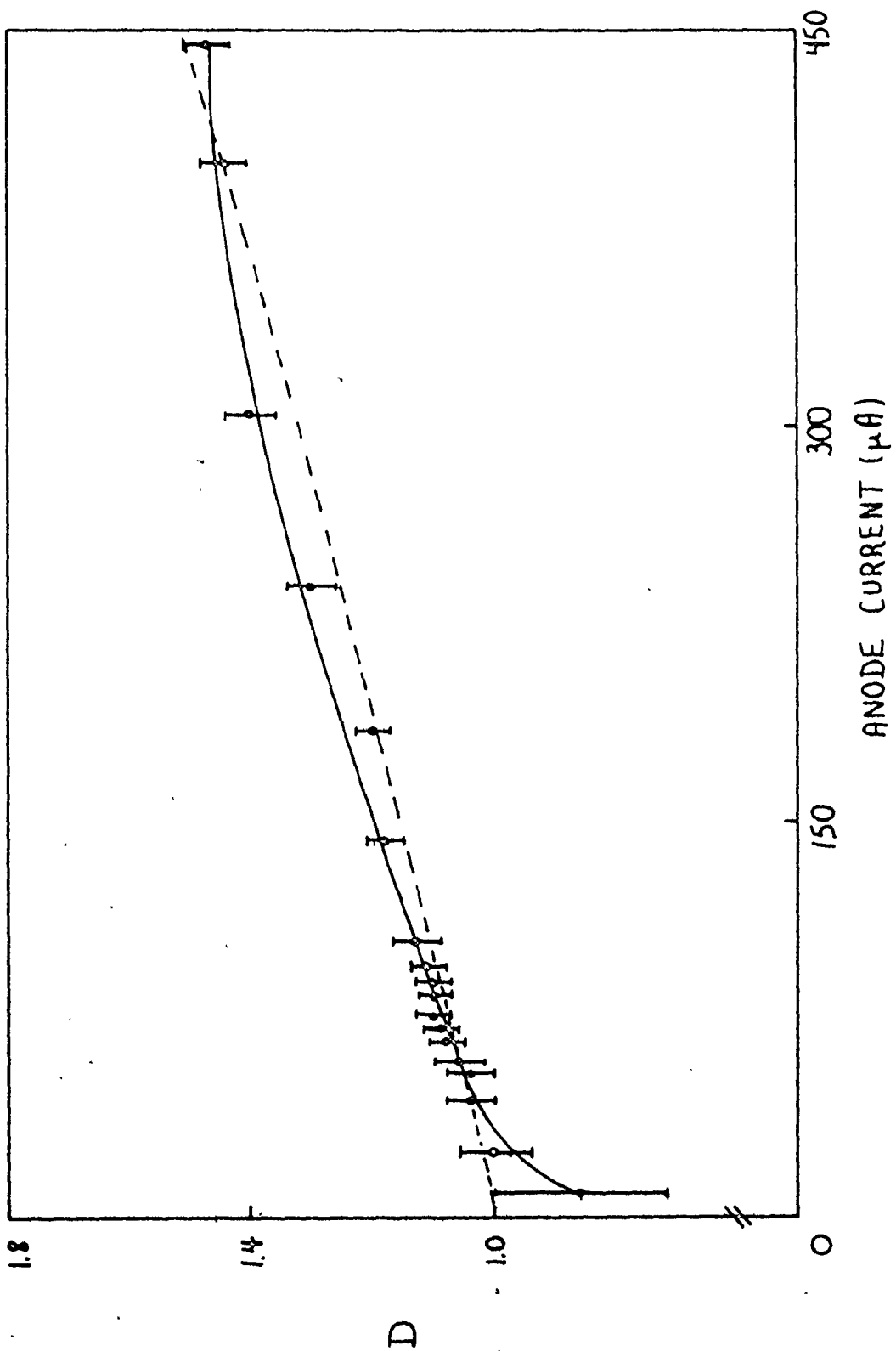


Fig. 3-11 Divergence (D) from linearity for photo-multiplier type RCA 6199 operating at 900V and in the dc mode. The theoretical curve (dashed) is from Lush et al. [34], with $k=1$ corresponding to a last stage resistance of $100\text{ K}\Omega$. Perfect linearity is achieved when $D=1$.



The space charge can easily explain the discrepancy between the experimental results and the theoretical predictions (Fig. 3-11). In fact, the space charge effect should occur at much lower currents in an elaborately focussed photomultiplier compared to a simply focussed photomultiplier (Fig. 3-10), owing to the much higher concentration of electrons in the former. The experimental results agree with these predictions.

We have seen (Figs. 3-9 to 3-11) that a high dynode current usually is larger than expected, and that the space charge effect tends to lower the anode current. These two effects can cancel each other to a certain extent (Figs. 3-9 and 3-10).

When the dynode current in the last stage reaches a value comparable to the chain current, the space charge effect becomes very strong. Then, the anode current is much lower than expected, and a third effect occurs, which results directly from Kirchhoff's law. The dynode current cannot be larger than the anode current, because their sum is a constant. Therefore, when the dynode current approaches a value equal to the chain current, it cannot increase further, whatever the intensity incident on the photocathode. More likely, at high intensities, the anode current can decrease from this maximum value due to space charge effects. This phenomenon explains the pronounced drop of the curve in Fig. 3-9 at ~ 0.4

mA (chain current is 0.5 mA). In Figs. 3-10 and 3-11, the chain current is ~ 0.75 mA, and a sharp drop is not observed for a dynode current of ~ 0.55 mA. It should be mentioned that when the chain current is properly chosen, then the photomultiplier is automatically protected against overload, i.e., the anode current will never be sufficient to cause permanent damage (in the dc mode).

Another observed limitation [32] comes from the photocathode. A radial voltage drop is set up at the photocathode (semi-transparent type) which is caused by sufficiently intense radiation generating large electron densities in the material. The equipotential pattern between the photocathode and the first dynode is modified, and the collection efficiency drops, resulting in a corresponding drop of the anode current. Magnetic fields and temperature changes will cause the output current to deviate from linearity, but this is a second order effect [32].

For the above reasons, i.e., voltage redistribution, space charge effect, dynode current limitation and photocathode saturation, the photomultiplier can behave very non-linearly with intense radiation. Consequently, when used either for absolute or relative intensity measurements, the anode current must be corrected to account for its non-linear behaviour. Figs. 3-9 to 3-18 show the behaviour of photomultiplier types RCA 6199 and HTV R212UH in different situations (dc and pulsed mode).

The dc mode has been studied almost exclusively in the literature. In the next sub-section, the pulsed mode is investigated. A comparison with the dc mode reveals some similarities between these two cases.

3.7.2 The Pulsed Mode

In the pulsed mode, the high dynode current in the last stages can last for a much shorter time than for the dc mode. Consequently, for sufficiently short periods of time, there should be much less space charge effect because of the much reduced number of electrons present in the photomultiplier. Moreover, with sufficiently large capacitors ($\sim 0.001 \mu\text{F}$) across each amplification stage, the voltage drop between each dynode is regulated, and there should be no voltage distribution, i.e., the sum of the dynode current and the chain current is no longer a constant because the capacitors provide current for the dynodes. This explains why, in Figs. 3-12 to 3-18, where dynode capacitors were used, an anode current up to 20 times larger than the chain current can be used. The current limitation occurs for a dynode current about 50 times larger than for the dc mode. Accordingly, much higher radiation intensity can be measured in the pulse mode than in the dc mode. This can be seen as follows.

First, the photomultiplier is operated in the normal dc mode (Fig. 3-12), but with a strong light pulse on the photo-

Fig. 3-12 Divergence (D) from linearity for photo-multiplier type HTV R212UH operating at 1000V. The on time of the light pulse is 600 ns (single pulse). The last chain resistor is 150 K Ω . Perfect linearity is achieved when D=1.

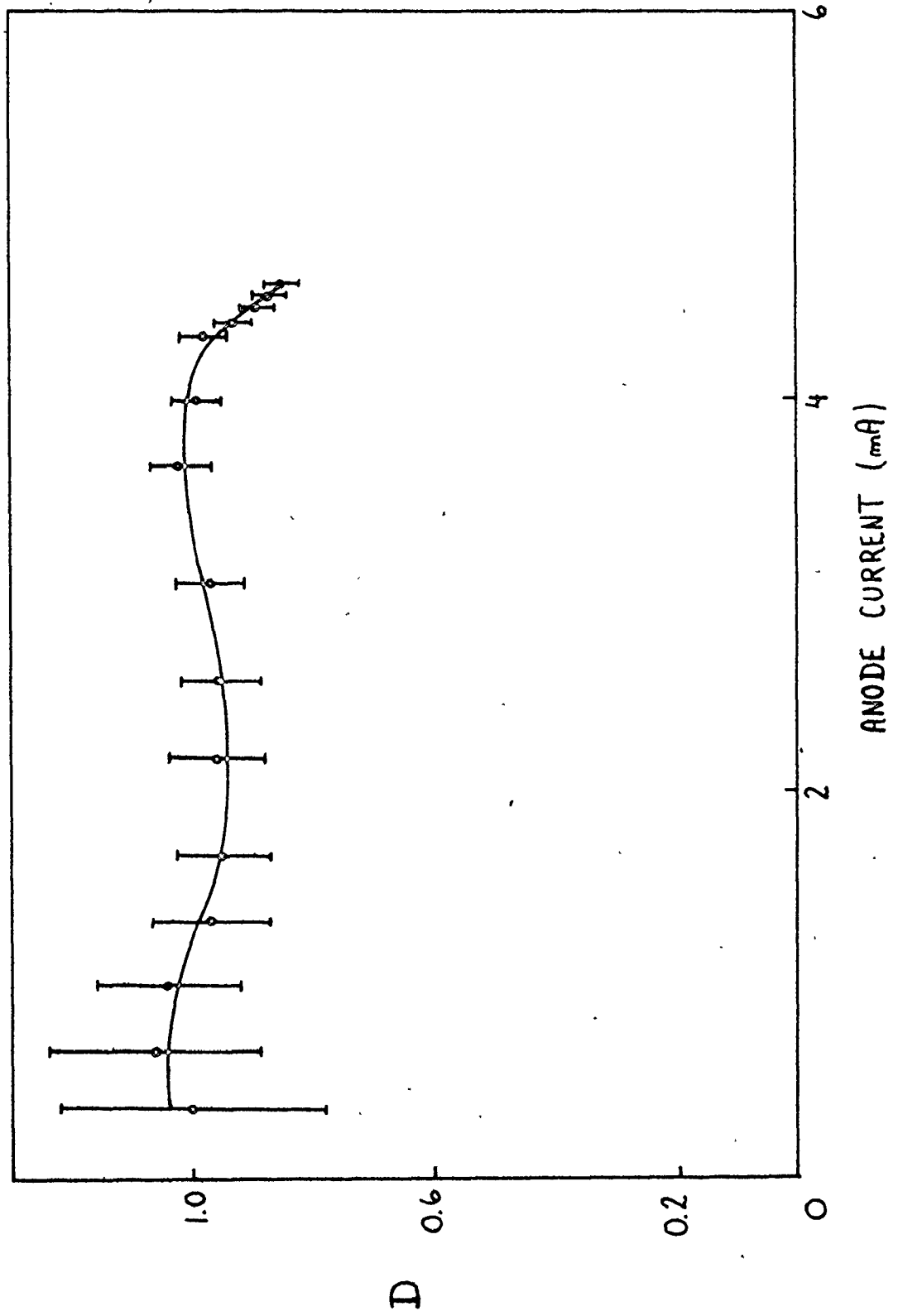
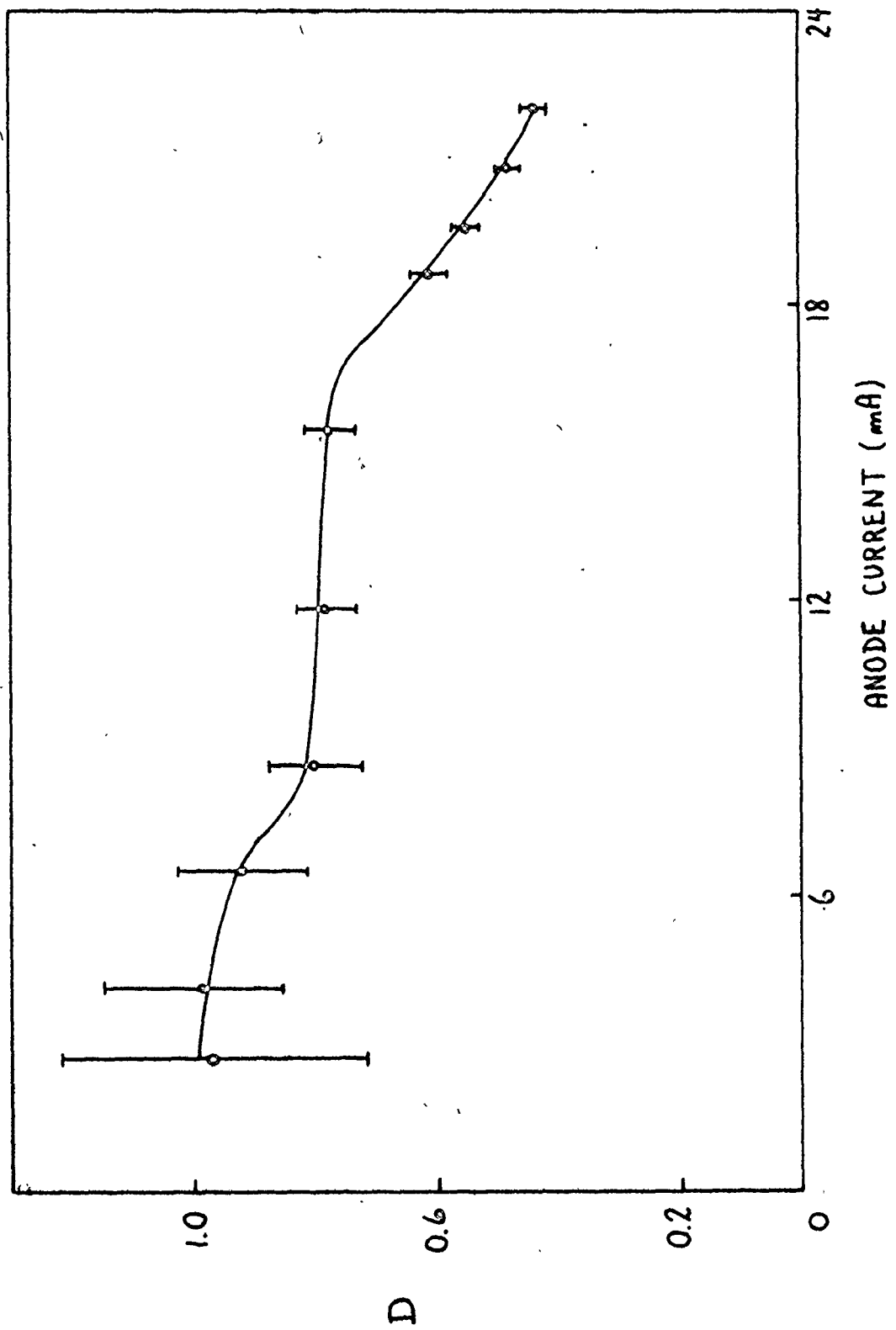


Fig. 3-13 Divergence (D) for linearity for photo-multiplier type HTV 212UH operating at 1000V. The on time is 8 ns during a light pulse lasting 600 ns. The last stage resistance is 150 K Ω . Perfect linearity is achieved when $D=1$.



cathode that lasts ~ 600 ns. Up to ~ 4.3 mA the anode current behaves linearly, to within experimental error. Then, quickly, the factor D, divergence from linearity, i.e., experimental value divided by expected value, drops to zero (at ~ 5 mA). This could be caused by the space charge effect, by too small capacitors or by saturation of the photocathode (as discussed earlier).

If the photomultiplier is now pulsed for a short interval (~ 8 ns) within 600 ns light pulse, the space charge effect and the capacitor discharge effect should be removed, but not the photocathode saturation since the light pulse is the same as before. This situation is depicted in Fig. 3-9 for 8 ns on time. A slight drop of the curve is observed at ~ 5 mA, but it is much less pronounced than in the previous case. A plateau is reached between ~ 8 mA and ~ 16 mA. Past ~ 16 mA, a monotonous drop brings the curve to zero. Compared with the previous case, the first drop could be related to the photocathode saturation. The plateau results from the combined effect of the photocathode saturation (decreases anode current) and the capacitor discharge that starts to allow a voltage redistribution (increases anode current). Finally, the last decrease could be due to discharge of capacitors, and/or to the space charge effect, and/or to a strong saturation of the photocathode.

By a comparison of Figs. 3-14 and 3-15, the focussed type (RCA) and elaborately focussed photomultiplier type (HTV) are compared, and the results agree with those observed in the

Fig. 3-14 Divergence (D) from linearity for photo-multiplier type RCA 6199 operating at 900V. The on time is 8 ns with a rate of 1 KHz. Perfect linearity is achieved when $D=1$.

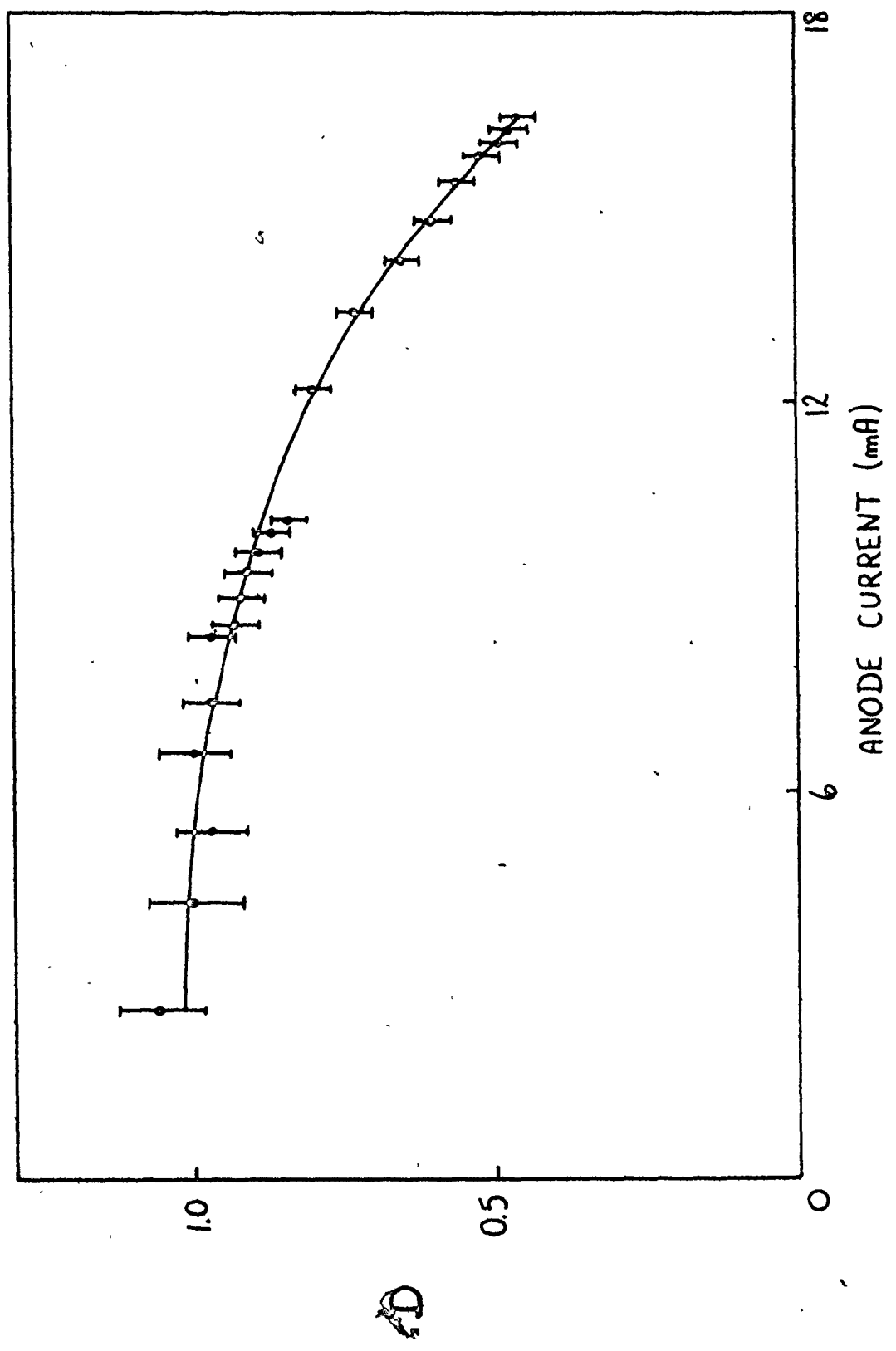
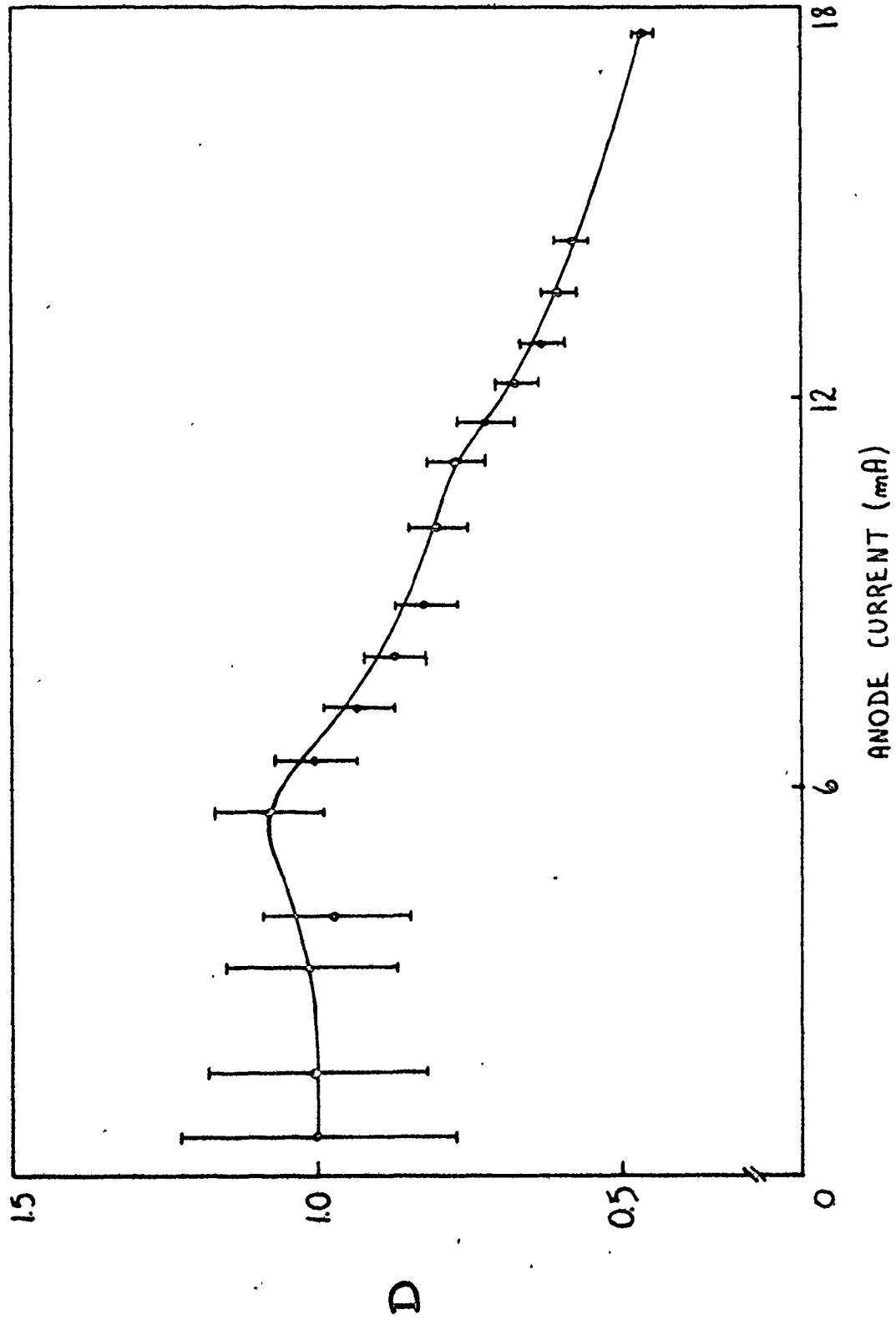


Fig. 3-15 Divergence (D) from linearity for photo-multiplier type HTV R212UH operating at 900V. The on time is 8 ns, at a rate of 1 KHz. The last stage resistance is 100 K Ω . Perfect linearity is achieved when D=1.



dc mode. Starting at $\sim 6\text{mA}$, the anode current behaves more non-linearly for the HTV. This strengthens the hypothesis that the space charge effect is more pronounced in the elaborately focussed photomultiplier. It should be noted that when a dc source is incident on the photocathode, the saturation by high electron densities is less obvious because a steady state is reached. Consequently, the effect is either reduced or not observed, as can be seen from Figs. 3-14 to 3-18. The saturation of the photocathode can be minimized by using a very narrow ($\sim 8\text{ ns}$) light pulse.

The effect of the capacitors can be observed when Figs. 3-16 and 3-17 are compared. For this data, the capacitor across the last stage (last dynode to anode) has been changed from $0.005\ \mu\text{F}$ to $0.002\ \mu\text{F}$. The capacitor discharges sooner when its capacitance is reduced. Consequently, a voltage redistribution appears at a smaller dynode current. This effect, i.e., $D > 1$, can be observed in Fig. 3-17. Logically, a larger capacitor should behave the same way as a smaller capacitor but at a higher anode current. However, this is not the case. In Fig. 3-16, the curve seems to go above $D=1$, but still remains in the linear region, to within experimental errors. The two curves, Figs. 3-16 and 3-17, drop at $\sim 12\ \text{mA}$, revealing the occurrence of the space charge effect. On Fig. 3-15, the space charge effect occurs at $\sim 6\ \text{mA}$ because a lower voltage is applied across the last stage (90V across $100\ \text{k}\Omega$) compared

Fig. 3-16 Divergences (D) from linearity for photo-multiplier type HTV R212UH operating at 800V. The last stage resistance is 150 K Ω and the last stage capacitance is 0.005 μ F. The on time is 8 ns with a rate of 1 KHz. Perfect linearity is achieved when D=1.

28

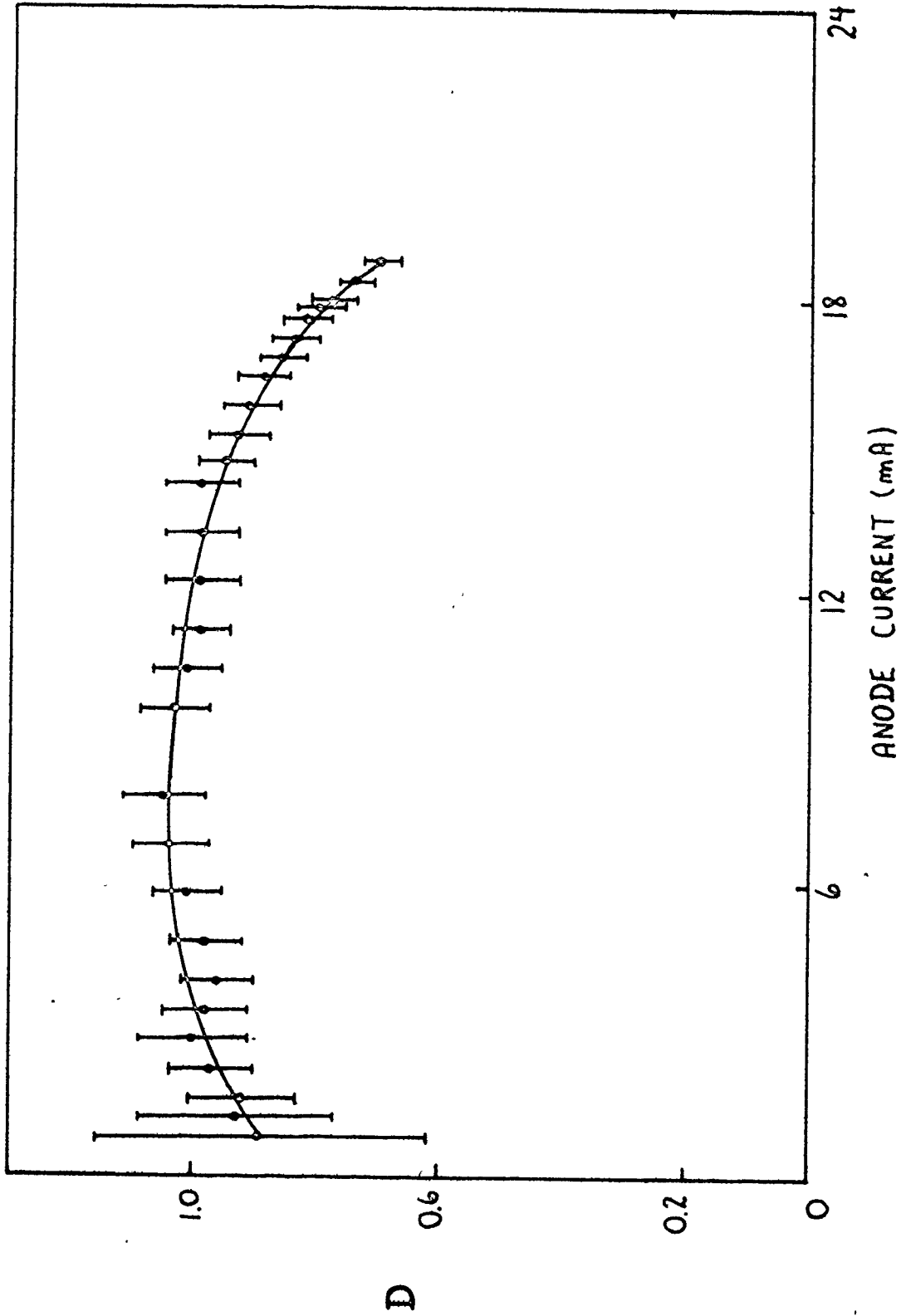


Fig. 3-17 Divergence (D) from linearity for photo-multiplier type HTV 212UH operating at 800V. The last stage resistance is 150 K Ω and the last stage capacitance is 0.002 μ F. The on time is 8 ns with a rate of 1 KHz. Perfect linearity is achieved when D=1.

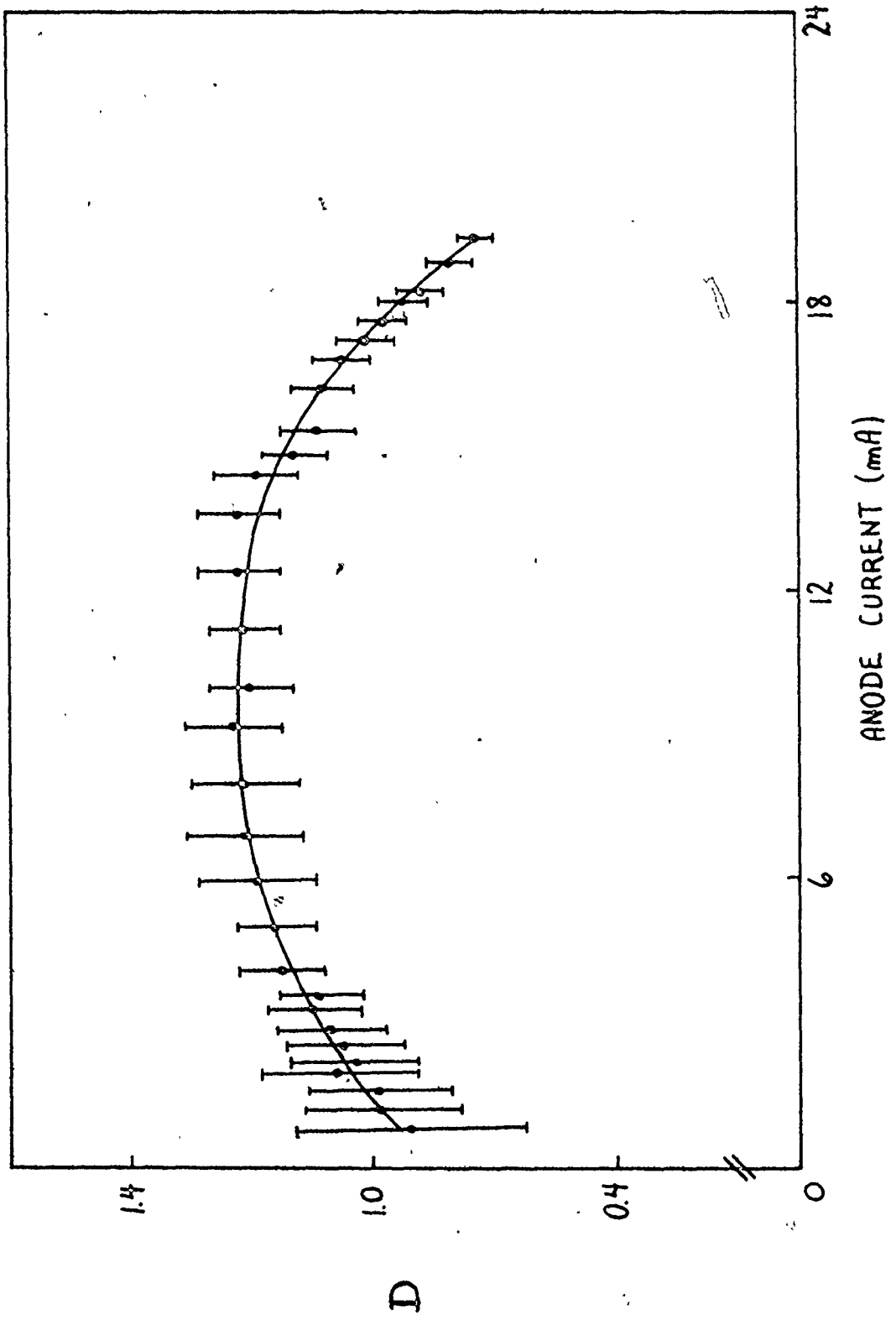
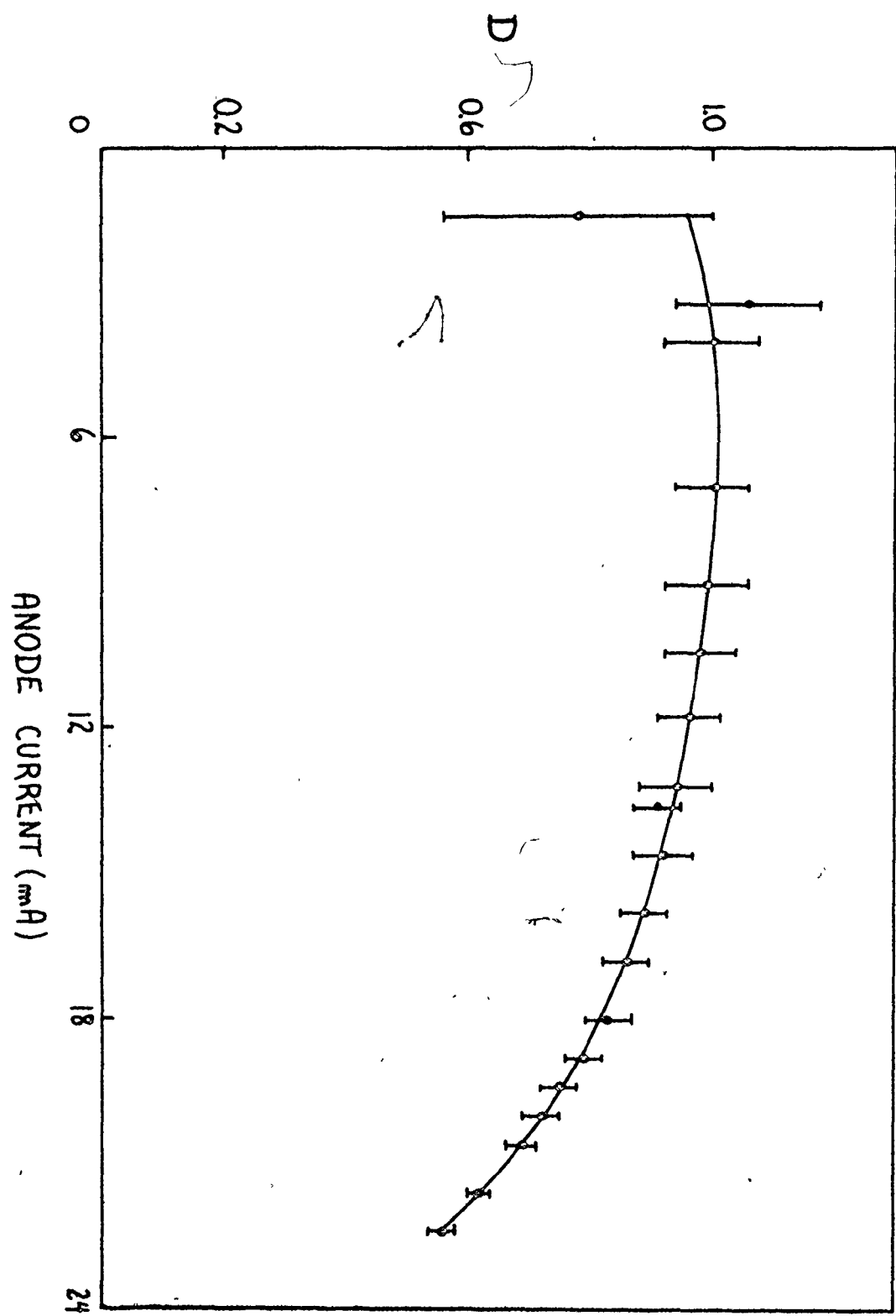


Fig. 3-18 Divergence (D) from linearity for photo-multiplier type HTV R212UH operating at 900V. The last stage resistance is 180 K Ω and the last stage capacitance is 0.005 μ F. The on time is 8 ns with a rate of 1 KHz. Perfect linearity is achieved when D=1.



to a higher voltage for the data in Figs. 3-16 and 3-17 (114V across 150 K Ω). This was done to emphasize the effect of the capacitors.

As has already been mentioned, the last stage resistor can be adjusted to decrease the effect of the space charge. Figs. 3-15, 3-16 and 3-18 represent the behaviour of the anode current for three different last stage resistors of 100 K Ω , 150 K Ω and 180 K Ω , respectively. However, care must be taken to avoid too large potential drop in order to avoid sparking between the anode and the dynode, which could permanently damage the dynode. The three figures reveal a net improvement in linearity with increasing last stage voltage. Furthermore, a higher anode current can be achieved. An increased voltage across the last stage also implies increased energy stored in the capacitor across that stage. Consequently, the capacitor is effective for a higher dynode current.

3.8 Conclusion

To tackle the problem which is the main concern of this thesis, a versatile gated photomultiplier has been built (Fig. 3-8). For the measurement of relative intensity changes during intense radiation, the behaviour of the anode current, when different dynodes are pulsed, has been studied in order to obtain the best cut-off ratio, together with the lowest electrical noise level.

Large anode currents are produced during intense radiations, in order to achieve good accuracy and high SNR. A know-

ledge of the behaviour of the anode current in the non-linear region is necessary. The non-linear effect has been studied in the dc mode, where it is best understood, and then compared with the pulsed mode. With the photomultiplier type HTV R212UH, the best linearity was achieved for the situation illustrated in Fig. 3-18.

In summary, the photomultiplier type HTV R212UH has been gated for an on time of 8 ns at a cut-off ratio of 1800, using positive gating pulses of 50V. The latter produced ~ 5 mV (across 25Ω) of spurious signal at the anode which is adequately small for a wide range of measurements. The output anode current deviates from linearity by 10% for ~ 16 mA, in the pulsed mode. This may be compared to $\sim 150 \mu\text{A}$ in the dc mode. Thus, the pulsed mode allows two orders of magnitude increase in the anode current.

CHAPTER 4

Time Dependence of Intense Light Pulses

4.1 Introduction

In this thesis, the gated photomultiplier is mainly intended for time resolved amplitude measurements of intense light pulses. Here, the term intense refers to any light pulse that can saturate a photomultiplier in its normal dc mode. One application, in this thesis, is for the study of light emitted by a flashlamp pumped dye amplifier.

In the first experiment, the gated photomultiplier and a high pressure Xe lamp were employed to investigate the gain of the dye amplifier as a function of time, with wavelength and pumping power. The relative changes in amplitude of the time resolved intensity measurements should provide accurate data to compute the gain of the dye amplifier. The experiment was intended to test the performance of the gated photomultiplier, using a very well characterized organic dye, Rhodamine 6G [21,24,26,27]. The saturated and unsaturated gain of dye amplifier has been extensively studied [16-23,27]. The theory relevant to this subject is described in the next section.

In the second experiment, the time dependent spectrum of

the amplified spontaneous emission (ASE) was investigated. These measurements were motivated by the failure to measure the gain using a high pressure Xe lamp as the source. Our goal remained the same, i.e., to test the performances of the gated photomultiplier for time resolved high intensity measurements. The theory, mentioned above, can also be applied to predict the spectrum of the ASE.

4.1.1 Literature Review

Gain measurements in amplifiers can be carried out in many different ways. Direct measurements, Huth [17], are commonly used where a laser beam of the right wavelength is passed through the amplifier and the amplified intensity is measured with a detector. This technique is suitable for most lasers, provided that a suitable source is available.

Burlamacchi et al. [20] employed double pass amplifiers and travelling-wave regenerative amplifiers to extract the data concerning the gain. With their technique, the amplification of the probe signal (laser beam) is enhanced, and the gain measurement accuracy is increased.

When the gain is high, in e.g., a dye laser, the narrowing of the amplified spontaneous emission (ASE) with increasing pump power provides the data to compute the gain [16,18,21,22,27]. The advantage of this technique is that there is not a probe signal to saturate the available gain.

Another alternative is to measure the intensity of the ASE from a full length cell and from, e.g., a half-length cell. The gain, as a function of wavelength (λ), can be computed from

$$G(\lambda) \approx \frac{2}{L} \ln(I_L(\lambda)/I_{L/2}(\lambda)) , \quad (4.1-1)$$

where I is the measured intensity and L the full length of the dye cell. The accurate reduction of the active medium length is not always possible and consequently the measurements may only give an approximation for the gain [16].

The last two techniques can be used only in a relatively low gain region. In general, the most simple technique is direct measurement using a probe source. The probe source must be weak enough not to saturate the available gain. Rhodamine 6G, e.g., has a broadband emission spectrum ($\sim 400 \text{ \AA}$) and required a tunable source for detailed gain measurements. Usually, a laser of the same type as the amplifier to be studied is used as a source. Our aim was to use a system of general application, i.e., one that can be used with most types of laser. Consequently, we needed a continuous probe source. The dye laser is the only suitable candidate among the lasers [23,25], but is an expensive and complicated system. A potential approach is to use a broadband lamp (e.g., a high-pressure Xe lamp) together with a monochromator. The first half of the experimental section in this chapter (4.4.1) deals

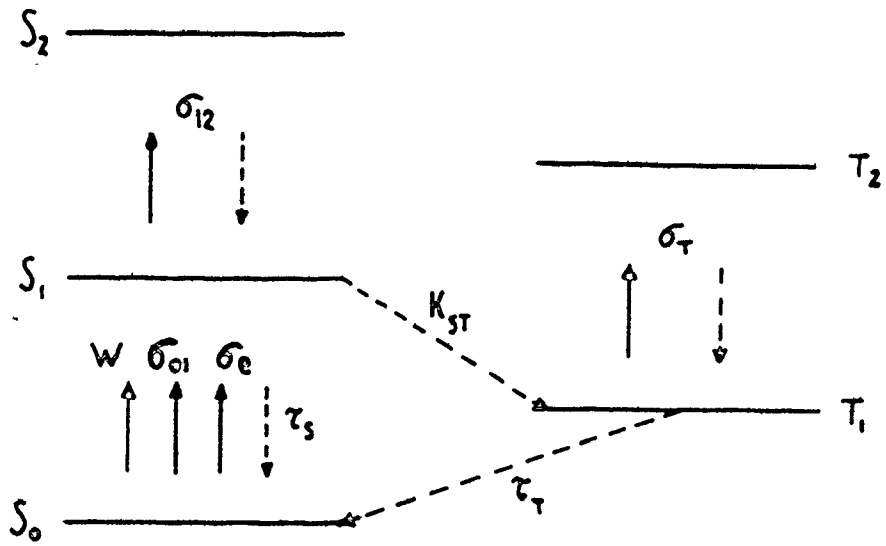
with such a system. First, we investigate theoretically the behaviour of Rhodamine 6G in a cylindrical cell surrounded by a coaxial flashlamp [19,25].

4.2 Theory of Gain in Rhodamine 6G

Rhodamine 6G (R6G) is a high gain and efficient dye for use in a dye laser. Marling et al. [24] give a comparison between seventeen dyes. The effect of flash excitation frequency and fluid filtration on the quality of the dye is discussed by Fletcher et al. [26]. The thermal effect, i.e., dye solution heating by the non-radiative transitions, and the loss of molecules due to the long triplet lifetime, are neglected. A concentration of 7.5×10^{-4} M/l of R6G in methanol, below the optimum concentration [18], has been chosen to minimize the intensity of ASE and maximize the available gain.

In order to compute the gain, we follow the model based on the rate equation approximation developed by Ganiel et al. [21]. We proceed in a way similar to that of Efthymiopoulos [16], which includes the model developed by Casper-son [22]. Fig. 4-1 gives the energy level diagram for the R6G. These energy levels have a semi-continuous structure consisting of all the vibrational and rotational energy states of the molecule. Owing to the fast thermalization process ($\sim 10^{-12}$ s) only the lowest levels of each state are

Fig. 4-1 Energy levels for Rhodamine 6G. S_0 is the ground state, S_1 and S_2 are the singlet states and, T_1 and T_2 are the triplet states. W is the pumping rate, σ_{01} is the ground state absorption cross-section, σ_e is the singlet state emission cross-section, σ_{12} is the singlet state absorption cross-section and σ_T is the triplet state absorption cross-section. τ_S and τ_T are the singlet state and triplet state lifetimes. K_{ST} is the singlet state to triplet state crossover rate.



filled. Moreover, the very fast non-radiative transitions, from the higher excited states (those not shown in Fig. 4.1) to the first excited state, depopulate these levels. So, zero population is assigned to the higher excited state. This is true also because the flashlamp provides a maximum pumping rate of about 10^7 photons per second [25]. The only populated levels considered are the ground state, the first excited singlet and triplet states. Then,

$$N_0(x,t) + N_S(x,t) + N_T(x,t) = N, \quad (4.2-1)$$

where t is time, x is distance along the axis of the cylindrical cell, N_0 is the ground state (S_0) population, N_S is the singlet state (S_1) population and N_T is the triplet state (T_1) population. N is the total number of molecules which can be calculated from the dye concentration used. The population of the S_1 and T_1 levels are governed by the following rate equations:

$$\begin{aligned} \frac{dN_S}{dt}(x,t) = & W(t)N_0(x,t) - \frac{N_S}{\tau_S}(x,t) - N_S(x,t) \int_{\lambda} \sigma_e(\lambda)I(x,t,\lambda)d\lambda \\ & + N_0(x,t) \int_{\lambda} \sigma_{01}(\lambda)I(x,t,\lambda)d\lambda - K_{st}N_S(x,t) - N_S(x,t) \int_{\lambda} \sigma_{12}(\lambda)I(x,t,\lambda)d\lambda \\ & - W'(t)N_T(x,t) \end{aligned} \quad (4.2-2)$$

$$\frac{dN_T}{dt}(x,t) = K_{st}N_S(x,t) - \frac{N_T}{\tau_T}(x,t) - N_T(x,t) \int_{\lambda} \sigma_T(\lambda)I(x,t,\lambda)d\lambda \quad (4.2-3)$$

Here $W(t)$ and $W'(t)$ are pumping rates, $\sigma_e(\lambda)$ is the emission cross-section from S_1 to S_0 , $\sigma_{01}(\lambda)$ is the absorption cross-section of S_0 , $\sigma_{12}(\lambda)$ is the S_1 absorption cross-section and $\sigma_T(\lambda)$ is the triplet state cross-section. K_{ST} is the S_1 to T_1 crossover rate, and τ_S and τ_T are the singlet and triplet state lifetime, respectively. $I(x,t,\lambda)$ is defined as the total photon flux per unit wavelength, or as the sum of the $-x$ and $+x$ propagation intensity, i.e.

$$I(x,t,\lambda) = I^+(x,t,\lambda) + I^-(x,t,\lambda) \quad (4.2-4)$$

The propagation in each direction can be considered independently. Taking account of the losses by absorption, and of the gain from the spontaneous and stimulated emission, we can write the rate equation for the photon flux as

$$\begin{aligned} \frac{dI^{\pm}}{dt}(x,t,\lambda) &= \frac{N_S}{\tau_S}(x,t)E(\lambda)g^{\pm}(x) + N_S(x,t)\sigma_e(\lambda)I(x,t,\lambda) \\ &- \sigma_{01}(\lambda)N_0(x,t)I^{\pm}(x,t,\lambda) - \sigma_T(\lambda)N_T(x,t)I^{\pm}(x,t,\lambda) \\ &- \sigma_{12}(\lambda)N_S(x,t)I^{\pm}(x,t,\lambda) \quad (4.2-5) \end{aligned}$$

The fluorescence spectrum $E(\lambda)$ is normalised so that

$$\int E(\lambda)d\lambda = \phi \quad (4.2-6)$$

where ϕ is the quantum efficiency (~ 0.84 for R6G in methanol). There is a relation between the emission cross-section and the fluorescence spectrum via

$$\sigma_e(\lambda) = \lambda^4 E(\lambda) / 8\pi\eta^2 c, \quad (4.2-7)$$

where c is the speed of light and η is the refractive index of the solution (1.3288 for methanol). The function $g^\pm(x)$ is an adjustable parameter for the coupling of the spontaneous emission in the cell (cylindrical). As a starting point,

$$g^+(x) = \frac{g}{2} \{1 - (L-x) / [(L-x)^2 + r^2]^{1/2}\}, \quad (4.2-8)$$

$$g^-(x) = \frac{g}{2} \{1 - x / [x^2 + r^2]^{1/2}\}, \quad (4.2-9)$$

where $g=1$, or any smaller value. Here r and L are the radius and length of the dye cell and x is taken along the symmetry axis of the dye cell. It should be noted that the pumping term $W'(t)N_s(x,t)$ in Eq. (4.2-2) is generally assumed negligible compared with $W(t)N_0(x,t)$ for a coaxial flashlamp pumped dye laser. [16], and therefore this term is omitted. The pumping term is defined as

$$W(t) = \frac{P(t)}{A} \int \sigma_{01}(\lambda) f(\lambda) \frac{\lambda}{hc} d\lambda, \quad (4.2-10)$$

where $P(t)$ is the power dumped into the dye cell by the flashlamp as a function of time, and A is the pumped area. With

an ablation flashlamp [16], $f(\lambda)$ is chosen to be the normalized blackbody radiation spectrum. Using

$$f(\lambda, T) = \frac{8\pi hc}{\lambda^5} (e^{hc/kT\lambda} - 1)^{-1}, \quad (4.2-11)$$

where k is the Boltzmann's constant and h is the Planck's constant. Integration over wavelength gives the normalized function,

$$f(\lambda) = \frac{f(\lambda, T)}{f(T)} = \frac{2\pi hc^2}{\sigma T^4} \cdot \frac{1}{\lambda^5} \cdot (e^{hc/kT\lambda} - 1)^{-1}, \quad (4.2-12)$$

where σ is the Stephan's constant. Because the light pulse from the flashlamp has a relatively slow variation with time, the pumping rate can be considered constant, which greatly simplifies the calculations. Thus

$$P(t) \equiv P = \frac{\alpha CV^2}{2.250 \text{ ns}} = \frac{3\alpha V^2}{5} \text{ J}\cdot\text{s}^{-1}, \quad (4.2-13)$$

where $C = 300 \text{ nF}$ refers to the capacitor driving the flashlamp, and 250 ns is the pumping pulse width (HWHM). The parameter α is the fraction of energy, stored in the capacitor, that is coupled into the dye cell. V is the voltage that appears across the capacitor and the flashlamp. The pumped area, although not clearly defined in this case, is assumed to be at radius r at the center of the absorption layer in the dye. The area is

$$A = 2\pi rL, \quad (4.2-14)$$

where L is the length of the active medium. With $L = 11.5$ cm and $r = 0.35$ cm

$$A = 2\pi \times 0.35 \times 11.5 = 25.29 \text{ cm}^2. \quad (4.2-15)$$

From Eqs. (4.2-10), (4.2-12), (4.2-13) and (4.2-15), the pumping rate becomes

$$W(t) \equiv W = \frac{1490\alpha cV^2}{\sigma T^4} \int_{\lambda} \sigma_{01}(\lambda) \cdot \frac{1}{\lambda^4} \cdot (e^{hc/kT\lambda} - 1)^{-1} d\lambda. \quad (4.2-16)$$

The limits of integration are determined by the absorption region of the dye [25]. The equivalent blackbody temperature is in the range 20,000°K to 30,000°K [16]. Eq. (4.2-16) is used to match theory with experimental results.

In our system, the pumping rate varied between 2.1×10^6 photons/s and 3.7×10^6 photons/s, which is above the minimum requirement of 1.08×10^6 photons/s which produces threshold gain at 5850 Å in 7.5×10^{-4} M/l of R6G in methanol.

Equations (4.2-1), (4.2-2), (4.2-3) and (4.2-5) form a system of non-linear coupled equations. These can not be solved analytically and must be treated numerically. The computer program written by Efthymiopoulos [16] has been followed closely.

Assuming a slowly varying pumping rate, Eq. (4.2-3) can be solved for the steady state, i.e.,

$$N_S(x, t) = \frac{N_T(x)}{K_{ST}} \left\{ \frac{1}{\tau_T} + \int_{\lambda} \sigma_T(\lambda) I(x, \lambda) d\lambda \right\}. \quad (4.2-17)$$

For a low pumping rate ($< 10^9$ photons/s), which is the case with a flashlamp, the integral in Eq. (4.2-17) is small compared to τ_T^{-1} . Therefore

$$N_T(x) = K_{ST} \tau_T N_S(x). \quad (4.2-18)$$

The same assumption applied to Eq. (4.2-2) gives

$$N_S(x) \left\{ \frac{1}{\tau_S} + \int_{\lambda} \sigma_e(\lambda) I(x, \lambda) d\lambda + K_{ST} + \int_{\lambda} \sigma_{12}(\lambda) I(x, \lambda) d\lambda \right\} = N_0(x) \left\{ W + \int_{\lambda} \sigma_{01}(\lambda) I(x, \lambda) d\lambda \right\}. \quad (4.2-19)$$

Combining Eq. (4.2-1) and Eq. (4.2-18) gives

$$N_0(x) = N - N_S(x) \{1 + K_{ST} \tau_T\}. \quad (4.2-20)$$

Substitution into Eq. (4.2-19) yields

$$N_S(x) = N \cdot \left\{ W + \int_{\lambda} \sigma_{01}(\lambda) I(x, \lambda) d\lambda \right\} / \left\{ K_{ST} + \frac{1}{\tau_S} + [1 + K_{ST} \tau_T] \left[W + \int_{\lambda} \sigma_{01}(\lambda) I(x, \lambda) d\lambda \right] + \int_{\lambda} \sigma_e(\lambda) I(x, \lambda) d\lambda + \int_{\lambda} \sigma_{12}(\lambda) I(x, \lambda) d\lambda \right\}. \quad (4.2-21)$$

Equations (4.2-18), (4.2-20) and (4.2-21) must be solved to find $N_S(x)$, $N_0(x)$ and $N_T(x)$. Both the unsaturated and

saturated gain are then computed using the expression

$$G(x, \lambda) = N_s(x)\sigma_e(\lambda) - N_0(x)\sigma_{01}(\lambda) - N_T(x)\sigma_T(\lambda) - N_s(x)\sigma_{12}(\lambda) \quad (4.2-22)$$

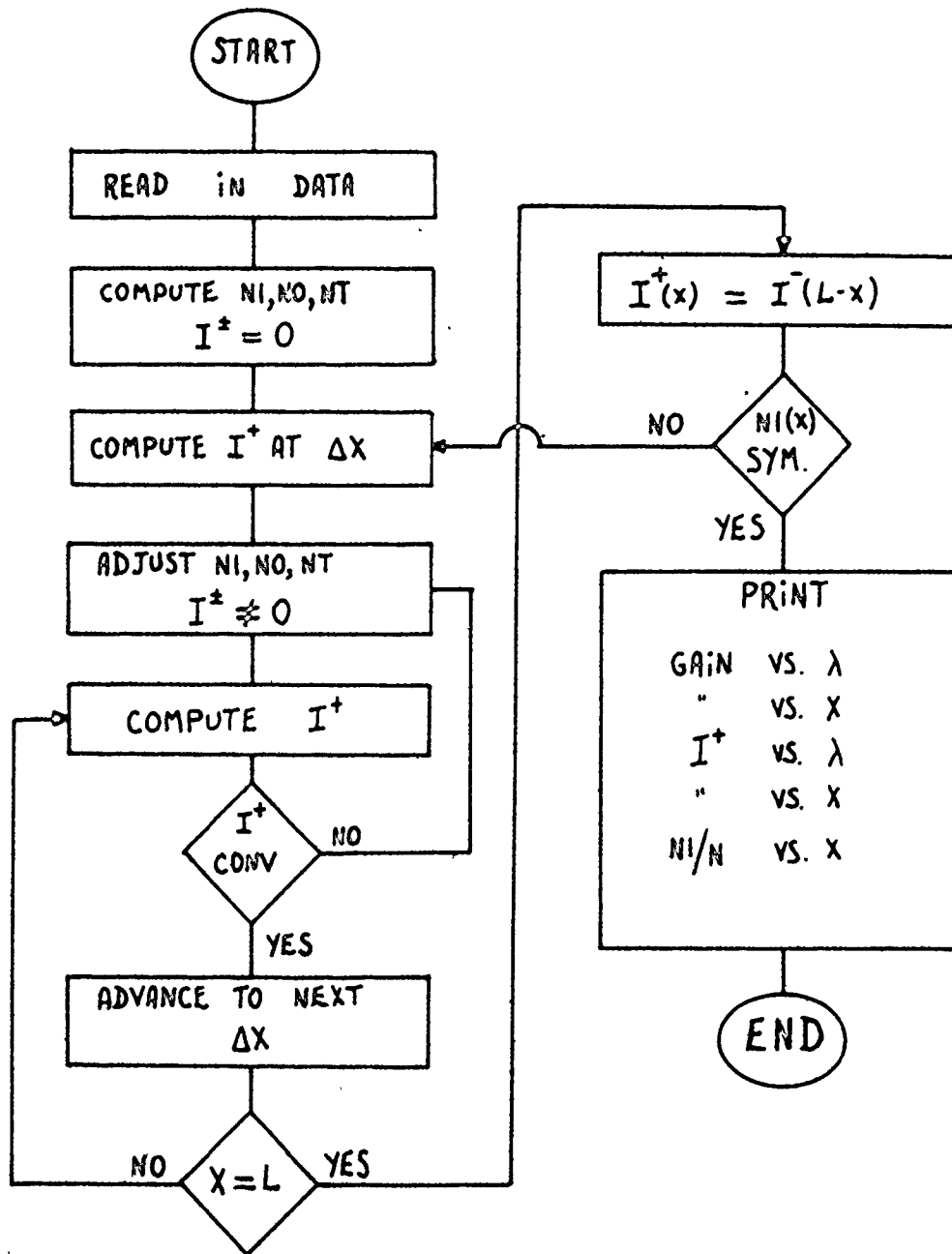
The results of this computation demonstrate the possibility of achieving an unsaturated gain as high as 0.8 cm^{-1} at a wavelength of 5960 \AA and employing a pumping rate of 2.5×10^6 photons/s with a concentration of $1.5 \times 10^{-3} \text{ M/l}$ of R6G in methanol. The probe source should then be amplified by a factor of 100 over the length of the dye cell. Equation (4.2-5) can also be computed to give the spectrum of the ASE.

4.2.1 The Computer Program : DYGAIN

The computer program created to solve the above equations follows closely the steps established by Efthymiopoulos [16] in his doctoral thesis. These steps are shown in the flow chart in Fig. 4.2. The starting point is to fix a pumping rate and a concentration. Then, I^+ and I^- in Eq. (4.2-19) and Eq. (4.2-21) are made equal to zero. This yields the first estimate for N_s , N_0 and N_T . Using Eq. (4.2-22), a first estimate for the gain is available, and the intensity traveling in the positive direction (I^+) can then be calculated from

$$\begin{aligned} ST &= ST' * \text{EXP}(G * \Delta x) \\ SP &= F(N_s) * E(\lambda) * \{\text{EXP}(G * \Delta x) - 1\} / G, \end{aligned} \quad (4.2-23)$$

Fig. 4-2 Flow chart of computer program DYGAIN.
N1, N0 and NT are the population of the singlet state,
the ground state and the triplet state, respectively.
 I^+ and I^- are the intensities travelling in the +x
or -x direction. Δx is a small interval into which
the length of the cell L is divided. CONV is for
convergence (test) and SYM is for symmetry (test).



where ST is the intensity of the stimulated emission in a certain range of wavelength and SP is the intensity of the spontaneous emission. ST' is the intensity of the stimulated emission coming from the precedent region (ΔX) of the cell. $F(N_s)$ is a function of N_s , $E(\lambda)$ is the emission spectrum of the spontaneous emission and G is the gain. The sum of ST and SP gives the intensity (I^+) in a particular location of the cell and in a given wavelength range.

The values of N_s , N_0 and N_T can be adjusted by including the new value of I^+ in Eqs. (4.2-19) and (4.2-21). This sequence is repeated until a reasonable convergence of I^+ is obtained. Then, the process is repeated for a new location (ΔX) in the cell. This is continued until the end of the cell is reached ($X = L$). Because both axial directions ($-x$ and $+x$) in the dye amplifier are identical, the intensity travelling in the negative direction should be identical to the intensity travelling in the positive direction. Therefore, there is a symmetrical distribution of N_s along x .

After the end of the cell is reached, the computation is repeated for each ΔX using both I^+ and I^- , instead of I^+ alone as in the first set of calculations. Each time the end of the cell is reached N_s is tested for symmetry with x . The computation is considered complete when the distribution of N_s is satisfactorily symmetrical. Typically, it requires four sets of calculations when the cell is divided into 100 steps (ΔX).

4.3 Experimental Arrangement

4.3.1 Gain Measurements in a Dye Amplifier

As mentioned earlier in this chapter, the probe source originates from a high pressure Xe lamp. The spectrum of the light emitted is reasonably uniform in the visible. The intensity drops off below about 250 nm. The total dc power input is 300W.

The light emitted by the lamp discharge volume is focused onto a 0.25 m monochromator (Jarell-Ash) by means of a 5 cm focal-length lens. The resolution of the monochromator establishes the bandwidth of the probe source, e.g., 10\AA for a 150 μm slit width. The output slit of the monochromator is focussed on the entrance window of the dye cell by means of a 5 cm focal-length lens. The reason for doing this is discussed later in the chapter. On the other side of the dye cell, a 10 cm focal-length lens couples the signal into a second monochromator (similar to the first). The gated photomultiplier is at the exit slit of the second monochromator. A second photomultiplier is used to synchronize the gating system and a storage scope with the light pulse from the dye amplifier flashlamp.

This experimental arrangement has to be optimized to maximize the intensity of the detected signal coming from the high pressure Xe lamp, and to minimize signals originating in the dye cell itself, such as spontaneous emission and ra-

diation directly from the flashlamp. In the initial experiments, there was no monochromator between the dye cell and the gated photomultiplier. Much effort was taken to filter out the background signal originating from the flashlamp and the spontaneous emission. This required the use of pinholes, and small apertures employing relatively long focal-length lenses. Light originating from the wall of the dye cell, i.e. coming from the flashlamp, were essentially eliminated. However, the spontaneous emission, coaxial with the probe beam, was too intense. Then a second monochromator was added to select only the spectral width of the probe beam. Unfortunately, owing to the length of the dye laser (~ 20 cm), it was impossible to couple all of the light from the probe beam into that second monochromator. Consequently, the detected amplitude became very small (~ 5 mV across 25Ω , corresponding to 2.5×10^{-9} W on the photocathode), while a strong signal was still present due to spontaneous emission in the system (~ 150 mV across 25Ω , corresponding to 7.5×10^{-8} W on the photocathode). The dye laser concentration was low at 5×10^{-5} M/l of R6G in methanol.

4.3.2 Problems and Discussion

From the above it can be seen that the probe signal is only 3% of the background signal. Furthermore, the concentration must be increased to measure gain, which means a con-

siderable background due to ASE. The contribution to the background by the direct light from the wall of the dye cell (i.e., from the flashlamp), when not removed by aperturing, is more than ten times stronger than the spontaneous emission. This can contribute on "on-axis" radiation by reflections from the cell windows. The dye cell is closed by quartz windows ($n_q = 1.4585$), with methanol on one side ($n_M = 1.3288$) and air on the other. The quartz-methanol interface gives 0.2% reflection and the quartz-air interface gives 3.5% reflection. It is reasonable to believe that part of the light coming from the flashlamp is coupled back along the axis of the cell after reflection at the interfaces. In order to eliminate that effect, which is equivalent to doubling the length of the cell (however, with effective wall intensity 3.5% of normal), several approaches were investigated. Roughened black-polyester disks were fixed on the far window at the quartz-methanol interface. The result was only a very small improvement. The next step was to remove the quartz window, and thus to put an extension on the dye cell (~ 20 cm long, filled with dye solution) so that the window was distant from the active medium. In addition, the window was inclined at 45° to avoid any coupling of the reflections along the axis of the cell. Again the improvement was not significant. These results indicated that the light coming along the symmetry axis of the dye cell came from the spontaneous emission alone. To confirm

this result, the central-part of the cell, which produces spontaneous emission, should be removed. The region close to the wall should remain the same, in order to test the ability of the aperture and optical system to remove light coming from the outer regions of the dye cell and from the flashlamp. For this test, a hollow glass tube, somewhat smaller than the inner diameter of the dye cell, was installed at the center of the dye cell to provide a symmetrical dye thickness of ~ 1 mm. Only air was present in the tube - windows were not employed. No background signals could be detected, which confirmed our previous results. Before the above test was performed, different low concentrations of dye were tried and a corresponding decrease in the intensity of the signal was observed.

Therefore, the major problem came from the intensity of the spontaneous emission. The difference of intensity between the probe signal from the Xe lamp, and the spontaneous emission from the dye amplifier could not be overcome. Consequently, the idea of probing the medium with a dc broadband light source had to be abandoned.

It would be mentioned that any measurements, using a relatively low power source are also very difficult owing to the photon noise. A simple calculation shows that, with $\sim 2.5 \times 10^{-9}$ W at the photocathode, only 80 photons (standard deviation of 9) reach the detector during a period of 8 ns and at a wavelength of 6000 Å. Therefore, this number is subjected to an appre-

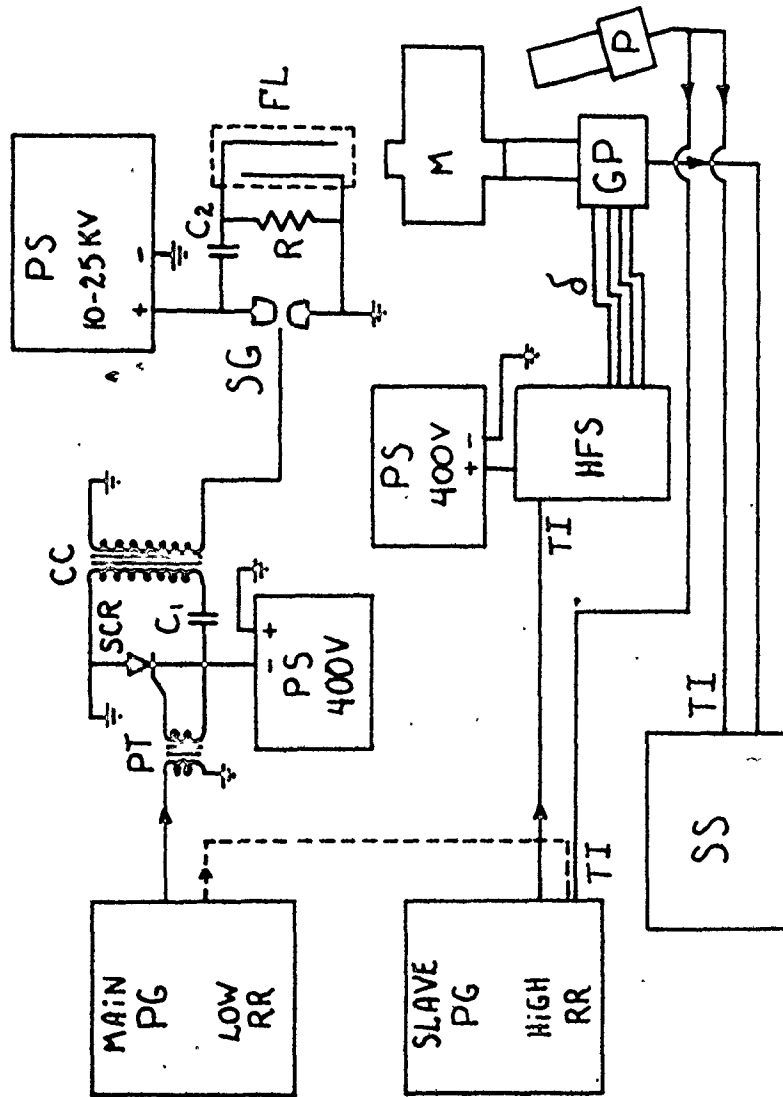
ciable fluctuation ($\sim 13\%$). Since these photons originate from a dc discharge, i.e., the signal changes from shot to shot. The way to make this technique work is to put more light into the system by, e.g., employing wider monochromator slits. However, the required width is so large that a considerable loss of resolution occurs as a consequence ($> 100 \text{ \AA}$). Another solution is to pulse the high pressure Xe lamp. Either solution was not practical in our case.

4.4 Time Dependent Spectrum of ASE

Experimental arrangement for measuring amplified spontaneous emission (ASE) is shown in Fig. 4-3. The aim of the measurements was to test the accuracy of the gated photomultiplier system when the signal intensity is very strong, i.e., up to the point where photomultiplier saturation begins.

The limiting accuracy of a gated photomultiplier, for low intensity signals, is determined by electrical noises. Part of this noise comes from gating pulses, as mentioned in Chapter 3. The rest is attributed to the electromagnetic fields generated by switching devices such as the spark gap, the flashlamp, and by high voltage cables and ground loops. With elaborate shielding, the total noise at the anode of the photomultiplier was $\sim 10 \text{ mV}$ across 25Ω , as obtained with a 100 MHz bandwidth oscilloscope.

Fig. 4-3 Schematic of the experimental arrangement. PG is the pulse generator, RR indicates repetition rate, PS means power supply, HFS means high frequency switch (chap. 2), GP is the gated photomultiplier and P is the photomultiplier used for triggering. M is the monochromator, PT is a pulse transform, CC is a standard car ignition coil, FL is the dye amplifier coaxial flashlamp and SG is the spark gap. The Silicon Controlled Rectifier (SCR) is a type 2N688, capacitor C_1 equals 10 μ F (400v), capacitor C_2 equals 300 nF (25 kv), and R is a 5K Ω resistor. δ represents the delay cables, TT the trigger input and finally, the signals were observed on a Tektronix type 466 storage oscilloscope (SS).



In Section 3.6, the behaviour of the gated photomultiplier was studied under short intense radiation pulses. The accuracy of the results, from this study, is important since the amplitude of the signals sent by the photomultiplier must be corrected, and consequently the errors must be added. Thus, the best accuracy is achieved for strong light pulses that will not drive the gated photomultiplier too far into saturation (< 40% of best linearity).

Fig. 4-4a shows the shape of the pumping pulse from the flashlamp and the corresponding shape of the ASE pulse. Fig. 4-4b represents the same situation, but only the ASE curve is shown, together with eight peaks representing the gated signals present at the anode of the gated photomultiplier. The location of each peak indicates the time when, during the ASE pulse, the photomultiplier was gated on.

The results, from the huge amount of data, are summarized in Figs. 4-5 to 4-12 and Fig. 4-13. The most interesting results are found in Fig. 4-13. This figure traces the evolution of the wavelength at the intensity peak and of the half width at half maximum (HWHM) of the spectrum, as the pumping rate is changed over a time interval of 700 ns, as shown in Fig. 4-4a.

The time characteristics of the laser emission spectra have been studied by Borisevich et al. [40], and their results for R6G correspond very well to what we have observed. For organic dye solutions, the time dependence is affected by the induced loss factors which are functions of wavelength. These

Fig. 4-4 Time dependence of light pulse shapes.

(a) Superposition of pumping pulse from the flash-lamp and of the ASE pulse. The vertical scales are not related. (b) Superposition of the ASE pulse and the sampled output from the gated photomultiplier. The vertical scales are not related.

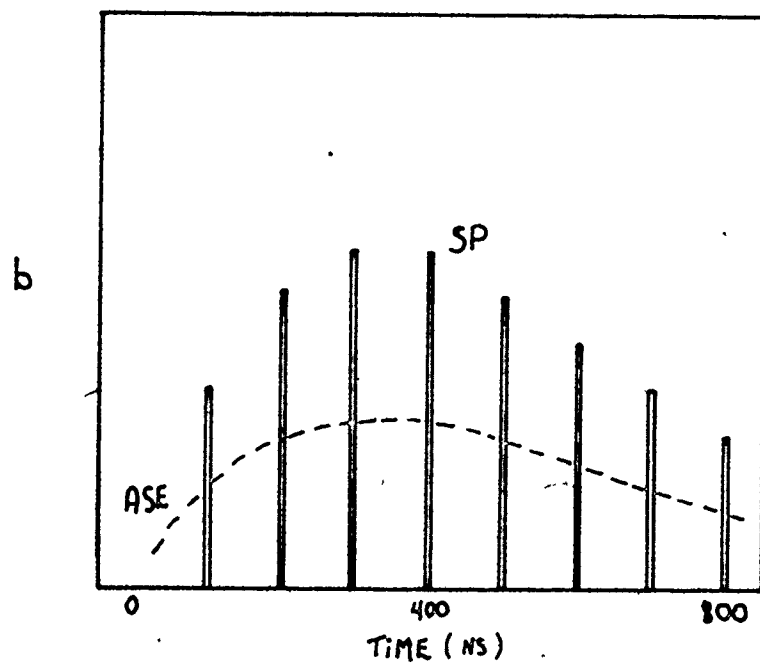
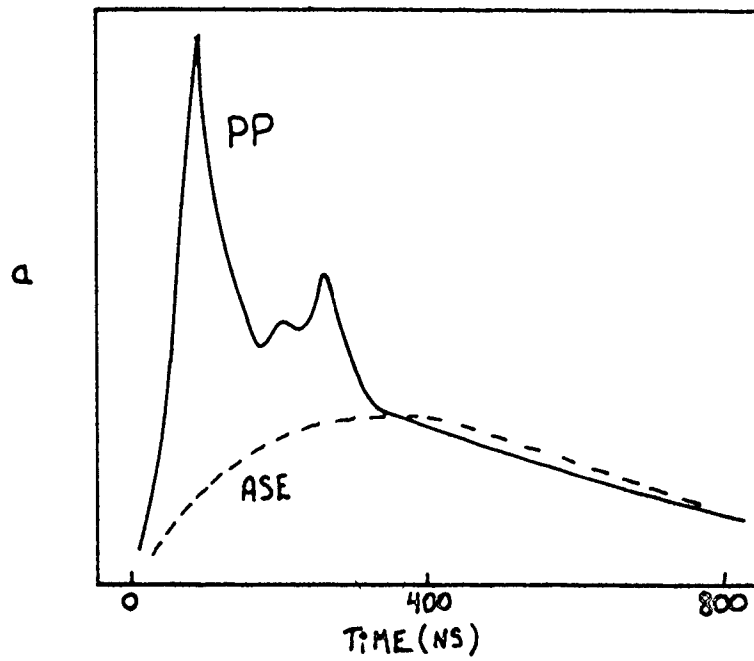


Fig. 4-5 ASE spectrum at time 0 ns. The spectral width is $225 \pm 8 \text{ \AA}$, the peak wavelength is $5960 \pm 8 \text{ \AA}$.

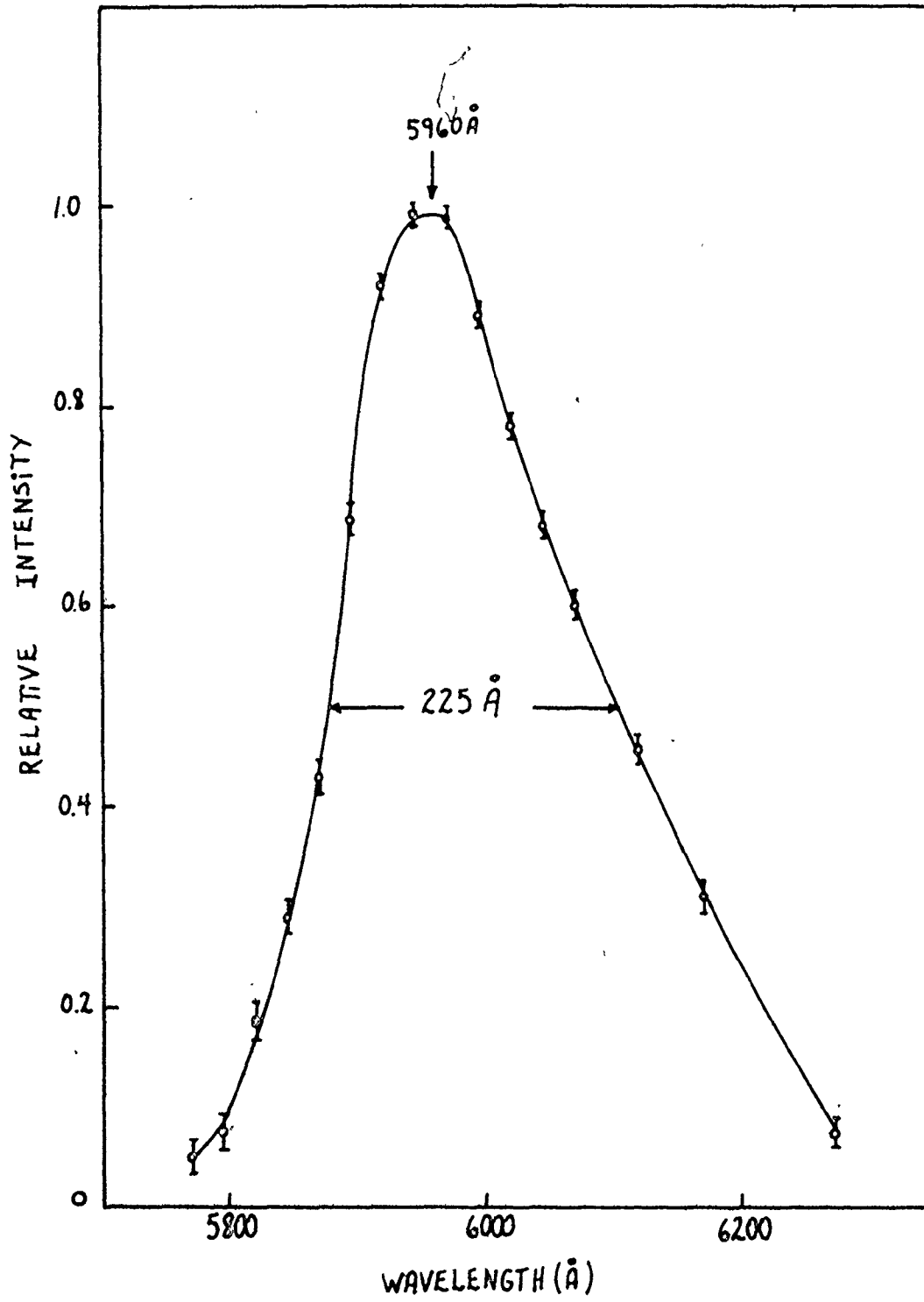


Fig. 4-6 ASE spectrum at time 100 ns. The spectral width is $307 \pm 8 \text{ \AA}$, the peak wavelength is $5960 \pm 8 \text{ \AA}$.

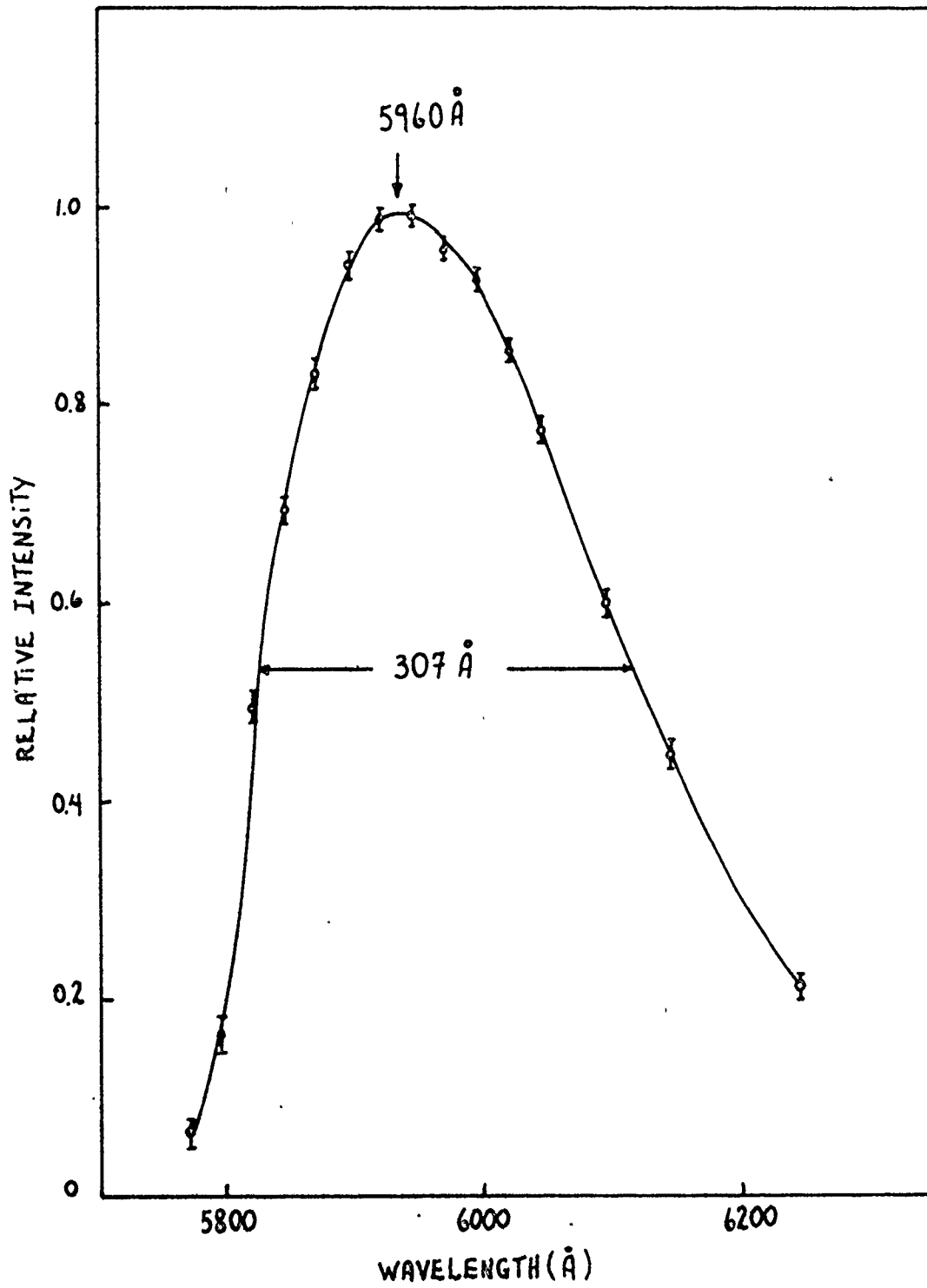


Fig. 4-7 ASE spectrum at time 200 ns. The spectral width is $325 \pm 8 \text{ \AA}$, the peak wavelength is $5965 \pm 8 \text{ \AA}$.

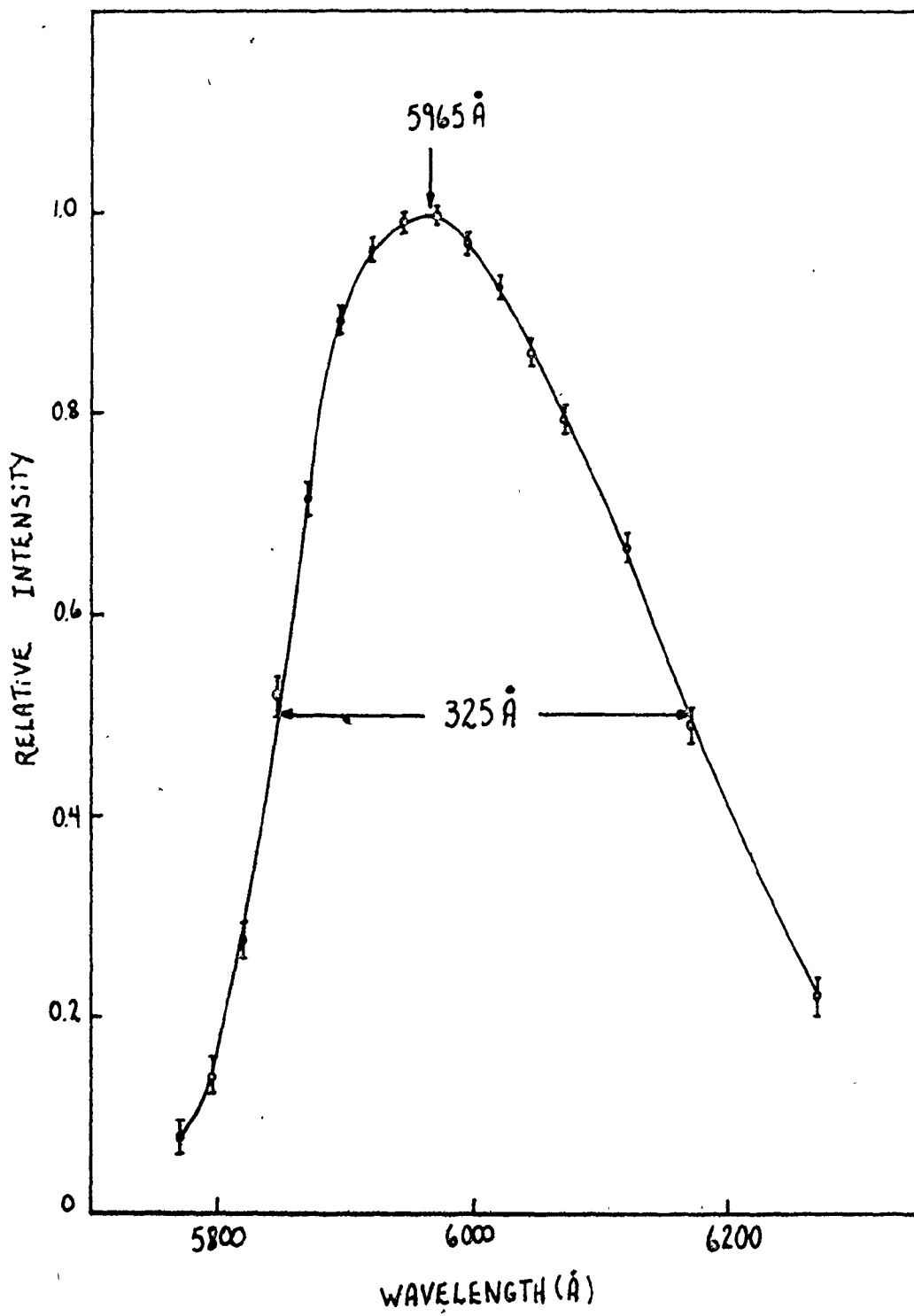


Fig. 4-8 ASE spectrum at time 300 ns. The spectral width is $350 \pm 8 \text{ \AA}$, the peak wavelength is $5855 \pm 8 \text{ \AA}$.

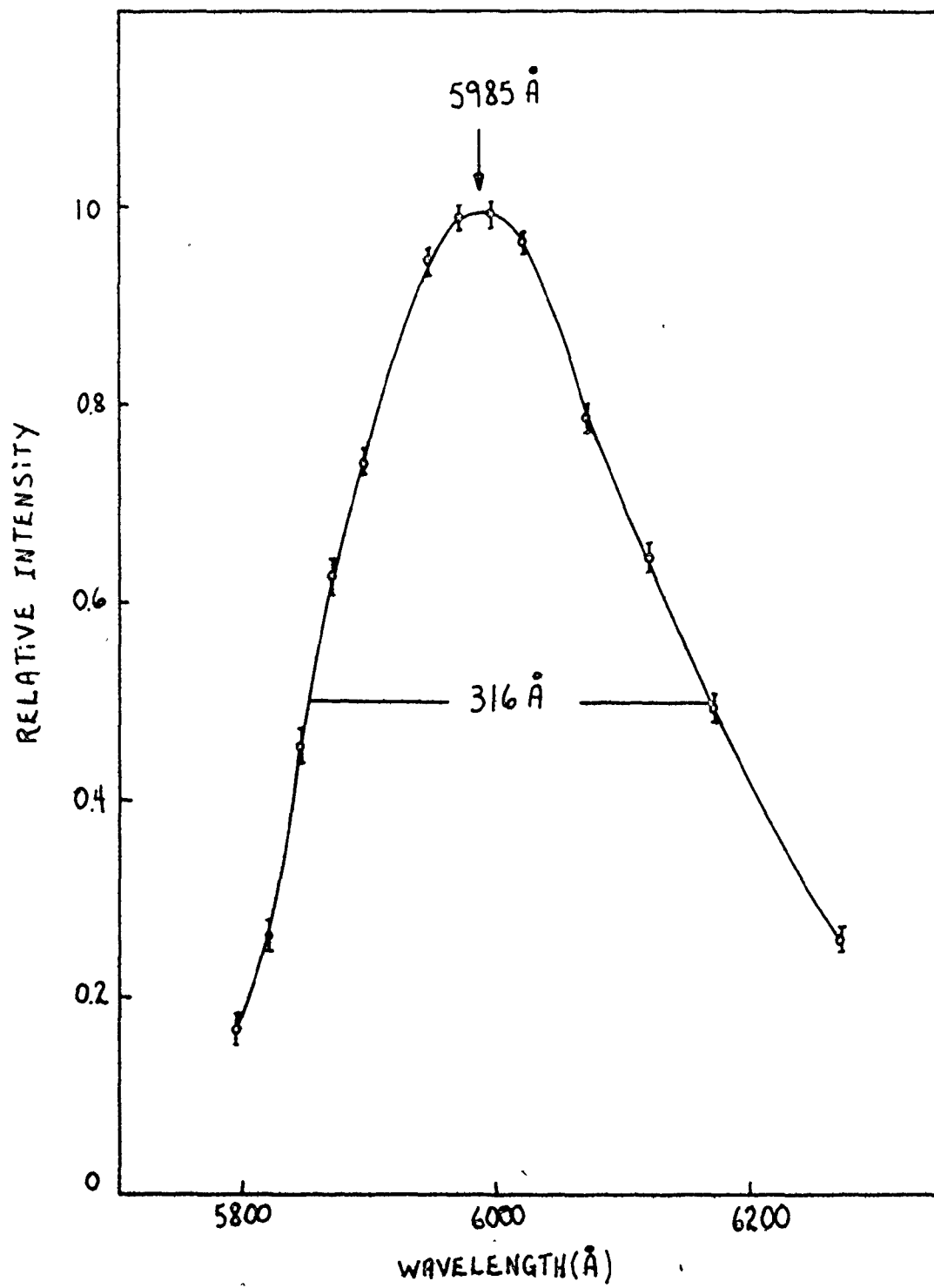
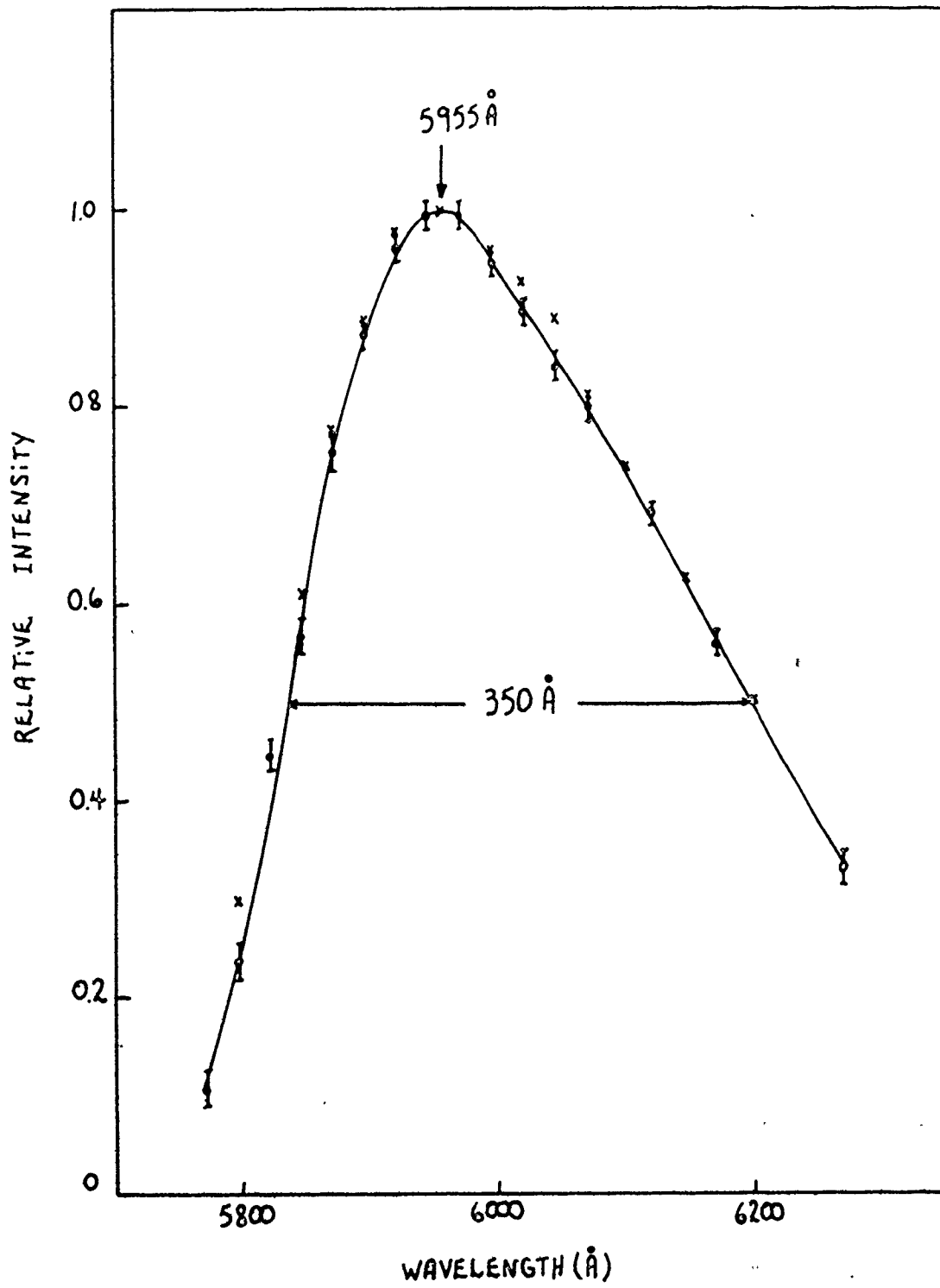


Fig. 4-9 ASE spectrum at time 400 ns. The spectral width is $316 \pm 8 \text{ \AA}$, the peak wavelength is $5985 \pm 8 \text{ \AA}$.






Fig. 4-10 ASE spectrum at time 500 ns. The spectral width is $297 \pm 8 \text{ \AA}$, the peak wavelength is $5955 \pm 8 \text{ \AA}$.

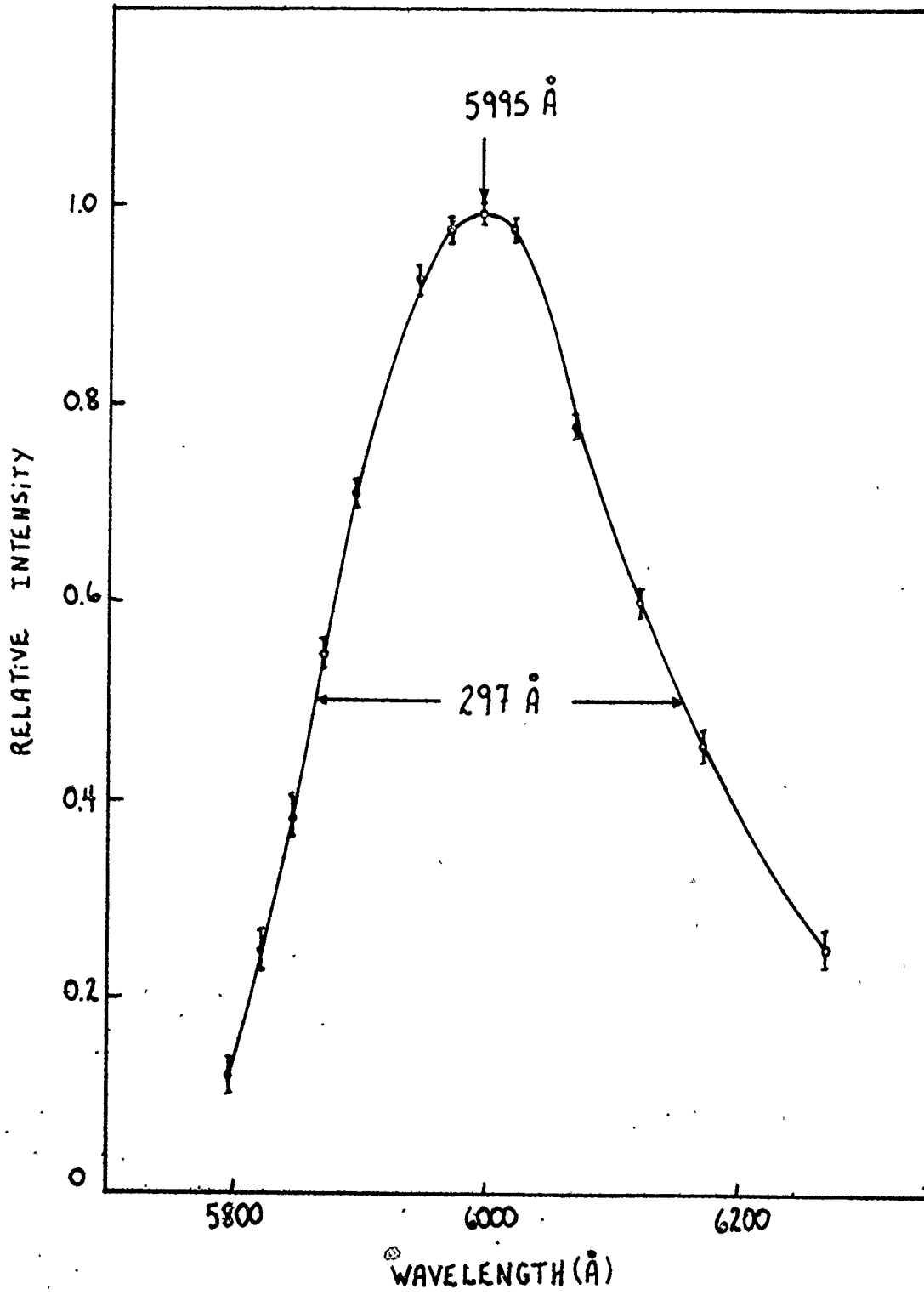


Fig. 4-11 ASE spectrum at time 600 ns. The spectral width is $270 \pm 8 \text{ \AA}$, the peak wavelength is $5995 \pm 8 \text{ \AA}$.

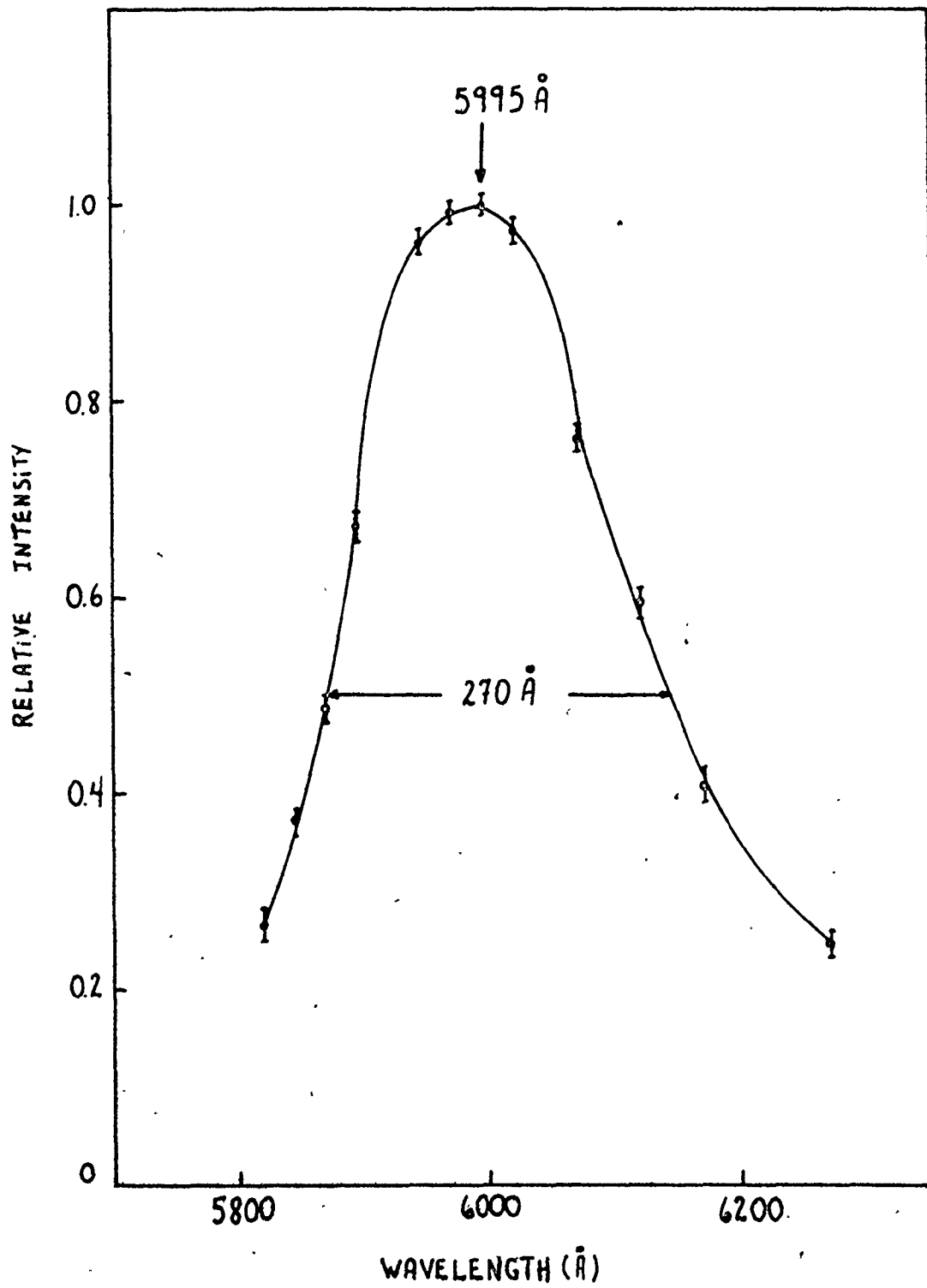
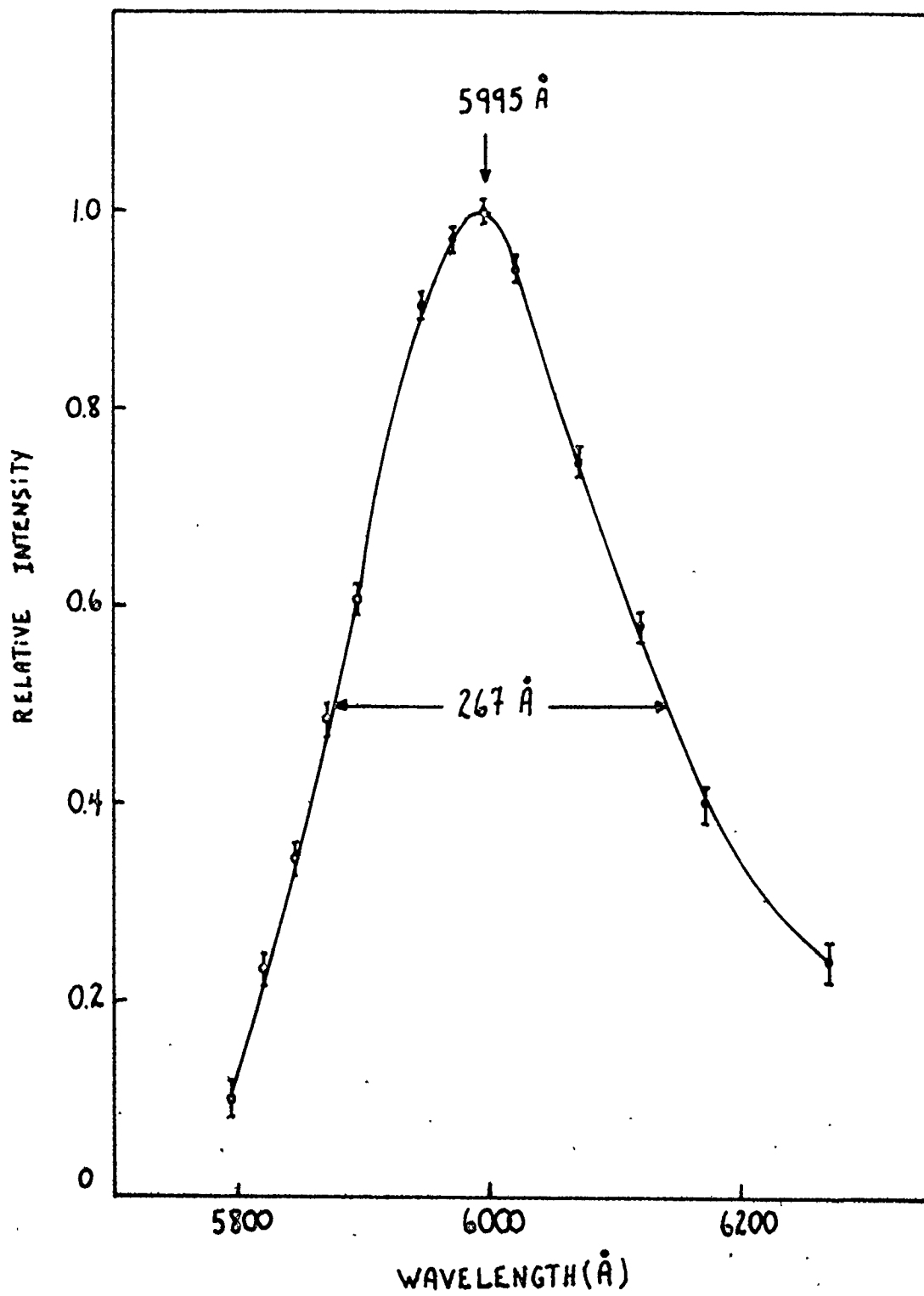


Fig. 4-12 ASE spectrum at time 700 ns. The spectral width is $267 \pm 8 \text{ \AA}$, the peak wavelength is $5995 \pm 8 \text{ \AA}$.

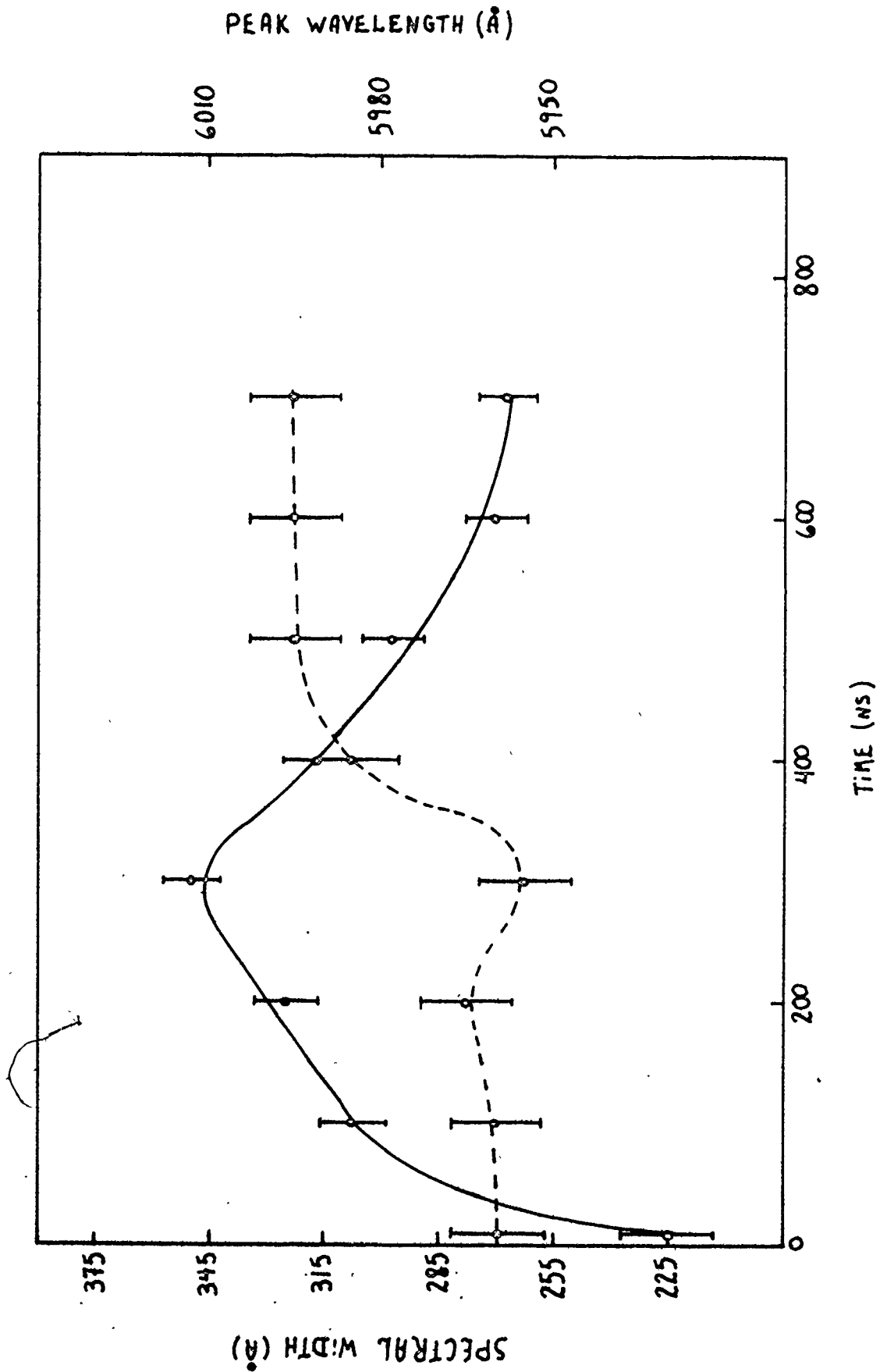


losses are principally

- a) increase of the population of the metastable triplet state,
- b) reabsorption of the emission by the ground state ($S_0 \rightarrow S_1$) or by the first excited state ($S_1 \rightarrow S_2$),
- c) deactivation of the molecules by the pumping radiation,
- d) increase in absorption, in the stimulated emission band, due to the formation of stable and short-lived photoreaction products,
- e) thermal and optoacoustic distortion of the medium.

Only two of these induced losses are found to have a considerable effect on the time dependence of the wavelength at the peak intensity and on the width of the ASE spectrum. The first of these is the triplet absorption, which shifts the wavelength at peak intensity toward the short wavelength region (because the absorption curve of the triplet state is located on the long wavelength side of the emission spectrum). The second is the absorption by photoreaction products which induces losses on the short wavelength side of the emission spectrum and, consequently, shift the wavelength at peak intensity to longer wavelengths. Borisevich et al. [40] have shown that the time behaviour of the wavelength at intensity peak is a competition between these two effects, and that the determining factor in this competition is the steepness of the leading edge of the pumping pulse. For a pumping pulse with a risetime of μs or less, the curve of Fig. 4-13 is typical for the behaviour

Fig. 4-13 Time characteristics of ASE spectra. The full curve represents the evolution of the spectrum width. The dashed curve represents the evolution of the peak wavelength.



of the wavelength at peak intensity.

For the first 200 ns, the pumping rate is high ($> 2.5 \times 10^6$ photons/s), the gain in the medium is high, and the ASE can withstand the losses from the ground state absorption. A typical shift of the wavelength at intensity peak to shorter wavelengths is observed (to $\sim 5960 \text{ \AA}$). After 300 ns, the triplet losses become important (triplet lifetime ~ 250 ns) and the wavelength at peak intensity is further shifted towards shorter wavelengths (to $\sim 5950 \text{ \AA}$). After 500 ns, the pumping rate has significantly decreased, the absorption by photoreaction products takes over, and a marked shift towards the long wavelength region is observed (to $\sim 5955 \text{ \AA}$).

The first plotted point, on the extreme left of Fig. 4-13, has a very high pumping rate, and therefore a high gain. Due to the non-uniform gain profile, as computed by DYGAIN, considerable narrowing is observed, the radiation intensity, near the peak of the gain profile, increases more rapidly than the radiation intensity near the edge of the gain profile. At very low pumping rates, no narrowing is assumed, and a spectral width of 420 \AA is predicted for a dye concentration of $1.5 \times 10^{-3} \text{ M/l}$. As the pumping rate decreases (after 300 ns) the spectral width broadens to 350 \AA . After 400 ns, the pumping rate is low and slowly decreasing. In such a case, it is typically observed [40] that the spectrum slowly narrows

and that the peak wavelength remains stable. This is probably due to the combined effect of the triplet losses and photoreaction products absorption acting simultaneously on both sides of the spectrum.

Finally, the computer program DYGAIN, inappropriate for a time dependent study of ASE, is able to match a steady state spectrum over the data points, corresponding to the time 400 ns in Fig. 4-13. This means that the situation has reached a steady state near the peak of the ASE curve (Fig. 4-4b). This demonstrates the accuracy of the steady state approximations.

4.5 Discussion and Conclusion

In our case, the greatest approximation comes from the assumption of a constant pumping rate. The wavelength at peak intensity is most affected by the steepness of the leading edge of the pumping pulse, as shown by Borisevich et al. [40] for pumping pulse risetimes greater than 1 μ s and by us for risetimes less than 1 μ s. Moreover, when the time characteristics of the ASE spectra are needed, the triplet losses and the photoreaction products absorption must be included in the numerical simulation. However, this is difficult because the triplet absorption band is not yet well defined, and even less is known about the photoreaction products absorption. We have observed a fluctuation of $\sim 40 \text{ \AA}$ in the wavelength of peak intensity (Fig. 4-13) over a period of 700 ns, for the pump

curve shown in Fig. 4-4a. The spectral width varies over $\sim 125 \text{ \AA}$ (from $\sim 225 \text{ \AA}$ to 350 \AA) in the same period of time. The error on these results is mainly governed by the resolution of the monochromator ($\sim 8 \text{ \AA}$).

Inspection of Figs. 4-5 to 4-12 reveals a typical accuracy of 2% for the results obtained with the gated photomultiplier when corrected for non-linearity following Fig. 3-9. The main source of error comes from the non-reproducibility of the pump pulse. The shape of the pulse is very constant, but the intensity typically varies by 5%. Therefore, a series of 20 flash discharges were recorded and averaged to obtain an accuracy of 1%. The limiting accuracy for intense light pulse is imposed by the trace width of the storage scope used (Tektronix 466). This accuracy degrades when the signal is weak, as observed in Figs. 4-5 to 4-12, due to electrical noise and to flash fluctuations. A 10% accuracy is available for a signal of $\sim 80 \text{ mV}$ across 25Ω .

The gated photomultiplier proved capable of providing reliable data on the time dependent spectrum of the ASE. Much more accurate results could be obtained if the pump was reproducible from pulse-to-pulse and if a high resolution spectrometer was available.

From the above work, we can conclude that a gated photomultiplier is suitable for accurate measurements of intense light pulses. This, together with the ability of good time resolution (2 ns), can be readily employed to investigate the time characteristics of such pulses.

CHAPTER 5
CONCLUSION

The main purpose of this work has been to develop a new high repetition rate sampling method for observing intense radiation sources. The basic unit consists of a high repetition rate high voltage pulse generator used to gate a photomultiplier.

The pulse generator is composed of six gates (transistor switches) triggered sequentially through coaxial cables which introduce the proper delay between each gate. A limit of six gates is imposed by the inherent mismatch between the coaxial cables and the different gates. We have operated the pulse generator at repetition rates as high as 75 MHz for six consecutive pulses, repeatedly every 2.5 μ s, and at a continuous rate of 2.5 MHz or less. The amplitudes of the gating pulses range between 0 and 220V. The risetime and faltime of such pulses is 2 ns, and the width is continuously adjustable. However, the width affects the highest repetition rate attainable.

The pulse generator is employed to gate a photomultiplier. The photomultiplier gating circuit proposed by Araki et al. [7] has been modified so as to be used either in normal dc operation or in the gated mode. This modification consists in the incorporation of three potentiometers

in the circuit of Fig. 3-7, instead of fixed resistors to bias the pulsed dynodes. This improves the ability to perform fine voltage adjustments in order to attain the best cut-off state consistent with minimum deterioration of gain when the photomultiplier is pulsed. In addition, it is possible to study the variations of gain when one or several dynodes are biased relative to their normal operating voltage. Such studies, together with comparison of the behaviour of photomultiplier types RCA 6199 (simply focussed) and HTV R212UH (elaborately focussed), showed that adequate cut-off is reached when the electron flow is defocussed in several locations of the multiplication stages. Consequently, an elaborately focussed photomultiplier is best for gating purposes. The results of these experimentations are discussed in Chapter 3.

The purpose of this work was to devise a sampling method specially adapted to deal with high intensity sources. Therefore, the non-linear behaviour of the anode current, at high radiation intensities, was studied. This study indicates that the linearity of the photomultiplier can be improved by a factor of ~ 50 when the photomultiplier is gating for very short period of time (~ 8 ns). This study also provided a good understanding of the causes and effects of anode current non-linearity. These results are summarized in Section 3-6.

Finally, this new high repetition sampling method has been applied to investigate the gain of a coaxial flashlamp

pumped dye amplifier. Also, the amplified spontaneous emission (ASE) has been investigated to estimate the system accuracy, and to complete the set of data published by Borisovich et al. [42]. The accuracy achieved by the gated photomultiplier, corrected for the non-linear behaviour of the anode current, was 2% for relative amplitude, and 3% for time. The accuracy on the peak wavelength and the spectral width of the ASE are determined by the resolution of the monochromator ($\sim 8 \text{ \AA}$). Data concerning the time characteristics of the ASE are provided in Chapter 4.

✱

APPENDIX A

A NANOSECOND LIGHT PULSER

When a photomultiplier is gated, e.g., as described in Chapter 3, the basic operating characteristics may be altered. The purpose of the light pulser is to measure the risetime, the transit time and the transit time spread of the photomultiplier in the gated mode. Ideally, the light pulse emitted from the light pulser should approach a delta function. Practically, the light pulse risetime and fall-time need only be shorter than the risetime of the photomultiplier.

A description of such a light pulser is given by McFarlane [36] and by Araki et al. [7]. It consists essentially of a LED which is driven by a voltage pulse generated by a transistor switch, similar to the one described in Chapter 2 (Fig. 2-2a), except that the charging cable is replaced by an adjustable capacitor. The light pulser circuit that we have designed is shown in Fig. A-1. Since this circuit operates in the same manner as the transistor switch described in Chapter 2, only the special features are discussed. These are the diodes to ground, the inductance and the LED.

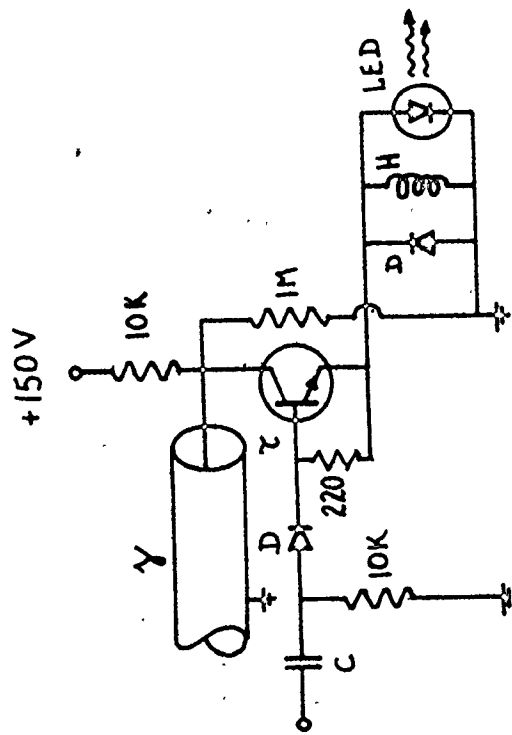
Fig. A-1 Circuit for a nanosecond light pulser.

LED is a light emitting diode, D is a diode (1N4148),

τ is a transistor (2N3725), γ is a charging cable

(RG58A/U), C is a capacitor (0.001 μ F) and H is an

inductance (\sim 50 nH).



Some resonances were observed because of circuit capacitance and inductance. Consequently, it was necessary to choose a LED type that minimizes these resonances, and that generates a light pulse with the best risetime and fall-time. The small inductance across the LED (~ 50 nH) is needed to provide a reverse current to the LED to speed up the recombination of the carriers and achieve a quicker extinction. This inductance must be selected for each LED.

LEDs type GL-56, GL-4484, GL-4850, FLV-340 and MV5253 were tested. The best results were obtained with LED type GL-4850 used with an inductance consisting of two turns of 22 gauge copper wire with inner diameter 5.5 mm and separation 1 mm. The diode to ground (1N4148) protects the LED from reverse breakdown caused by high voltage transients (~ 100 V).

In order to test the photomultiplier, the characteristics of the light pulse (risetime, falltime and FWHM) must be known. These characteristics could not be measured with an available photodiode (risetime 0.3 ns) because the intensity was too low. Consequently, we had to rely on relative measurements, i.e., we compared the shape of the light pulse as seen by the photomultiplier in normal dc operation, in the gated mode and in the cut-off state (cut-off ratio ~ 100). There were no differences between regular dc operation and gated mode operation, where the latter was broader than the

light pulse. Even with a dynode voltage distribution such that the gain was reduced by 100, the risetime and the transit time spread are not changed, to within 0.3 ns. The transit time is also not affected to within 1 ns. Again reduction of more than 100 could not be used, because the intensity was too low. However, it is possible that the pulse characteristics of the photomultiplier, discussed in this appendix, might be altered significantly for a gain reduction of 1800 because of strong defocussing of the electron flow.

APPENDIX B
PULSE TRANSFORMER FOR USE AS A
NANOSECOND PULSE INVERTER

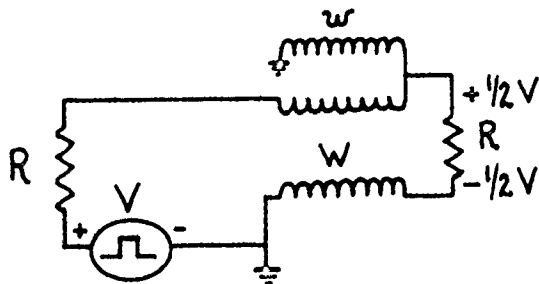
Figs. 3-3, 3-4, 3-5 and 3-6 indicate that, depending on the situation, some dynodes must be gated by a positive voltage pulse and some others by a negative voltage pulse. The pulse generator described in Chapter 2 can generate voltage pulses with either a positive or a negative polarity, but always with the same polarity for all the gated dynodes. Therefore, a pulse inverter is required to provide opposite polarity pulses, when necessary.

Very small ferrite toroids are useful for making nanosecond pulse inverters. The basic information is provided in an article by Smith [37]. The best inverter for our application (high voltage nanosecond pulses) are broad-band nanosecond bifilar wound transforms with a finite toroid core (Philips 4C6) [38,39].

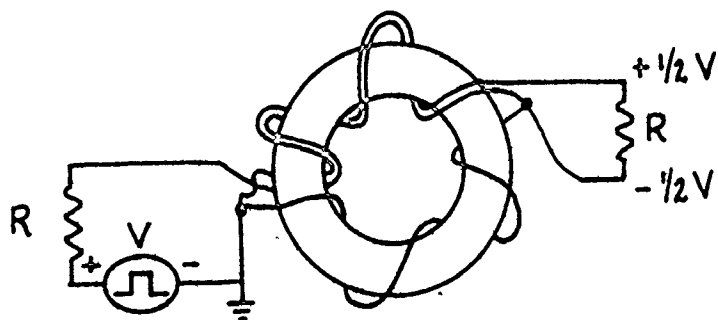
In a bifilar transformer (Fig. B-1) the primary and the secondary winding form a transmission line. In conventional transformers, the interwinding capacity resonates with the leakage inductance to produce a loss peak. This mechanism limits the high frequency response. In transmission line transformers, the windings are so arranged that the interwinding capacitance is a component of the characteristic im-

Fig. B-1 A nanosecond pulse transformer. (a) is the transmission line form of the windings. W is the transmission line and w is an additional winding. R is the matched impedance. (b) represents the transformer built following the bifilar arrangement of (a). Some 32 gauge enameled copper wire was used on a ferrite toroid core (Philips type 4C6). Voltage +V or -V are available when the opposite end of R is grounded.

a)



b)



pedance of the line, and as such forms no resonances which seriously limit the bandwidth. The current trend is to wind very small diameter commercial coaxial cables directly on the toroid [39]. However, we employed wire windings because of availability.

The following sample calculation is based on Ref. [37]. The ferrite core employed (Philips type 4C6) has a relative permeability $\mu' \sim 100$, and is 2 mm thick by 4 mm ID by 6 mm OD.

Only two parameters determine the quality of a pulse inverter - the pulse risetime and droop. The adequately small droop is of the order of 5%. It is difficult to achieve a risetime of better than ~ 1 ns because of the finite characteristics. First, assume that the pulse has a width of 4 ns. The primary inductance is given by

$$L_p \approx 20TR = 2\mu\text{H} \quad (\text{A.1})$$

where T is the pulse width (4 ns) and R is the generator and load impedance connected in parallel (25 Ω). The number of turns in the bifilar winding is

$$N = \left(\frac{\ell L_p}{A\mu_0\mu'} \right)^{\frac{1}{2}} = 15 \text{ turns} , \quad (\text{A.2})$$

where ℓ is the winding length (3 cm), μ_0 is the permeability of free space and A is the cross-sectional area of the core (0.02 cm²). The risetime of the transformer and the load impedance for best matching can be calculated from

$$t_R = \pi(L_L C_p)^{1/2} . \quad (A.3)$$

The load impedance is given by

$$R_L = (L_L / C_p)^{1/2} , \quad (A.4)$$

where L_L , the leakage inductance referred to the primary is calculated from,

$$L_L \approx \frac{N^2 \delta D \mu_0}{\ell} = 40 \text{ nH} , \quad (A.5)$$

and C_p , the stray capacitance referred to the secondary, is calculated using

$$C_p \approx \frac{\epsilon \epsilon_0 D}{\delta} = 3.5 \text{ pF} , \quad (A.6)$$

where D is the mean circumference of the windings, ϵ is 1, ϵ_0 is the permittivity of free space, and δ is the insulation thickness (0.1 cm). The risetime becomes approximately 1 ns and the transmission line impedance is $\sim 92 \Omega$. Finally, the strength of the magnetic field is checked to verify that the ferrite core does not saturate. The field is given by

$$B = \frac{V_p I}{NA} \times 10^8 = 28 \text{ gauss} ,$$

where V_p is the voltage across the primary. For the grade of ferrite material commonly used, a core would saturate at ~ 2500 gauss.

In conclusion, the most important criteria, i.e. the best risetime, is achieved for a small toroid and a small

number of turns as can be seen from Eqs. (A.3) to (A.6). It should be noted that the extra winding (w in Fig. B-1) is required to complete the path for the magnetizing current. Moreover, an unmatched impedance, compared to the transmission line impedance, creates a dip in the frequency response curve, at a frequency equivalent to a transmission line length of $\lambda/4$. For small toroid transformers, this occurs in the GHz region.

REFERENCES

1. U. Farinelli and R. Malvano, Rev. Sci. Instrum., 29, 699 (1958).
2. F. De Martini and K. P. Wacks, Rev. Sci. Instrum., 38, 866 (1967).
3. F. De Marco and E. Penco, Rev. Sci. Instrum., 40, 1158 (1969).
4. T. Ushida and S. Minami, Japan J. Appl. Phys., 10, 1744 (1971).
5. M. Rossetto and D. Mauzerall, Rev. Sci. Instrum., 43, 1244 (1972).
6. D. G. Jameson and J. J. Martin, J. Phys. E: Sci. Instr., 8, 636 (1975).
7. T. Araki, T. Ushida and S. Minami, Japan J. Appl. Phys., 15, 2421 (1976).
8. J. Sharpe, Elec. Tech., 38, 251 (1961).
9. F. J. Lombard and F. Martin, Rev. Sci. Instrum., 32, 200 (1960).
10. N. A. Koshilev et al., Instr. Exp. Tech., 20, 521 (1977).
11. M. Yamashita, Rev. Sci. Instrum., 45, 956 (1974).
12. Millman and Taub, Pulse Digital and Switching Waveform, McGraw-Hill, 1965.
13. L. A. Dalhom, Design and Application of Transistor Switching Circuit, McGraw-Hill, 1968.
14. Motorola, High Speed Switching Transistors Handbook, Semiconductor Product Division.

15. D. T. Comer, Large-Signal Transistor Circuit, Prentice-Hall, 1967.
16. T. Efthymiopoulos, Flashlamp Pumped Dye Laser, Ph.D. Thesis, McMaster U., 1978.
17. B. G. Huth, Appl. Phys. Lett., 16, 185 (1969).
18. M. Gassman and H. Weber, Opto-Electronics, 3, 173 (1971).
19. P. Burlamacchi, R. Pratesi and L. Ronchi, Appl. Optics, 14, 79 (1975).
20. P. Burlamacchi, R. Pratesi and R. Salimbeni, Appl. Optics, 14, 1311 (1975).
21. U. Ganiel, A. Hardy, G. Neumann and D. Treves, J. Quant. Electr., QE-11, 881 (1975).
22. L. W. Casperson, J. Appl. Phys., 48, 256 (1977).
23. R. B. Green, J. Chem. Educ., 54, A365 (1977).
24. J. B. Marling, J. G. Hawley, E. M. Liston and W. B. Grant, Appl. Optics, 13, 2317 (1974).
25. P. Dal Pozzo, R. Polloni and F. Zaraga, Opt. Acta, 23, 919 (1976).
26. A. N. Fletcher, D. A. Fine and D. E. Bliss, Appl. Phys., 12, 39 (1977).
27. W. Falkenstein, A. Penzkofer and W. Kaiser, Opt. Commun., 27, 151 (1978).
28. J. R. Prescott, Nucl. Instr. Methods, 39, 173 (1966).
29. G. G. Albach and J. Meyer, Rev. Sci. Instr., 44, 615 (1973).

30. O. H. Sacherlotzky and V. J. Belanger, Trans. Nucl. Sci., NS-19, 68 (1972).
31. D. J. Baker and C. L. Wyatt, Appl. Optics, 3, 89 (1964).
32. D. H. Hartmann, Rev. Sci. Instr., 49, 1130 (1978).
33. P. Moatti, Onde Electr., 43, 787 (1963).
34. H. J. Lush, Rev. Sci. Instr., 42, 597 (1965).
35. R. Stump and H. E. Talley, Rev. Sci. Instr., 25, 1132 (1954).
36. W. K. McFarlane, Rev. Sci. Instr., 45, 286 (1973).
37. J. H. Smith, Electr. Eng., nov., 551 (1957).
38. C. L. Ruthroff, IRE Proceedings, 1337 (1959).
39. R. Bosshard, C. Zajde and H. Zyngier, Rev. Sci. Instr., 38, 942 (1967).
40. N. A. Borisevich, V. V. Gruzinskii and S. V. Davidov, Sov. J. Quant. Electr., 4, 947 (1975).